UNIVERSITÀ DEGLI STUDI DI MILANO-BICOCCA
European Doctorate in Materials Science
Dipartimento di Scienza dei Materiali

CHARGE TRANSPORT PROPERTIES OF ORGANIC SEMICONDUCTORS: APPLICATION TO FIELD EFFECT TRANSISTORS

Daniele Braga

a joint thesis with the University Paris VII

Thesis Directors:

Prof. Alessandro Borghesi
Prof. Gilles Horowitz

MILANO

DECEMBER 2009

1. Reviewer:

2. Reviewer:

Day of the defense:

Signature from head of PhD committee:

Abstract

Organic Field Effect Transistors (OFETs) are the fundamental building blocks of many flexible and low cost electronic systems, i.e. radio-frequency identification (RFID) tags and active matrices of organic light-emitting displays. Moreover, they represent unique tools to study charge transport in an organic semiconductor, by giving direct access to the most important electrical parameter: the mobility of the charge carriers. In spite of the importance of these devices, unique descriptions of their working principles are nowadays not available, especially because there are no consistent understandings of the material properties.

For this reason, in order to go deeper in the knowledge of the device fundamentals, we have characterized different typologies of OFETs using rubrene single crystals. The latter are highly ordered organic semiconductors with which high mobility transistors can be fabricated. First to consider field effect devices, we have obtained a detailed picture about the properties of a rubrene single crystal, by analyzing the current-voltage ($I-V$) characteristics of symmetric diodes with the Space Charge Limited Current (SCLC) theory. A low density of defects and a low density of intrinsic thermally generated carriers have been found to characterize this material. On this basis, we have analyzed metal-semiconductor-field-effect-transistors (MESFETs) made on the same semiconductor. These non-conventional devices have been proved to be efficient organic FETs, in which the process of charge carrier injection from the ohmic source contact is controlled by the voltage applied to a non-ohmic gate electrode. Their working principles are extremely different compared to the inorganic case, because there is no depletion layer in the rubrene single crystal close to the non-ohmic contact. This peculiarity reflects well the low density of free charges in the material.

Finally, single crystal metal-insulator-semiconductor field effect transistors (MISFETs) have been considered. Inconsistencies with respect to the inorganic case have been found also in this case. Indeed, the $I-V$ trend below the threshold voltage is not exponential, as predicted by the diffusion theory developed for the inorganic MOSFET; instead, it is linear with the gate voltage and it follows a pseudo-exponential behavior only in a narrow transition region. An alternative semi-analytical description has been provided here by taking into account the effect of a localized trap level on the distribution of free charges. The presence of this discrete trap level was highlighted by the previously conducted SCLC analysis.

Résumé

Les transistors organiques à effet de champ (OFETs pour Organic Field-Effect Transistors) sont les briques de bases de nombreux systèmes électroniques flexibles et à faible coût, tels que les radio-étiquettes (RFID pour RadioFrequency IDentification) et les matrices actives dans les dispositifs électroluminescents. De plus, ils représentent un outil d'étude du transport de charge à l'intérieur d'un semiconducteur organique, permettant ainsi un accès direct au paramètre électrique le plus important pour un semiconducteur, la mobilité des porteurs de charge. En dépit de l'importance de tels dispositifs, actuellement il y a aucune description unanime sur leur principe de fonctionnement, notamment à cause du manque de compréhension des propriétés des semiconducteurs organiques. Pour cette raison et dans le but d'améliorer les connaissances dans les fondamentaux de tels dispositifs, nous avons élaboré et caractérisé différents configurations d'OFETs en utilisant des monocristaux de rubrène. Ce dernier est un matériau organique fortement ordonné avec lequel il est possible d'obtenir des transistors ayant une mobilité élevée. Tout d'abord, avant de s'intéresser aux transistors à effet de champ, nous avons étudié et obtenu une image détaillée des propriétés du monocristal de rubrène, en analysant les caractéristiques courant-tension ($I - V$) de diodes symétriques à l'aide de la théorie du courant limité par la charge d'espace (SCLC pour Space Charge Limited Current). Cette étude nous a permis de montrer que ce matériau se caractérise par une faible densité de défauts ainsi qu'une faible densité de porteurs de charge intrinsèques générés thermiquement. A partir de ce résultat, nous avons analysé transistors organiques à effet de champ à jonction métal/semiconducteur (MESFETs pour Metal-Semiconductor Field Effect Transistors) fait avec le même matériau. Ces dispositifs non-conventionnels se sont révélés être des FETs performants, où l'injection des porteurs de charges de la source est contrôlée par la tension appliquée à la grille, choisie de manière à former un contact non-ohmique avec le semiconducteur. Nous avons trouvé que ces MESFETs organiques fonctionnent différemment de leurs équivalents inorganiques du fait de l'absence d'une zone de dépletion proche du contact non-ohmique. Cette particularité traduit bien la faible densité de charges libres dans les monocristaux de rubrène. Finalement, nous avons étudié les transistors à effet de champ à jonction métal/isolant/semiconducteur (MISFETs pour Metal Insulator Semiconductor Field-Effect Transistors). Des divergences avec les semiconducteurs inorganiques ont également été observées dans ce cas: le comportement ($I-V$) en-dessous de la tension de seuil ne varie pas de fonction exponentielle, contrairement à la prédiction de la théorie de diffusion développée pour les MOSFETs inorganiques. En effet, un comportement linéaire, fonction de la tension de grille, est observé excepté sur une région étroite de transition

dans laquelle le comportement est pseudo-exponentiel. Une description semi-analytique alternative a été établie en prenant en compte l'effet d'un niveau de pièges localisé sur la distribution de charges libres dans le canal. Niveau dont la présence a été précédemment mise en évidence lors de l'analyse SCLC.

Contents

Chapter 1

Introduction

This preface is a short introduction to the field of organic electronics. Through some important examples, the state of the art is outlined, along with the presentation of the open problems this thesis addresses. The main goal of this thesis is to provide, on the basis of the differences between organic and inorganic semiconductors, an alternative description of some organic electronic devices. For this scope, in spite of their low processability, rubrene single crystal devices have been chosen as ideal systems, with which the fundamental properties of an organic device can be investigated. In the last section, the structure of the thesis is also briefly presented.

1.1 General Overview

1.1.1 State of the Art

In the past century the identification of a particular class of organic compounds that, under an appropriate stimulus, could emit visible electromagnetic radiation and through which a current could flows, has been of particular importance. The marking element of these "organic molecular semiconductors" was the presence of a π-conjugated system. Materials derived from the condensation of these molecules, that for years remained pure research topics, nowadays begin to be put beside (or take the place of) the conventional inorganic semiconductors in all the applications that require low production costs and high frame flexibility. Even if still in a prototype form, small logic circuits working on polymeric substrates (e.g. RFID tags), large size flat displays and flexible solar cells can be produced with these materials. An innovative technological market sector, characterized by extremely low production costs, could be opened in the oncoming future, thanks to the increased performances of organic light emitting diodes (OLEDs), organic field effect transistors (OFETs) and solar cells. However, nowadays a number of intrinsic problems are still to be resolved. The stability and the charge carrier mobility of the active layer have to be increased and, more importantly, a deeper knowledge of the physical fundamentals governing the device operation has to be reached.
Behind their technological interest, field effect transistors (FETs) represent unique tools to study charge transport in an organic semiconductor; their characterization gives direct access to the most important electrical parameter in the semiconductor: the mobility of

the charge carriers. However, this statement would be true only when dealing with "ideal" systems, in which the mobility is a quasi-constant parameter, only slightly influenced by the voltage applied to the gate electrode. On the contrary, describing the operation of a disordered thin film field effect transistor (TFT) is still not a straightforward task. The formation of the conductive channel and the injection of charge carriers from the metal electrodes into the semiconductor are still not well understood interface processes, in which the high density of defects masks the intrinsic properties of the device. [1] However, it is not pointless to underline that the first fabricated and studied organic devices were thin film transistors [2], OLEDs [3] and solar cells. Utilization of single crystals in electronic devices was limited by the absence of established methods to integrate the fragile active layer in the system, without its damage. [4] This is in strong contrast with the inorganic case, where the advanced electronic applications use single crystals of high structural and chemical quality. In any case, from the beginning of the fast development of organic electronics, an accurate understanding of the principles underlying devices seemed to be only a marginal problem; the characteristics were mainly analyzed using theories developed for the inorganic case. On the contrary, it is nowadays evident that the physics of organic devices is different from the latter case. Considering the differences between the two classes of materials, [5] several innovative interpretations about the device fundamentals have already been provided [6, 7, 8]. However, in spite of important efforts, satisfying descriptions are not available yet [9] and several inconsistencies can be also found, for example, in the theories describing the formation of the simple metal/semiconductor interface. [10] This is especially due to the amorphous or polycrystalline nature of the analyzed semiconductor. These inconsistences in the description of this device building block cause several problems to the analysis of more complex structures. In the case of organic diodes, the commonly used "inorganic-like" interpretations [11, 12, 13, 14] are in contrast with alternative explications in which the differences between organic and an inorganic semiconductors are kept into account. [15, 6] Sometimes the former approach has been consider as not suitable for the organic case by the authors themselves. [16]

These common examples strongly highlight the lack of clearness in the description of the working principles of thin film devices. However, it has already been recognized that crystalline samples can give an important contribution in this field. [17] Single crystals are often used, for example, to explore the upper limit of carrier mobility in an organic semiconductor and to better understand the charge transport mechanisms in a field effect device. The low density of defects in the active layer and the limited influence of the insulator and the metal electrodes on its structural properties allow fundamental investigations about the intrinsic characteristics of the devices. For FET analysis, rubrene single crystals are recognized as a benchmark among the most characterized semiconductors. [18, 19] The low density of defects [20] and the high charge carrier mobility related to a high cofacial π-stacking interaction in the b-direction [21] enable to investigate the device performance limit and to identify its intrinsic characteristics. These important pieces of information are then used as a term of comparison during the analysis of more complex structures (e.g. thin film transistors) [22]. Several characteristics of an "ideal" device have already been clarified using this tool: the anisotropy of the mobility [23] and its independence on the gate voltage [24], the influence of the insulator dielectric constant [25] and the delocalized

nature of the charge carriers at the semiconductor surface. [26] However, also the picture about the working principle of an ideal organic FET is not complete and a number of different problems are still to be elucidated.

1.1.2 Aim of the Thesis

It is nowadays clear that a further development in the field of organic electronics can be achieved only by considering organic semiconductors as an innovative class of materials with its own peculiarities and different from the inorganic one. New interpretations of experimental results, most of the time closely resembling the conventional case (inorganic case), have therefore to be provided.
The aim of this thesis is to go deeper into the knowledge about the fundamentals of organic devices, in particular of field effect transistors. For this reason, in spite of their poor mechanical properties and their difficult integration in large scale commercial applications, high quality rubrene single crystals are used. In this way it is possible to work with "ideal" systems, suitable to elucidate the intrinsic properties of the considered devices. This route was in the past successful in exploring the characteristics of conventional inorganic devices. The same approach should help to define a clear demarcation between the inorganic and organic cases, and go beyond the "easy" interpretation of the device working principles within the inorganic theory. In addition, since the models developed for the inorganic case have been developed considering the properties of high quality single crystals, a direct comparison between the two cases is however more appropriate.
The analysis we have carried out on each device represents a part of the same electrical characterization, in which focus is given to the properties of the active layer and to their influence on the devices operation mechanisms. The degree of complexity of the considered structures increases at each step, reaching the upmost level with the metal-insulator-field effect transistor (MISFET). Before its analysis, the bulk electrical properties of the active layer and the characteristics of more simple structures are determined. The reliability of these results is assured by the reproducibility of the experimental data and by the high quality of the used active layers.

1.2 Synthetic Work Description

By considering the organic single crystal as an ideal material with different properties with respect to the inorganic case, several attempts to describe the operation of organic electronic devices have been made during the scientific work for this thesis. On the basis of fundamental information about the single crystal bulk electrical properties, significant results have been obtained in the characterization of field effect transistors with different configurations and operation principles.
By analyzing the current-voltage ($I-V$) characteristics of two terminal symmetrical devices with the Space Charge Limited Current (SCLC) theory, we have firstly determined the bulk properties of a rubrene single crystal. This technique has given full evidence of the presence of a discrete charge trap level in the active layer and, through the achievement of the trap-free regime, it has provided the "effective" charge carrier mobility in the semicon-

ductor. Also, the density of intrinsic free charges in the bulk of a rubrene single crystal has been obtained. Then, the latter information has been used to read the characteristics of asymmetric contact diodes. These devices have been fabricated by placing a single crystal on the surface of a metal substrate and evaporating a non-injecting metal contact on the opposite crystalline surface. By analyzing their responses to an applied static or alternating electric field, we did not find any evidence of a depletion layer in the rubrene single crystal close to the non-ohmic contact. This behavior can be understood by considering the low density of free charges in the rubrene single crystal, as extracted from the SCLC analysis. The inaccuracy of the model developed for the inorganic metal/semiconductor interface is therefore evident, as it is evident from the first characterizations the different nature of an organic semiconductor with respect to an inorganic one. On this basis and using the same non-injecting metal/semiconductor couple, metal-semiconductor field effect transistors (MESFETs) have been fabricated and characterized. This is a non conventional FET structure in which the current is modulated by the voltage applied to a non-injecting gate electrode. In spite of the simple operation principle of the inorganic MESFET, which works through the depletion layer formed at the rectifying metal/semiconductor interface, no similar explanations can be given for the corresponding organic device. Indeed, the analysis of the diode characteristics excludes the presence of a depletion layer at the rectifying metal/semiconductor contact. An organic MESFET is therefore proposed to be an interface controlled device, in which the carriers injection from the ohmic source contact is modulated by the applied gate voltage. No depleted region close to the Schottky contact is considered in this case.
Finally, introducing a polymeric insulator between the active layer and the gate electrode, single crystal metal-insulator-semiconductor field effect transistors (MISFETs) have been fabricated. Their characteristics have been analyzed by changing the device configuration and using different polymeric insulators. On the basis of the previous results, whereby a solid picture about the properties of the active layer has been outlined, the non-exponential current-voltage behavior between the transistor ON and OFF states ("sub-threshold regime") has been understood. Once again, the observed trend can not be explained with the theory developed for the inorganic case. Therefore, an alternative semi-analytical description based on the multiple trapping and thermal release (MTR) concept [27] has been provided. The latter takes into account the effect of localized trap levels on the distribution of free charges in the channel. This approach is validated in our case by the results obtained with the SCLC analysis, where the presence of a discrete level in the gap between the semiconductor HOMO and LUMO levels has been pointed out.

1.3 Thesis Structure

In order to provide a useful introduction to the experimental results obtained and to their interpretation, we start this thesis describing the properties of the materials in Chap. (2. We consider here both classes of semiconductors, since the knowledge about the characteristics of inorganic materials is essential for the comparison developed during the whole thesis; in this Chapter a short description of the building blocks of inorganic

devices is also provided. Techniques and theories used to analyze and to describe the working principles of our devices are presented in Chapter (3). These two chapters represent together the first part of the manuscript, the one dedicated to the physics of the devices and of the materials used as their active layer. We illustrate how it is possible to pass from a rubrene single crystal to an electronic device in the second part of the thesis (Chaps. (4) and (5)). In Chap. (4) a detailed description of the rubrene single crystal properties is provided, whereas in Chap. (5) we discuss about the device preparation processes and about all non-electrical characterizations performed on materials and devices. The first two parts of the thesis provide all the elements needed for the description of our experimental results and for their analysis. Chapters (6), (7) and (8) represent the innovative part of the thesis. Here the results obtained for the different devices are presented, starting from the most simple structure: the two terminal symmetric device (Chapter (6)). The analysis of diodes and MESFETs is reported in Chapter (7), whereas Chapter (8) is devoted to the analysis of MISFETs. At the end, a short summary is given, together with some ideas for possible further work.

Part I

Physics of Materials and Devices

Chapter 2

Material Properties and Device Building Blocks

We describe here organic molecular semiconductors, without considering polymeric materials except for some details used for the sake of comparison. The attention is given to the electrical properties of small molecular weight semiconductors, and to the differences existing between this class of materials and the inorganic semiconductors. In the first part of the chapter inorganic semiconductors are widely presented, along with the necesary description of inorganic metal/semiconductor interface and metal-insulator-semiconductor capacitor. This section is not supposed to be an exhaustive picture on the physics of the inorganic building blocks, but a general overview useful to underline the differences between the organic and inorganic cases.

2.1 Inorganic Semiconductors

2.1.1 Material Properties

Exhaustive descriptions about the structural and electronic properties of inorganic semiconductors are available in several textbooks [28, 29, 30, 31]. Accordingly, they are not reported here except for some peculiarity, useful for understanding of the physics of organic molecular semiconductors.
Semiconductors are a group of materials that have electrical conductivity intermediate between insulators and metals. Inorganic semiconductors for advanced electronic applications are, in general, high quality single crystals, with which high speed and low operation voltage, nanoscale devices can be fabricated. Several growth techniques are available for these materials [32] and several grades of purity, for different applications, can be reached. Amorphous or polycrystalline systems can also be produced and different low cost devices, distributed over large areas and operating on plastic substrates, can be obtained. [33] In an inorganic single crystal, charge carriers, under an electric field or because of carrier concentration gradients, move in a partially filled energy band, as "free charges", giving a net drift or a diffusion current, respectively. The ballistic motion of the carriers suffers from a number of scattering processes, due to lattice vibrations (because of the crystal thermal

energy) and structural or chemical defects, that may alter the periodicity of the carrier Bloch function. In this case, the mobility is ultimately determined by the carrier effective mass and by the average time between collisions. Defects have also a direct influence on the mean density of free carriers in the band, and therefore the current, because they can act as trap states for the carriers. Indeed, at each defect is associated a localized state in the semiconductor energy gap, in which charges can be trapped and released, so that the mean carrier velocity depends on the density of free and immobilized charges.
However, a localized energy level in the gap is, in any case, not only a trapping center; its nature depends on the distance from the band edge. If the energy required to promote a free charge in the conduction or valence band is substantially low (comparable with that of thermal energy), a localized level can also act as charge "donor" or "acceptor" state. The density of these shallow levels is generally strictly controlled and depends on the amount of doping elements intentionally introduced into the semiconductor. An inorganic material, suitable for optoelectronic applications is not an intrinsic semiconductor, in which the majority of free carriers come from the outermost electron shell of the atoms. In this case, the semiconductor would be a high resistivity material, with an equal amount of negative (electron) and positive (holes) charges and in which the electrical properties strongly depend on the temperature. Different types and concentrations of impurities are generally introduced into the host crystal to donate or to accept electrons to or from its conduction/valence band. In this way, materials in which electrons (n-type semiconductor) or holes (p-type semiconductor) are the majority carriers can be obtained and a higher stability with respect to the temperature can be achieved. A small amount of dopants in the pure semiconductor drastically change its properties, making it suitable (or better tunable) for different electronic applications.
The development of inorganic electronics has been closely related to the ability of controlling the inclusion of dopants into the pure material. [34] However, not only the properties of the semiconductor determine the operation of the devices, since most of the processes do not occur in the semiconductor bulk, but at the interfaces between the active layer and the other device components. Besides the semiconductor itself, the metal/semiconductor and the insulator/semiconductor interfaces represent therefore highly characterized building blocks, peculiar to a given electronic device.

2.1.2 Metal-Semiconductor Interface

Ohmic Contact

When a semiconductor and a metal are brought into contact, diffusion of carriers always takes place, until achievement of thermal equilibrium, in which the Fermi levels of the two materials are aligned. Depending on the position of these levels with respect to the vacuum, an ohmic or a blocking contact can be formed. An ohmic contact is, by definition, a metal-semiconductor junction that has a linear (non-rectifying) $I - V$ characteristic. This is an essential element for the connection of the single device with the other components of the electronic circuit, in which the metal acts like a infinite reservoir of charges; the current is, in this case, not determined by the volume of the injecting material. This statement is usually formulated by setting the boundary conditions $E_0 = 0$ and $n_0 = \infty$, where E_0 and

n_0 are respectively the electric field and the charge density at the contact. The resistance of the contact R over a certain area A defines the quality of an ohmic interface. The normalized resistance is called the specific contact resistance R_c and is given by $R_c = RA$. The latter has to be negligible with respect to the resistance of the semiconductor itself, with no significant voltage drop across the interface. The semiconductor is, in this case, the element in which processes limiting the current flow occur.

Injection Limiting Barrier

Aside from the described ohmic behavior, the metal-semiconductor junction can also be a rectifying element with a non linear current-voltage ($I-V$) characteristic. In the case of a p-type semiconductor, a non-ohmic interface is formed if, in the vacuum, the Fermi level of the metal ϕ_m is at lower energy with respect to that of the semiconductor ϕ_s, that is when the condition $\phi_m < \phi_s$ is fulfilled. This is shown in Fig. 2.1(a), where E_{Fm} and E_{Fs} are respectively the metal and semiconductor Fermi levels, whereas E_V and E_C are the semiconductor valence and conduction bands. After the contact has been made and at thermodynamic equilibrium, where the Fermi levels are aligned through transfer of holes from the semiconductor to the metal, the semiconductor bands are bent downward and a charge depleted zone W forms close to the interface (Fig. 2.1(b)). When equilibrium is reached, a further migration of holes from the semiconductor to the metal is prevented by the built-in potential V_{bi}, whereas injection of holes from the metal to the semiconductor (under the influence of a suitable applied voltage) is limited by a "Schottky" barrier ϕ_b at the interface.

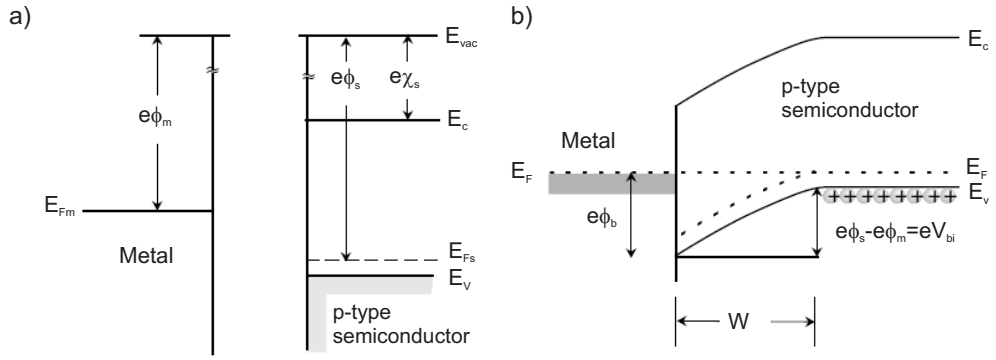

Figure 2.1: A draft showing the formation of the ideal p-type Schottky barrier (a) before the contact, underlining the positions of the energy levels in the metal and the semiconductor compared to vacuum, and (b) after the contact, showing the formation of a depletion region of width W at the interface and the presence of a junction potential ϕ_b.

We point out that this is, in any case, a simplified picture, in which no trap states are included in the semiconductor band-gap. These states would cause the barrier height to be nearly independent on the metal work function but to depend, above all, on the distribution of localized states in the semiconductor. [28]
Our focus of interest in the picture above is the non-equipotential region close to the interface, in which an uniformly distributed and fixed space charge is present; its formation

in the organic case is still a debated question. [6] We consider the width W of the depleted zone:

$$W = \sqrt{\frac{2\varepsilon(V_{bi} - V)}{qN_A}} \tag{2.1}$$

in which ε is the permittivity of the semiconductor, N_A the volume density of dopant, q the elementary charge, V_{bi} the built-in potential, and V the applied voltage. Note its dependence on the applied potential and, above all, on the concentration of semiconductor dopant, which, at room temperature, corresponds to the density of free charges in the semiconductor (in this case, all the impurities are ionized). The presence of a depleted zone at the interface can be easily determined experimentally. As we can see from Eq. (2.1), the width of the depletion region W falls to zero after the condition $V \simeq V_{bi}$ is reached. This threshold voltage corresponds therefore to the voltage point in which the capacitance associated with the depleted zone C reaches infinity and can be easily found by plotting $1/C^2$ vs. V. Rewriting the equation for W as a function of the depletion capacitance, the simple relation of Mott-Schottky can be obtained:

$$C^{-2} = \frac{2(V_{bi} - V)}{q\varepsilon N_A} \tag{2.2}$$

in which C is the depletion layer capacitance per unit area. The simple condition for the existence of an ideal Schottky barrier is therefore that the reciprocal of the depletion region capacitance $1/C^2$ vs. V should be a straight line. The density of ionized dopant atoms and the built-in potential at the interface can be extracted, in this case, from a simple measure of the capacitance associated with the depletion region.

An important consideration can be made on the width of the depletion region and its influence on the operation of a rectifying diode. In a silicon Schottky diode, in which $\varepsilon = 11.2$ and the density of impurities is typically $N_A = 1 \times 10^{16}$ cm^{-3}, the depletion width is W= 350 nm, that is a reasonable dimension with respect to the thickness of the semiconductor. However, the density of free charges in an organic semiconductor is at least four orders of magnitude lower than that value. [35] Is therefore the depletion region a useful parameter in the characterization of an organic diode? We will return back to this question in Chap. (7), where the characteristics of our rubrene single cystal diodes will be presented.

A point to note is also that the characteristics of an inorganic rectifying diode only depend on the properties of the Schottky junction. In this case, the high mobility of the bulk does not affect strongly the device performances, except at high forward biases where the contribution of the bulk resistance R_c needs to be considered. Accordingly, the current-voltage characteristic of the device can be understood, by considering only charge injection processes at the rectifying interface. In the organic case, since the strong influence of the semi-insulating bulk cannot be neglected, rectifying diodes are not single interface devices, but complex systems in which several contributions related to bulk and contact effects have to be kept into account. For this reason, we will describe the $I - V$ characteristics of the diodes only in Chapter (3), where the physics of the real devices is considered. Several effects will cause us to redraw the simple picture given in this paragraph.

2.1.3 Metal-Insulator-Semiconductor Capacitor

The metal-insulator-semiconductor (MIS) structure represents an important tool for the study of the semiconductor surface properties. [36] Moreover, it is the basic element in a field effect transistor, through which current flow between the source and drain contacts is modulated. In Fig. 2.2 a draft of the alignment of the energy levels at the insulator/semiconductor interface is reported for a p-type semiconductor. Each case displays different conditions of applied bias. Even if the the equilibrium condition $V_{appl} = 0$ has been omitted an important consideration about the properties of the MIS at equilibrium must be done: at zero voltage, the metal and semiconductor Fermi levels are supposed to be at the same energy. This condition assures no band bending nor charge accumulation at the interface when no potential is applied to the structure.

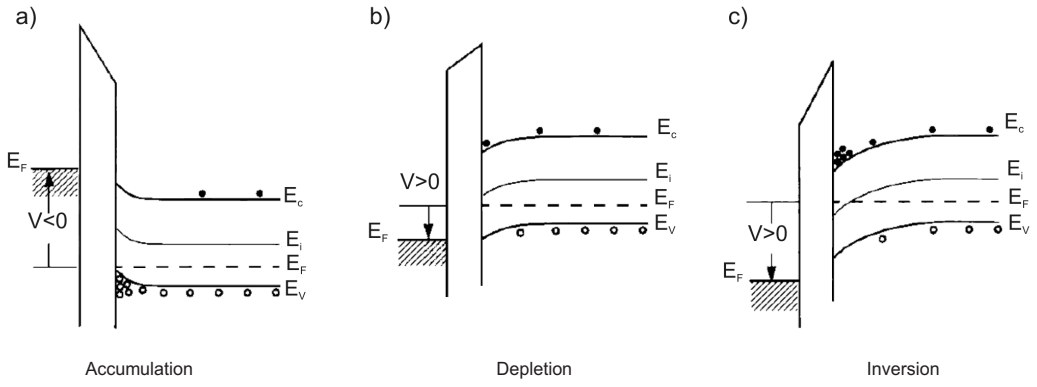

Figure 2.2: Energy band diagram for an ideal MIS structure in the case of a p-type semiconductor. When the system is biased with positive o negative voltage the carriers charge density at the interface changes from a) accumulation to b) depletion and c) inversion. Due to the low density of thermal free charge, only the charge accumulation process is feasible in the organic case.

When a negative voltage is applied to the metal (Fig. 2.2.(a)), accumulation of holes (majority carriers) occurs in the semiconductor close to the insulator surface. On the contrary, holes are pushed away from the insulator/semiconductor interface at applied positive bias. In this case, a zone depleted of holes (Fig. 2.2.(b)) and an inversion region (Fig. 2.2.(c)) are created near the boundary, following the increasing voltage. The inversion region is a thin slab close to the interface, in which the concentration of minority carriers is higher than the density of dopants in the semiconductor bulk and that, in strong inversion, is isolated from the bulk by a depletion region formed behind it. Roughly speaking, strong inversion occurs at a "threshold voltage", the bias at which the Fermi level at the interface crosses the middle of the semiconductor gap (Fig. 2.2). However, in the operational voltage range of a real device, strong inversion can be reached only when the structure is not far from steady-state conditions, and only if the MIS is fabricated with a high intrinsic charge density semiconductors (e.g. silicon). This is because V_T depends both on the density of dopants N_A, and on the density of intrinsic charge n_i, according to the relation $V_T \propto (2kT/q)\ln(N_A/n_i)$. Moreover, since the applied voltage partly appears across the insulator and partly across the semiconductor, also the capacitance of the insulating layer

C_i and the permittivity of the semiconductor ε_s determine the value of the threshold. Only when strong inversion has been achieved, the capacitance of the MIS structure is equal to C_i, the maximum capacitance of the system, that is also equal to the capacitance achieved in accumulation mode.

2.2 Organic Molecular Solids

2.2.1 Material Properties

A solid condensate of organic molecules is typically an amorphous or crystalline material with insulating behavior. However, if the constituent molecules contain π-conjugated groups, a number of electrons are only weakly bonded to the molecule and can drift under an external applied field. These molecular solids can be considered therefore as semiconducting materials, with a low mobility and low intrinsic free-charge density, but suitable for many optoelectronic applications. Their properties can be also easily tuned by exploiting the versatile organic chemistry.
Organic molecular semiconductors can be broadly classified into two groups on the basis of their molecular weight: oligomers (low molecular weight compounds) and polymers. [37] In spite of their high molecular weight, conjugated polymers useful for optoelectronic applications are soluble semiconducting materials, with which large area electro-optical devices can be prepared using low-cost processes. Polymeric condensed phases can be prepared, for example, by spinning the solution onto a substrate and then making the solvent evaporate. However, only amorphous or polycrystalline films with variable degree of disorder can be obtained in this way. The lack of long range order and the high density of defects of the active layer have therefore to be considered in the (not simple) analysis of a polymeric device.
On the other hand, oligomers are quite often insoluble molecules, typically deposited via vacuum sublimation. Also in this case, the molecular condensation results in amorphous or polycristalline film formation, but an easier control of the molecular characteristics and of the film growth parameters have provided an easier determination of the charge transport mechanisms, together with the improvement of the device performances. Moreover, single crystals with low density of defects and high structural quality can be easily prepared with these materials. These single crystals are small brittle materials, not suitable for commercial applications, but they represent, in any case, ideal active layers useful to underline the intrinsic properties of organic materials. The characteristics of polycrystalline films devices tend, indeed, toward those of single crystals when active layers with high degree of order are used. [38] However, in spite of the same molecular composition, the polycrystalline or amorphous nature of the thin film generally induces a completely different electrical behavior with respect to the single crystal case. Indeed, the charge transport in an organic solid is strongly determined by the complex interaction between the charge carriers and the molecular surrounding. [17] We will, therefore, consider separately the charge transport problem in single crystals and thin films, continuing to describe here only the features common to both systems.
Because of its large band-gap E_g, an organic semiconductor essentially behaves like an

insulator, i.e. its density of thermally induced charge carriers is very low, orders of magnitude lower than what is found in conventional inorganic semiconductors. For this reason, one of the most important processes in an organic device is the injection of charges via a suitable metal contact. Charge flow is also influenced by the the low density of intrinsic free charges and the low mobility: accumulation of injected charges always occurs in the material. The voltage dependence of the current is therefore not linear, as in the inorganic case, but depends on the complex distribution of the electric field. The latter is determined by the space charge distribution and it is also strongly influenced by the presence of defects.

Some definitions regarding the semiconductor characteristics, even if similar to the inorganic case, have to be reconsidered on the basis of these peculiarities. It is important to remark, for example, that even if organic semiconductors are classified as either p-type or n-type, this definition is strictly not correct if we only consider the intrinsic properties of the organic material. A correct classification is not possible without keeping into account especially the metal/semiconductor couple, instead of the organic layer itself. The latter statement should be clear if we consider the result obtained, with the time-of-flight (TOF) technique, on ultrapure single crystals of naphthalene: both charge carriers (holes and electrons) have nearly the same mobility, when they are generated by a suitable electromagnetic stimulus. [39] This points out the inadequacy of the conventional explanation for the generally observed low electron mobility of an organic system. The latter is not an intrinsic of the material but it is due to the more difficult charge injection with respect to the p-type case, and to a stronger influence of charge traps on the electron motion. [40] The latter it is a common process, for example, close to the FET insulator interface, where water, oxygen, or terminal hydroxyl groups are present. [41, 42] In this respect, an alternative definition must be provided. An organic p-type semiconductor is a material in which, because of its low ionization potential, holes are better injected from a high work function metal electrode. On the contrary an n-type semiconductor is an active layer in which, because of its high electron affinity, electrons are better injected from a low work function metal. On the basis of this definition, it is easy to imagine that an organic molecular semiconductor can be both n and p-type depending on the properties of the contact and of the insulator/semiconductor interface (in the case of a FET). This peculiarity allows, for example, preparation of interesting ambipolar field effect devices on the same active layer, as the ones reported by using rubrene [43] and pentacene. [44]

It is important to reconsider, also, the formation of the metal/semiconductor contact. In the inorganic case, thanks to the high quality of the used semiconductor, heavy dopant implantations are used to fabricate ohmic junctions. On the contrary, an organic semiconductor is generally not a pure material, in which the control of the doping level is extremely difficult; even if doping at the surface of organic semiconductors has demonstrated to be useful in the reduction of the contact resistance, [45, 46, 47] this procedure is generally not used. Generally, ohmic contacts are fabricated by using high work function metal, with which a good matching between the metal Fermi level and the conduction level of the semiconductor can be obtained. [48] The latter is a necessary condition in order to obtain efficient charge injection. Indeed, the picture we have previously reported to show the formation of the inorganic/metal interface is not wholly correct; there is no band bend-

ing at the interface between an organic semiconductor and a metal, because insufficient carrier diffusion takes place during the contact between these materials. Accordingly, in the absence of an applied voltage, the contact should be considered as a "blocking" one. [49] However, application of an external field causes incline of the energetic levels in the semiconductor, so that injection of charges from the metallic electrode occurs (by tunneling or by thermoelectronic emission). With a suitable matching between the metal Fermi level and the semiconductor transport level, these mechanisms are able to provide the amount of charge necessary to satisfy the condition for ohmic injection $n_{inj} >> n_0$. In the latter, n_{inj} and n_0 are respectively the charge density injected from the electrode and the semiconductor intrinsic charge density (order of magnitude lower than in the inorganic case). A point to note is that, even if several metals can be used to provide ohmic injection with high ionization potential materials (p-type semiconductors), the case for n-type conduction is different: there, a more difficult matching between the semiconductor LUMO level and the Fermi level of the available low work-function metals can be obtained. [50]

2.2.2 Single Crystals

The main motivation for fabricating single crystal devices is surely to determine the intrinsic limitations of an organic electronic system, in the hope that the ultimate properties of the material can be achieved. Even if the first experimental attempts reported a mobility of the charge carriers not higher than that in thin film devices, [51] the importance of single crystals in fundamental research is nowadays established. High efficiency single crystal devices can be fabricated without damaging the fragile active layer, [52] so that, consistent experimental results are available to confirm/invalidate the theoretical predictions. Moreover, the latter procedure is made particularly meaningful by the high structural order and low density of defects of the semiconductor.
The crystal structure of a molecular organic material is controlled by the interplay between intramolecular forces and weak interactions, i.e. dipolar, hydrogen bonds, or π-π interactions, between different molecular units. The latter are hard to control and it is almost impossible to exactly forecast the crystal structure adopted by a compound. Several polymorphs of comparable cohesion energy are also generally obtained by starting from the same material and by working at slightly different growth conditions (the growth temperature is a fundamental parameter, determining the molecular packing and the shape of the crystal). In order to obtain the desired structure the most common approach is therefore to select a promising system, then tailoring its structure and properties through molecular modifications. [53]
In spite of low intermolecular interactions, some peculiarities can be found in the molecular structure of the commonly used oligomeric crystalline condensates. Single crystals of non polar aromatic compounds are generally quite densely packed, with a 2D layered structure in which the molecular long axis is perpendicular (or slightly tilted) with respect to the molecular layer. For this reason, the highest intermolecular overlap, and therefore the highest charge carrier mobility, is found along the in-plane crystallographic directions [54, 55] However, depending on the molecular size and on the overall effect of the intermolecular forces (attraction and repulsion), some different molecular arrangements are possible in a

single crystal (Fig. 2.3).

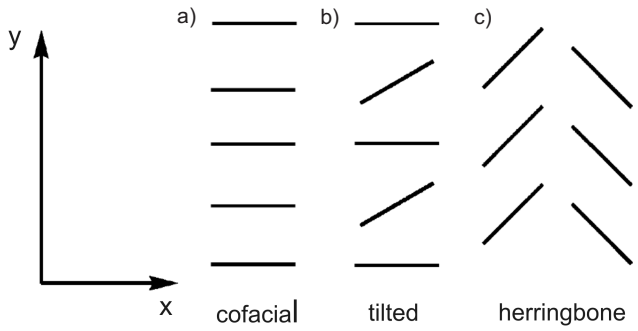

Figure 2.3: Among different in-plane π-stacking motifs, the herringbone one is the most common in organic single crystals. The latter assures a lower repulsion with respect to the cofacial disposition, but it suffers for a poor orbitals overlap.

The face to face configuration (Fig. 2.3(a)) is the most desirable π-staking for high performance organic devices; a high intermolecular π overlap provides a large bandwidth and therefore a high mobility. On the other hand, in the tilted (Fig. 2.3(b)) and herringbone motifs (Fig. 2.3(c)), the π-π overlap between adjacent molecules is clearly reduced, with a significant decrease of the charge carrier transfer probability. However, in this cases, the lattice energy is minimized thanks to a higher packing density, combined with favorable short-range interactions and lower repulsive interactions between the inner electrons. Considerable stabilization exists therefore in an herringbone and tilted motif with respect to the cofacial arrangement. Indeed, as we can see from Fig. 2.3(a), repulsive interactions are important in the cofacial motif that, for this reason, is a rarely encountered geometry in real systems. Real molecular structures generally exhibit a herringbone-like arrangement, in which the molecular units are in an edge-to-face disposition.
Different oligomers have been used as active layer in organic devices and several important characteristics have already been elucidated. [56] In single crystals of oligothiophenes and oligoacenes, two important families of organic semiconductors, the bandwidth and the carrier mobility have been found to increase with the molecular size. [57, 58] However, a unique correlation between this parameter and the charge mobility is not possible either, because of the significant dependence of the mobility on the molecular packing. Mobility has been also demonstrated to be an inverse function of temperature (it considerably increases with the decrease of the temperature), by fundamental TOF studies made on ultrapure single crystals [39, 59], and by the analysis of several single crystal FETs and diodes. [60, 61, 62] Similarly to the inorganic case, these results point to a band-like charge transport mechanism, even if several important differences exist between the two cases. While inorganic semiconductors can be well described via the one-electron approximation, organic semiconductors require both electron-electron and electron-phonon coupling to be taken into account. Indeed, in an organic solid, molecules are held together by weak intermolecular forces that only slightly influence the single unit properties; accordingly, the molecule retains its individuality. The band-width in an organic molecular

crystal is, therefore, extremely narrow, two orders of magnitude less than that of silicon, as found for rubrene single crystals, where it ranges between 0.1 and 0.5 eV. [63] For this reason, the excess charge carrier suffers from a strong localization; it is a "polaron", a quasiparticle composed of a charge and a lattice polarization cloud, which is bound to the charge itself. [64, 65] The grade of delocalization of the polaron depends on the interplay between the electron-electron and electron-phonon coupling; only highly localized "small polaron" are observed in an organic material (with the exception of ultrapure single crystals at low temperature), because of the importance of the electron-phonon term with respect to the electronic coupling.
Using the polaron concept, interpretations of the mobility dependence on the temperature in organic single crystal have been provided. [65] Roughly speaking, it is easy to imagine that, due to the strong interaction with the lattice, the properties of a polaron strongly depend on the temperature. At low temperature polarons move in a conduction band that, even if extremely narrow, is significant with respect to the lattice thermal energy. In this case, the mobility temperature dependence is the same as the one observed in the inorganic case. However, in contrast to the bare bandwidth of a conventional semiconductor, the bandwidth in a organic single crystal decreases with increasing temperature. At high temperatures, where higher is the interaction between the charge and the lattice, the polaron becomes localized and transport starts to be dominated by "hopping" processes. The charge drift is no more a band-like process, but it occurs through thermally activated hops between localized states, adjacent in position and not far in energy.
Several experimental results, obtained with single crystal FETs and diodes, have been interpreted, by considering the polaronic nature of charge carriers. In rubrene single crystals transistors, the properties of the polaron have been found to be strongly dependent on the polarizability of the gate dielectric [66], and on the density of charge carriers in the conducting channel. [67] However, in spite of much evidence reported in the literature, a point to note is that the description of the charge motion using polarons is not unique and it is not always accepted. [68, 69] In fact, up till now there is no ultimate theory to define which is the real charge transport mechanism in an organic semiconductor.

2.2.3 Thin Films

In a single crystal device, the structural quality of the active layer is not influenced by the surrounding elements. As previously seen, this peculiarity enables the comparison between experimental results and theoretical predictions. On the contrary, the properties of a thin film device are strongly determined by the substrate. The molecular packing of the first monolayers in the film can be, for example, different from the one found in the bulk, [70] baffling any theoretical efforts, in which this effect is not considered. [71, 72] Hence, since the first experimental results, it was clear that thin films could not permit a full determination of the carrier transport mechanisms in organic semiconductors. [73] In spite of this limitation, it is important to remark that only thin film devices can be mass-produced for promising organic optoelectronic applications, so that understanding their characteristics is a necessary step toward the real commercialization of organic devices.
Charge carrier mobility in thin film devices is orders of magnitude lower that in single crys-

tals. Moreover, it depends on the applied electric field and it follows another dependence on the temperature, i.e. it increases with the increasing temperature. These peculiarities are a consequence of the strong influence of disorder on the motion of charge carriers. [74] Depending on the degree of order, several models have been developed to describe charge transport in thin film devices. Differently from the situation in a single crystal, in which the charge drift is limited by phonons scattering (band-like mechanism), charge transport is an established example of hopping at all temperatures. The charge hop process is temperature assisted and occurs along the direction parallel to the applied electric field, between localized energy states. In the most common picture, the latter are seen as distributed in energy according to a Gaussian function (Bässel model for hopping transport). [75] Anyway, this description is not unique, especially in the case of polycrystalline thin films. Alternative models, like the multiple trapping and release (MTR), [27, 76] have been proposed. The MTR model is an alternative description to hopping transport, that also predicts thermally activated mobility and its dependence on the applied gate voltage. It well describes an intermediate situation, in which the band transport coexists with an influent charge trapping/releasing process, to and from localized levels in the band gap. The latter is the mechanism that limits the conduction. Accordingly, the localized trap distribution does not enable hopping motion like in the Bässel description, but it represents, rather, the tail of a delocalized transport band in which charge carriers are immobilize.
We note an important aspect of this model. If traps are uniformly distributed in the organic layer (highly disordered film), a temperature dependent mobility can be predicted similarly to the hopping case. On the contrary, if traps are localized only at the grain boundaries (high quality polycrystalline film), a higher mobility with a less pronounced dependence on temperature is predicted. [77] This result points out the influence of disorder on the characteristic of organic devices and it underlines, once again, the importance of single crystals for fundamental studies on the properties of these systems.

2.3 Difference Between Inorganic and Organic Cases

It is clear from the previous discussion that an organic semiconducting material is closer to an insulator than to an inorganic semiconductor, because of its low free charge density and charge carrier mobility. Other differences can be found in the two cases:

- Organic single crystals are brittle materials not suitable for device mass-production.
- Due to the low charge density, the most important process in an organic device is the charge injection/extraction at the metal/semiconductor contact.
- The bulk transport phenomena are extremely complex in an organic material because of the polaronic nature of the charge carriers.
- Differently from the organic case, no electronic polarization has to be considered in an inorganic semiconductor. Here the localization time of the charge carrier in a site ($\simeq 10^{-16}$ s) is lower than the electronic relaxation time (10^{-15} s). [49]

- The properties of an inorganic material can be tuned by dopant addition. A useful doping requires high purity of the starting material and a fine control of the effects related to structural defects. On the contrary, a significant amount of intercalated molecules used for synthesis and non expected sub-products are generally present in nominally pure organic compounds. The used materials are therefore non intentionally doped semiconductors, that contain approximately equal amounts of donor and acceptor impurities (in this respect organics are compensated semiconductors). The effect of intentional doping in organic semiconductors only appears for large densities of dopants, where the material act as conductor (e.g. PEDOT:PSS) and it is not useful as device active layer.

- The n-type and p-type character of an organic semiconductor is definitively not an intrinsic property of the material, but mostly of the metal/organic couple.

- Ohmic metal/semiconductor interfaces can be obtained in the organic case only by a suitable choice of the metal electrode; there must be a natural matching between the metal Fermi level and the HOMO/LUMO level of the semiconductor.

- The voltage dependence of the current in the organic case is not linear, but it is related to the complex distribution of the space charge electric field.

It is therefore clear that the physics of organic semiconductor devices is a complex interface science, in which several contributions related to the non periodicity and the high density of defects in the active layer have to be considered. Moreover, difficulties in the control of the device fabrication procedures and the consequent spread of the obtained experimental results prevent the correct theoretical analysis of the mechanism occurring in the semiconducting layer. On the contrary, inorganic single crystals of high structural and chemical quality provide the basis for the most important electronic applications. Here, the high control of the semiconductor growth parameters and of the device processing permits a direct comparison between experiments and theoretical predictions.

Table 2.1: Comparison between the electrical properties of two benchmarks among inorganic and organic semiconductors.

	Si	Pentacene
Energy gap (eV)	1.12	1.8÷2.8
Dielectric constant	11.9	3
Molecular density (cm^{-3})	10^{23}	10^{21}
Intrinsic charge density (cm^{-3})	10^{10}	100
Mobility (cm^2/Vs)	100÷1000	1÷10
Doping level (cm^{-3})	10^{-9}	10^{-3}÷10^{-1}

For this reason, several models, describing the electrical properties of inorganic materials and devices, are nowadays fully developed and established. However, only in exceptional cases the same models are also appropriate for the analysis of organic optoelectronic devices. This is a clear statement, if we further underline the difference between the two

classes, by taking as an example the properties of two of the most used organic and inorganic semiconductors, pentacene and silicon (Table 2.1). [74] Note the strong difference (orders of magnitude) between the mobility, the intrinsic charge density, and the doping level in the two cases. These peculiarities will be fundamental in the interpretation of the results we obtained with asymmetric single crystal diodes and field effect transistors.

Chapter 3

Devices and Techniques for their Electrical Characterization

In this chapter we describe the organic devices of our interest and the techniques used for their analysis. Even if the description is divided with respect to the devices typology, it is important to underline that each section represents a part of the same electrical characterization. The latter starts with the analysis of symmetric diodes $I-V$ characteristics, by using the space charge limited current (SCLC) theory. This is how the properties of the material are determined. This information is then used to go deeper into the physics of more complex systems: diodes with asymmetrical contacts and field effect devices. In the latter case, both metal-semiconductor field effect transistors (MESFETs), and metal-insulator-semiconductor field effect transistors (MISFETs) are considered.

3.1 Space Charge Limited Current Theory

3.1.1 Introduction

The Space charge limited current theory describes the steady state response of an organic material (or in general of an insulator), to an applied bias. As pointed out in Chap. (2), charge injection in a conventional semiconductor occurs without accumulation of charge, because of the high mobility of the charge carriers. On the other hand, an organic semiconductor is usually quite an electrically insulating material with a low density of thermally generated free carriers n_0. As soon as the density of the injected charges is higher than n_0, the material becomes charged with a stationary space charge that, depending on the properties of the materials, can be free or trapped in localized states. This space charge has a strong influence on the electric field distribution that, in this case, is in not constant through the bulk of the material.
In the simplest description, an organic semiconductor placed between two metal electrodes can be seen as a plane capacitor with a dielectric layer between the plates. [78] We can therefore describe the space charge limited current in the active layer by starting from the basic equation that describes the current flow $J = \sigma F = en\mu F$, in which F is the electric field, n and μ the charge carrier density and mobility, respectively, and by assuming that

the injected charge is homogeneously distributed in the material and it is equal to the maximum charge presented on the metallic plates of the capacitor $nqAd = CV$. Here, A and d are the area and the distance between the two electrodes, respectively. By simply considering the capacitance of the system as $C = \varepsilon A/d$ and the electric field between the two electrodes as $F = V/d$, a quadratic dependence of the current on the applied voltage $J = \varepsilon\mu(V^2/d^3)$ can be obtained. The latter, in spite of the simplicity of our reasoning, adequately describes the current-voltage characteristics of a trap-free insulating material under charge injection from an ohmic contact, and it is only slightly different from the formal treatment proposed by Mott and Gurney to describe the same system. [79] However, it is generally not an exhaustive description of a real device, in which localized trap states influence the concentration of free charge and the space charge distribution and consequently the dependence of the current on the applied voltage. [78, 80, 81] In this case, analysis of the $I - V$ characteristics, even considering a two terminal devices with ohmic contacts, is not a straightforward process. Furthermore, the high density of defects and the dependence of the mobility on the applied voltage do not permit a unique determination of the basic electrical properties of the material (i.e. mobility, charge density). Nevertheless, as we will see in Chap. (6), only the effect of a discrete trap level needs to be included in the formal treatment of a single crystal device. The latter, thanks to its high structural order, represents a favourable condition in which a complete characterization of the material can be carried out. Accordingly, in the next section, we do not consider the problem of space charge formation in the presence of energetically distributed trap states. We will rather focus on another important aspect: the influence of the system geometry. Two theories, developed to describe ideal systems with different dimensionality, will be presented. The first one applies to the 3D case, in which the material is sandwiched between two electrodes, whereas the second one is valid for the 2D case, in which a system with two coplanar electrodes located on the same side of the semiconducting thin layer is considered.

3.1.2 Mott-Gurney Analysis

The first important description of space charge effects in an insulator was given by Mott and Gurney, [79] that considered a trap-free material sandwiched between two plane and parallel electrodes. Then the system has been extended by the inclusion of several contributions: the influence of distributed trap states, [82, 78, 83] the effects of the electric field on the trap depth, [84] and the effect of non-ohmic metal/insulator interfaces. [85, 86] Generally, these models are complex mathematical formulations that do not provide a unique description of the material under analysis. However, when only discrete trap levels influence the space charge current, simple analytical equations are available and several parameters, regarding the charge carrier mobility, the density of thermal free carriers and the density/depth of charge traps, can be obtained by the analysis of a single $I - V$ characteristic. Even if, the first detailed description of charge trap effects in an insulating material has been formulated by Rose, [82, 87] all the theories developed for the 3D case are collected here under the term Mott-Gurney analysis. This is, in fact, the first important demonstration that a current can flow even in the insulator sandwiched between two metal electrodes if substantial charge carrier injection occurs.

The SCLC theory developed for the ideal 3D case is based on the following important assumptions:

- Only single carrier injection occurs from the ohmic metallic contact. The contact has no effect on the current.
- The material is assumed to be an insulator with a low density of free charge.
- Localized states, acting as traps of charge carriers are assumed to be uniformly distributed along the insulator.
- The electric field is assumed to be high enough to neglect current due to diffusion. Only drift of the charge carriers is considered.
- The mobility is assumed to be constant on the applied voltage.

These conditions turn the description of the space charge into an easy to resolve analytical problem.
Fig. 3.1(a) shows the ideal SCL behavior of an insulating material, in which a single discrete trap level is present. This is reported along with a draft showing the position in energy of the trap (that it is spread because of the naturally statistical distribution of an energetic level) (Fig. 3.1(b)).

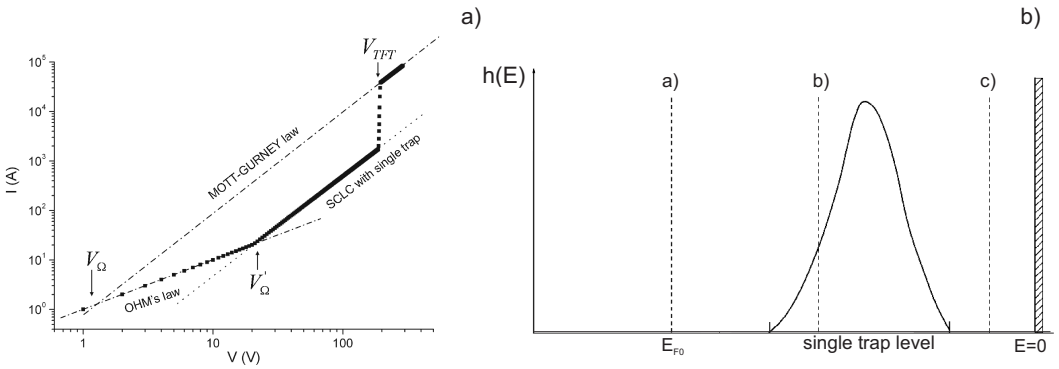

Figure 3.1: a) Ideal $I-V$ characteristic for an insulating material with a discrete trap level and b) energy position of the thermodynamic quasi-Fermi level E_{F0} with respect to the conduction band. At low electric field, the behavior is ohmic, whereas at higher fields, the injected charge concentration exceeds the equilibrium (before injection) charge concentration, leading to a space-charge-limited current (SCLC). With the increasing bias the quasi-Fermi level moves toward the edge of the conduction band. The trap in the conduction pathway is filled when E_F passes the trap level, leading to a dramatic increase in current (the trap filling regime). With a further slight increase in potential, the trap-free SCLC region is attained.

The $I-V$ characteristics presents four regions with different slope, that are related to different conduction processes. At low electric field, the current increases linearly with the applied voltage. The density of injected charges does not exceed the density of intrinsic thermal charges; an ohmic contribution is observed, because the drift of the thermal free carriers is not influenced by space charge effects. In this case, the quasi-Fermi level in

the semiconductor is at its thermodynamic equilibrium value E_{F0} (Fig. 3.1(b).a)). The second region begins at the voltage $V_{\Omega'}$, when the density of injected free-charge n_{inj} is comparable to the density of thermal charges n_0. The conduction is here limited by the presence of the trap level. With the increasing applied voltage, the quasi-Fermi level has, in fact, moved toward the edge of the conduction band and has crossed the discrete trap level (Fig. 3.1(b).b)) A first general consideration on the trap effects is that a marked reduction of the current compared with the trap-free case occurs. Most of the injected carriers are, in fact, immobilized by the trap, whereas the amount of excess charge injected from the electrodes is the same, since it is the maximum that can be stored in a parallel-plate capacitor. The observed current-voltage trend can be described by the equation:

$$J = \frac{9}{8}\theta\varepsilon\mu\frac{V^2}{L^3} \tag{3.1}$$

where the trap parameter $\theta = n/(n + n_t)$ is, in a first approximation, the constant ratio between the density of free carriers achieved under injection n, and the total density of injected carriers (trapped n_t, and free). Note that when the trap substantially affects the monopolar injection current, the density of trapped charges is higher than the free one $n_t >> n$, and the trap parameter reduces to $\theta \approx n/n_t << 1$. This condition is fulfilled until the trap remains shallow, e.g. until the quasi-Fermi level lies below the trap energy E_t. When at the applied voltage V_{TFL} the trap is filled and E_F has passed the trap level, we can observe a dramatic current increase. This transition-voltage depends on the density of traps N_t, according to the relation $V_{TFL} = eN_tL^2/\varepsilon$, where e is the elementary charge and L is the distance between the metal electrodes. With a further increase of the applied voltage, the trap-free SCLC region described by the Mott-Gurney equation is finally attained. The sample behaves, in this case, as a trap-free insulating material. At V_{TFL} the amount of charge injected by the contact is, in fact, sufficient to fill all the traps, so that the quasi-Fermi level establishes at a level above the trap distribution within the energy gap. (Fig. 3.1(b).c)) Reaching the trap-free regime allows to estimate the free-electron mobility μ from Eq. (3.1), by simply fixing $\theta = 1$.

We note that, when only a discrete trap level is present, no significant differences compared with the trap-free case are found in the current-voltage tendency. A direct comparison between the two cases is easily obtained by introducing an effective charge carrier mobility $\mu_{eff} = \theta\mu$, that represents the mobility of the entire body of injected charges, trapped and free. However, this is not common in real systems. Generally, the $I - V$ characteristics in the trap limited region present a superlinear trend $J \backsim V^m$ with $m > 2$, that depends on the energetic profile of the trap distribution. [78]

In the simple case we have described, several electrical bulk parameters can be extracted from the analysis of the experimental $I - V$ curves. From Fig. 3.1(a) we see that the presence of shallow trapping centers delays the finish of the ohmic regime from the critical voltage V_Ω to $V_{\Omega'}$. The latter clearly depends on the trapped charge density and is $1/\theta$ times the crossover voltage of the trap-free case V_Ω. Through the simple ratio between these two experimentally accessible quantities, the fundamental trap parameter θ (so that information about the density of free and trap charge) can be therefore obtained. Given the voltage $V_{\Omega'}$, the thermally generated electron density n_0 can be also estimated, by

using the equation:

$$n_0 = \frac{V_{\Omega'}\theta\varepsilon}{eL^2} \tag{3.2}$$

Finally we note also that the knowledge of V_{TFL} makes it possible to determine the density of traps N_t.
It is important to remark that the characteristics of a real high quality single crystal device, although similar to the ideal case (Fig. 3.1(a)), present some important differences. The current-voltage trends are not strictly proportional to the described shallow trap square law but present, up to the trap-free limit voltage, a slightly voltage dependent slope. θ is, in fact, a voltage dependent parameter, that can be assumed as constant only when all the injected carriers are trapped charges (at low applied voltage). Moreover, a trap level is always distributed in energy and the concept of a discrete mono-energetic level is only an oversimplification of the real case. In addition, even if the simple SCLC theory predicts a perfectly vertical "jump" at V_{TFL}, smoother transitions are generally observed in the real case. More complex theories, like the Lambert regional approximation method, are needed to take into account these effects. [78]

3.1.3 Configuration with Coplanar Electrodes

The Mott-Gurney formalism can be applied only in a 3D sandwich configuration, in which the lateral dimensions of the metal contacts are higher that their separation. Other approaches have to be used to describe the planar SCL current flowing in a "gap-type" structure, in which the distance between the electrodes L is larger than, at least, one of the transversal dimensions of the active layer. This important configuration, in which both the electrodes are on the same side of the semiconducting material, is common, for example, in field effect transistors. However, even if for the simple two terminal structure the SCL problem can still be resolved, different is the FET case in which this is a not simple task. In fact, in a 2D structure the lines of force related to the injected charges are not confined to the bulk active layer, so that the complete description of the problem would need to take into account the influence of the surrounding materials (gate electrode and dielectric). For this reason, space charge effects are usually not considered in the description of organic FETs. Like in the conventional case, the "gradual channel approximation" by Schockley is a plausible simplification.
The current-voltage characteristics of insulating materials in a gap-type structure present, at low applied voltage, an ohmic behavior, followed by a transition to a new regime in which the current shows a quadratic dependence on the voltage, like in the 3D case. However, the dependence of the current on the distance between the two electrodes is different. The SCL planar current generally follows a $I \propto V^2/L^2$ relation, in contrast to the $1/L^3$ dependence expected from the 3D analysis. This general feature has been firstly pointed out by Geurst [88] and Zuleeg [89]. A formal treatment has been later provided by Grinberg and co-workers. [90] In the Geurst argumentation, both the current-voltage, and the current-thickness dependencies are explained by looking at the electric field perpendicular to the semiconducting layer and therefore normal to the one that drives the charges over the distance L. This is the field that determines the space charge density in the thin active

layer. Considering the thickness of this layer as infinitesimal, a general relation for the dependence of the current on the voltage and on the separation between the electrodes, can be obtained:

$$I = \frac{2\varepsilon\mu}{\pi}\frac{V^2}{L^2} \tag{3.3}$$

where W is the width of the structure. This theory is only an illustration of the real problem. In any case, it delineates its essential features. More complex theories, in which the finite thickness of the active layer is considered, only give a different numerical coefficient with respect to Eq. 3.3. However, they predict an interesting transition between a 2D SCL conduction to a 3D transport, upon increase of the thickness. [90] The latter has been experimentally found during the analysis of our rubrene single crystal two terminal devices.

3.1.4 SCLC Differential Method

The space-charge-limited-current differential method is a general starting point to determine the depth and density of localized states, that was firstly proposed by Nevspurek and co-workers. [91, 92] It is based on the assumption that the position in energy of E_F depends on the density of injected charge and therefore on the voltage applied between the two electrodes. The quasi-Fermi level represents the demarcation between empty and filled traps (actually this is only true at low temperature, when the Fermi-Dirac distribution can be approximated to a step function), so that the distribution of traps for which the occupancy is changed can be determined by direct analysis of a single current-voltage characteristic.
In the framework of the SCLC analysis, using the zero temperature approximation, it is possible to estimate the parameters of an arbitrary distribution of traps, by knowing the function that describes the distribution $h(E_F)$ and the position of the quasi-Fermi level at the non-injecting electrode $E_F(L)$. The trap distribution is given by $h(E_F) = \mathrm{d}n_t(L)/\mathrm{d}E_F(L)$ or even better (after some manipulations) by:

$$h(E_F) = \frac{\kappa_1\kappa_2\epsilon V}{2eL^2kT(m-1)} \tag{3.4}$$

On the contrary, the quasi-Fermi level at the non-injecting electrode $E_F(L)$ is obtained by simply combining the equation for the current $J = e\mu n_f(x)F(x)$, with the density of free charge given by the Fermi-Dirac statistic $n_f = N_v \exp(-E_F(x)/kT)$. By knowing the relation between the potential and the electric field $F(x) = V(x)/L$ we have:

$$E_F(L) = kT \ln\frac{L}{\kappa_1 N_v e\mu} + kT \ln\frac{J}{V} \tag{3.5}$$

In both the equations $m = d\ln J/d\ln V$, L is the distance between the electrodes and N_v the effective density of states in the highest occupied molecular orbital. The parameters κ_1 and κ_2 are respectively, the average distance of the injected charges from the anode, and the ratio of the carrier concentration at the anode on the concentration of the total injected carriers. These parameters correlate the value of the field and the density of

trapped carriers at the non-injecting electrode, to their mean values. By knowing the slope of the characteristic m, they can be calculated by using the equations: [93]

$$\kappa_1 = \frac{2m-1}{m} \tag{3.6}$$

$$\kappa_2 = \frac{m-1}{m}(1+B) \tag{3.7}$$

where B is a second-order correction that can be neglected to a first approximation. Equations (3.4) and (3.5) allow us to extract, in principle, an energy distribution of states directly from a single experimental $I-V$ curve. However, an obvious problem is that, according to Eq. (3.5), the effective density of states N_v should be previously known in order to find the correct values of the trap energy depth. This need, combined with the approximation of uniformity in the trap distribution, makes the calculated trap depth E_t only an estimation of the real value, altered by an error that may be as great as several kT. It is also important to remark that this method is valid only at low temperature and under the condition $\theta << 1$. The latter corresponds to the low injection level, in which the quasi-Fermi level is far from the edge of the trap distribution that is at (Fig. 3.1(b)).

3.2 Diode

3.2.1 Introduction

An asymmetric diode is generally a planar structure, in which the active layer is sandwiched between two different metal electrodes. An ohmic interface is formed at the first metal/semiconductor contact, whereas a Schottky barrier at the second. The devices is therefore a low-voltage, high-current rectifier, in which the current flow is limited by the non-ohmic interface. This one, and more complicated structures (double carrier devices), are widely used in the organic electronic field as, for example, rectifying elements in simple logic circuit [94, 95], light emitting diodes, and solar cells. [96]
In spite of its simple structure, understanding the working principles of a single carrier organic diode is not straightforward, especially because of the complex nature of the active layer. In this case, amorphous films are normally used. Moreover, even if the properties of the Schottky diode are mainly determined by the characteristics of the non ohmic interface, the same is not true in the organic case. A strong contribution from the low conductivity bulk of the active layer must be considered, along with several unclear effects at the organic/metal interface. [97] This interplay between charge injection and drift of the carriers (limited by space charge effects) complicates the description of the problem. [9] A commonly used technique to determine which of the two processes is the limiting one is, for example, to examine the dependence of the current on the temperature and on the thickness of the active layer. Another option is to analyze the device AC characteristics, even if this technique generally provides not unique and incomplete results, because of the complexity of the equivalent circuits used to fit the data.
Besides all these problems, there is still lack of clearness about the energy band alignment at the non-ohmic metal/semiconductor interface. The process described in the previous

chapter, in which part of the active layer is depleted of charges, is often unaccepted. Evidence for the formation of a depletion layer in the active layer has been reported and then refuted by other experiences on similar devices, in which the active layer is seen as fully depleted. Contradictions can be found, both in the analysis of polymeric systems, [98, 99] and in devices made with small molecular weight materials. [13, 100]
In our characterization of single crystal diodes we have chosen to focus our attention essentially on the latter problem (Chapter (7)). Anyway, for the sake of clarity, we will briefly describe in the next section the processes determining the current-voltage characteristics of a diode. Moreover, attention will be given to the techniques used to determine the properties of the depletion region at the rectifying contact.

3.2.2 I-V Characteristics

Inorganic case

The characteristics of an inorganic diode depend on the properties of the Schottky interface. As visible in Fig. 2.1, at thermodynamic equilibrium and in the absence of any external bias, no current flows in the device. Flow of holes from the semiconductor to the metal $I_{s\to m}$ is balanced by the flow from the metal to the semiconductor $I_{m\to s}$. If forward bias is applied to the structure (- on the metal, and + on the semiconductor), the built-in potential on the semiconductor side decreases, whereas the potential barrier ϕ_b at the interface is unchanged. As a result, a net current from the semiconductor into the metal is observed. On the other hand, when reverse bias is applied to the structure, the built-in potential V_{bi} increases, so that $I_{s\to m}$ is reduced, while flow of holes from the metal remains unchanged. A small reverse current is therefore measured in this case.
Besides this simple picture, several models have been developed to describe the rectifying DC behavior of a Schottky diode. [28] The applicability of the theory depends on the properties of the active layer: thermionic-emission theory in the case of high mobility semiconductors, and diffusion model in the case of low mobility materials. A general unifying treatment has been also proposed: the thermionic-emission-diffusion model. In all the mentioned cases the current has the form $J = J_0[\exp(qV/nkT) - 1]$, in which n is the ideality factor of the diode, that is close to 1 for inorganic Schottky devices. In order to consider the effect of the bulk equipotential region in series with the depletion layer, a resistive term R_s is also added to the previous equation, giving:

$$J = J_0 \left[\exp\left(\frac{q(V - IR_s)}{nkT} \right) - 1 \right] \tag{3.8}$$

This equation provides better results at high forward bias, where the high current flowing in the device is influenced by the resistance of the semiconductor bulk, although it is very low. The previous equation is widely used also in for organic devices, even if the different nature of the active layer suggests its inadequacy.

Organic case

The previous description (Eq. 3.8) is widely used also to describe the characteristics of organic diodes, especially when single crystals are used as active layers. [101, 102] In the

latter case, the applicability of this simple approach is justified by the low density of defects at the interface and in the semiconductor bulk. Anyway, even if Eq. 3.8 is reasonable for a low resistance inorganic device, in which typical values are R_s =10 − 100 Ω, [103] a natural question about its validity in the organic case would arise. In the case of rubrene single crystal diodes, R_s has been found to be around 1 GΩ, revealing a clear insulating contribution of the crystal bulk. Thus, is it plausible to have a partially depleted structure, in which a high resistance (semi-insulating) bulk is in series with an insulating depleted region close to the interface? What should be the difference between the depleted region and the low free charge density bulk? We will try to answer to these questions during our discussion in Chap. (7).
In more realistic but complex descriptions, injection of charge in localized trap states is taken into account, along with effects induced by the formation of space charge. In this case, the most common approach is firstly to consider both the contributions [104] and, later on, to discriminate between them by the analysis of the experimental evidence. Which of these ones is the limiting contribution depends on the charge carriers mobility and on the interface barrier high. Unified models of hopping carrier injection and space charge limited current in the organic bulk have been formulated, [105, 106] as well as interpretation in which the SCLC is considered to be the not limiting process [107, 108]. Generally speaking, as we have previously seen, a higher barrier at the contact prevents the formation of a space charge, making the charge injection the limiting processes to the conduction. [109]

3.2.3 Impedance Spectroscopy

Important information about the properties of a diode can be obtained by analyzing its response to an AC stimulus superimposed on a static applied voltage. The device impedance is due to the composition of all phenomena occurring in the material and at the interfaces with the electrodes, [110] so that by the analysis of its dependence on the applied voltage and on the frequency of the monochromatic AC signal, considerations about the characteristics of the rectifying interface and of the semiconductor bulk can be made.
The impedance $Z(\omega)$ is defined as the ratio between the variable small amplitude signal applied to the sample $V(t) = V_m \sin(\omega t)$ and the resulting steady state current $I(t) = I_m \sin(\omega t + \theta)$, in which $\nu = \omega 2\pi$ is the frequency and θ is the phase difference between the voltage and the current. This is an imaginary quantity $Z(\omega) = Z^{'}(\omega) + iZ^{''}(\omega)$, that becomes real only for pure dissipative phenomena, in which a phase relation between $V(t)$ e $I(t)$ exists. $Z^{'}$ and $Z^{''}$ are the real and imaginary part of the impedance, respectively equal to $Z^{'} = |Z|\cos(\theta)$ and $Z^{''} = |Z|\sin(\theta)$. By plotting the real against the imaginary part (Argand representation), a complex plane plot showing the device different contributions to the impedance can be obtained. A suitable fitting procedure, in which the diode response is compared with the one of an electrical circuit formed by the parallel or series combination of ideal resistors (R) and capacitors (C), can then provide the capacitance and resistance associated with each element. The characteristics of the used equivalent circuit depend on the complexity of the system under analysis. By increasing the number of the

elements, the approximation of the impedance data with the presumable circuit become not unique; several different RC elements combination can give the same AC response.
In the inorganic case, the analysis of the capacitance-voltage dependencies gives information about the properties of the depletion layer at the Schottky interface, as discussed in Chap. (2). On the contrary, in order to describe the response of an organic device, complex circuits are generally used. The presence of a high resistivity bulk complicates the single parallel RC circuit suitable for the description of a conventional diode. In the most simple case, the equivalent circuit is formed by two RC elements in series, that keep into account interface effects and the resistance/capacitance associated with the semiconductor bulk. [111] This description is made even more complicated by the presence of trap states in the bulk and at the interface. [112] An easy determination of the capacitance associated to the depletion region is therefore not possible, unless complete impedance-frequency spectra at different applied voltage are available. However, it is not pointless to remark that, also in this case, the problem can be resolved only when the resonances of the RC elements are not superimposed; in this case the Argand plots show well resolved semicircles that can be fitted by using the expected equivalent circuit.

3.3 Metal-Semiconductor Field Effect Transistor

3.3.1 Introduction

The inorganic Metal-Semiconductor Field Effect Transistor (MESFET) is one of the simplest three terminal devices that can be fabricated and for which the basic working principles can be easily understood. In any case, the analytical treatment necessary for the analysis of its characteristics is quite complex and it will not be reported here. Once again, more important to the aim of this thesis is to provide only a qualitative description, that can be used to remark the differences between inorganic and organic devices. On the basis of this description and considering that reported in Chap. (2) about non-ohmic metal/semiconductor interfaces, we will show in Chap. (7) that organic MESFET are undoubtedly a new class of devices, for which innovative models are needed.

3.3.2 Device Functioning

MESFETs are field effect devices, in which the lateral current between source and drain is controlled by the voltage applied to a metallic gate electrode. No insulating layer is interposed between this electrode and the active layer and field effect is achieved by using a suitable rectifying metal/semiconductor couple. The most common semiconductor in conventional MESFETs is GaAs. With this high mobility material, efficient Schottky contact can be obtained, for example, by using aluminum as gate metal. [113]
Fig. 3.2 is a draft showing the device operation principles in the case of p-type semiconductor.

Two ohmic source S and drain D contacts are on the same surface of a high conductivity layer and are coplanar to the gate electrode G. The active semiconducting layer, of

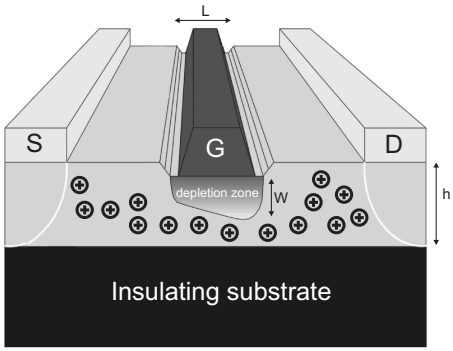

Figure 3.2: Draft of the working operation of a MESFET. In these figures G is the gate, S and D are the device source and drain electrode.

thickness h, is grown on the surface of an insulating substrate. When a positive bias is applied to the Schottky gate electrode, the width W of the a depletion zone at the non-ohmic metal/semiconductor interface changes (as described in Chap. (2)), so that the thickness of the conductive channel changes. The current is therefore controlled by reduction/increase of the region in the active layer, in which charge transport occurs $(h - W)$. In the case of p-type semiconductor, as V_G became more positive, the drift current I_D decreases because of the increasing depletion width.
The width of the space charge region is also controlled by the the potential difference between source and drain electrodes V_D. By increasing V_D, the depletion region becomes asymmetrical (Fig 3.2), until W, in the region close to the drain electrode, is equal to the channel depth h. At this point, a complete "pinch-off" of the channel occurs $(h - W) \simeq 0$ and the current stops following the increase of the drain voltage. This corresponds to the transistor saturation region. The $I - V$ output characteristic of this device is strictly similar to that one of the MISFET. At constant gate voltage V_G and at low V_D the current is linear, whereas it saturates for higher applied V_D after that the channel pinch-off occurs.
Efficient high-speed field effect operations can be obtained using inorganic depletion-mode devices. However, this is not a favourable configuration in the organic case. Extremely low current can be supported in an organic device, because of the low mobility and free charge carrier density in the active layer. This prevents hypothetically integration of organic MESFET in more complex electronic systems, in which generally high current densities have to be supported during the switch ON state. For this reason, the conventional MISFET, in which a high charge density layer is formed at the insulator/semiconductor interface, is generally preferred. However, MESFETs have to be considered important systems, with which fundamental studies on the properties of organic materials can be conducted (as we will show in Chap. (7)).

3.4 Metal-Insulator-Semiconductor Field Effect Transistor

3.4.1 General Description

In an Organic Metal-Insulator-Semiconductor Field Effect Transistor (OMISFET) an insulating layer is interposed between the gate electrode and the semiconductor, forming a MIS structure (Fig. 2.2). The lateral current, flowing between source and drain, is therefore controlled by modulation of the charge density close to the insulator/semiconductor interface. This field effect device can be viewed as a plane capacitor, where one of the plates is constituted by the gate, while the thin conductive channel formed at the interface composes the second plate. The two other electrodes are coplanar ohmic contacts, spaced by a channel length L, that are generally made by high work function metals (most usually Au, but also Pd [114], Pt [115] and Ni [116]), to provide a good matching between the metal Fermi level and the HOMO level of the commonly used, high ionization potential semiconductors. Even if the $I - V$ characteristics of an organic and inorganic MISFET are quite similar, the working principles of these devices are strongly different. The MIS structure in an organic ON device is polarized in accumulation mode (ref. to Fig. 2.2), so that no depletion region separates the conductive channel to the active layer bulk. In any case, the latter has no influence on the device characteristics, because of its low intrinsic free charge density. A low leakage current, in the transistor OFF state, is also assured by the total depletion of the semiconductor below threshold voltage. [117, 118]
Depending on the respective position of the three electrodes, various field-effect structure can be fabricated. The most used are shown in Figure 3.3.

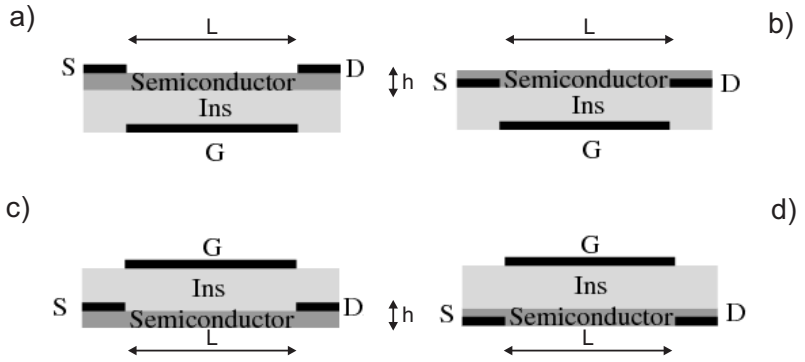

Figure 3.3: Draft of the different OFET structures. a) bottom-gate/top-contacts b) bottom-gate/bottom-contacts c) top-gate/top-contacts and d) top-gate/bottom-contacts. In these figures G=gate, S=source, D=drain, Ins=dielectric layer.

Here, L is the transistor channel length, h is the thickness of the semiconducting layer and S, D, G are respectively the source, drain and gate electrode.
Because of the semi-insulating nature of an organic semiconductor, only a low current flows between source and drain, when no gate voltage V_G is applied. On the contrary, if the gate is polarized, the density of charge in a thin layer close to the insulator surface changes.

When V_G goes beyond a given threshold voltage V_T, a high charge density channel is formed close to the insulator/semiconductor interface and a significant current flows between the two coplanar ohmic electrodes. In a ON transistor far from the threshold, the sign of the gate voltage is opposite to that of the charges in the conducting channel, that is, positive for an n-channel and negative for a p-channel. In any case, the exact position of V_T depends not only on the nature of the semiconductor, but also on the properties of the insulator and its interface with the active layer.
Under ohmic charge injection and under control of a constant gate bias above V_T, the drain current I_D grows linearly with V_D, until $V_D \simeq (V_G - V_T)$. By increasing V_D, the reduction of the potential difference between drain and gate electrode results to a gradual thinning of the channel close to the drain electrode, so that the charge density is no longer uniform (as for the case of low V_D). When $V_D \simeq (V_G - V_T)$, the potential at a point of the channel close to the drain electrode falls to zero. The channel is therefore pinched off; a further increase of V_D only moves the pinch-off point toward the source electrode, but it does not effect its potential. In a long channel device, in which the shortening of the channel is negligible with respect to its length L , no increase of the current is observed after this point; the transistor is in the saturation regime. Equations (3.9) and (3.10) give the drain current in the linear and saturation regimes, respectively.

$$I_D = \frac{W}{L} C_i \mu \left(V_G - V_T - \frac{V_D}{2} \right) V_D \tag{3.9}$$

$$I_D = \frac{W}{2L} C_i \mu (V_G - V_T)^2 \tag{3.10}$$

Here, C_i is the capacitance of the insulating layer, W the channel width and μ the constant mobility of the charge carriers. Looking to these equations, the importance of a field effect transistor as tool for the characterization of a semiconductor is evident. The analysis of the transistor characteristics, by means of Eqs. 3.9 and 3.10, allows a direct determination of the charge carriers mobility, both in the linear, and in the saturation regime; in the former case this can be done by simply deriving Eq. (3.9), whereas in the latter by plotting the square root of I_D on V_G.
Eqs. (3.9) and (3.10) are similar to the ones used for conventional MOSFETs. However, a point to note is that here, we have only described an ideal case, in which several assumptions have been made:

- The distance between the source/drain electrode has to be considerably higher that the separation between the conductive channel and the gate electrode. As previously mentioned, this condition supports the gradual channel approximation, in which the electric field normal to the channel is considered much larger than the parallel field. Effects related to the influence of channel length shortening and formation of space charge are neglected.

- The source/drain contacts are supposed to be ohmic and their resistance to be lower than the resistance of the channel.

- The mobility is constant.

- The leakage current in the device OFF state is negligible.

Although these conditions fit well with the characteristics of an inorganic MOSFET, it is clear, nowadays, that several other effects must be taken into account when dealing with organic devices. Actually, in a real organic MISFET, the charge carrier mobility is a voltage-dependent function $\mu(V_G)$, [119, 120, 121] that largely depends on various parameters, which include the density of charge carriers. The previously described approaches for the determination of the mobility cannot be formally applied, because there is no simple linear relation between the drain current and the applied gate voltage. This is especially true in the saturation regime, where the density of charge varies considerably along the channel, so that the mobility is not constant; the extracted value only represents a mean value. For this reason, it is often more judicious to extract the mobility in the linear regime, where the density of charge is more uniform. Also in the case of gate-dependent mobility a meaningful determination of this parameter can be done by determining V_T with one of the available techniques (to be described in the next section) and by using Eq. 3.9 without any differentiation. [122] However, it is also important to note that the value extracted with this method represents a "contact limited"' mobility, in which the effect of the contact series resistance R_c is still present. In an real organic device, in fact, the resistance associated to the source and drain contacts is generally not negligible [123, 124]. An "intrinsic" mobility can be obtained only by determining R_c by extrapolation from the trend of the device total resistance on the channel length, and by including the resistance effect in a modified version of equation (3.9). [125] In this case, the voltage dependence of the intrinsic mobility on the applied gate voltage can be determined.
When comparing the performance of different devices, we must note also that the highest values reported in the literature refer to a "four-terminal" mobility μ^{4T}, which is not affected by contact effects, and, for this reason, is referred to as the "intrinsic" mobility. In the four terminal measurement, two additional electrodes are, in fact, introduced within the space that separates the source and the drain; by measuring the voltage difference between them, no limitations from the source and drain contacts have to be considered. [126, 127] The mobility is therefore always greater than that extracted by means of the methods present before.

3.4.2 Threshold voltage

Determination of the threshold voltage

In the conventional MOSFET, the threshold V_T is defined as the gate voltage at which the density of carriers at the semiconductor surface equals the dopant concentration, that is, when strong inversion takes place. [28] At this point a conductive channel close to the insulator/semiconductor interface is formed and a considerable current starts to flow. The latter statement is correct also in the organic case, even if an alternative definition for V_T should be given, since the conductive channel is formed by accumulation of charges at the interface. [128] Without considering an inversion layer, the threshold can be simply defined as a measure of the charge needed to switch on ohmic conduction in the channel. [129]

From the description of the ideal MIS structure (Fig. (2.2), we see that accumulation of charges comes off only under one voltage polarity, depending on the nature of the semiconductor (p or n-type). We should therefore expect a zero value of the threshold voltage, contrary to what observed in real devices. A point to note is that our description of the MIS assumes no band banding at thermodynamic equilibrium. Important effects, derive from the work function difference between the gate metal and the semiconductor and from misaligning of the materials vacuum levels at the interface have, in fact, been omitted. Also, the presence of fixed charge due to distribution of trap levels at the insulator/semiconductor interface has not been considered. These effects give rise to charge accumulation also at zero applied voltage and therefore to a non-null V_T. At this point all the traps become filled, the fixed charge is neutralized, and flat-band condition at the interface is reached. Above the threshold, charge carriers are essentially free and a substantial increase of the source to drain current is observed.
An accurate extraction of the threshold voltage is required to obtain a reliable estimation of the charge carrier mobility and to compare the characteristics of different devices. Several techniques, derived from the consolidated experience in the analysis of inorganic devices, can be used [130] but only in few case meaningful results can be obtained. Looking at Eqs. 3.9 and 3.10, we note, for example, that at low drain voltage and at constant V_G, the threshold is given by the extrapolation of the linear I_D/V_G characteristic down to zero current. The same technique gives V_T also in the saturation regime, if $\sqrt{I_D}$ is plotted against V_G. Anyway, several contributions usually determine the departure of the transistor characteristics from what expected by Eqs. 3.9 and 3.10, making the described methods inaccurate. Each method presents its weakness and, even when more complicated derivative techniques are used, a comparison among the obtained results is extremely difficult, in particular when different transistor regimes are considered. [131]
During our analysis we have chosen to work with the transconductance change (TC) method developed by Wong and coworkers [132]. In its simplest description, it is easy to understand that, since the threshold voltage is the transition point from a region of zero current to another where the current is proportional to V_G, the first derivative of the transfer curve should be a step function and its second derivative a delta function. The latter looks like a broad peak in real cases, where a non-zero current below threshold exists. The TC is a powerful method insensitive to non-ideal effects (such as parasitic resistance and the gate-voltage dependence of the mobility), which yields physically meaningful results. Anyway, it is important to focus on the fact that this second derivative technique can be performed only when low noise experimental characteristics are available. Otherwise, the peak could not be distinguished from the unstable and oscillating shape of the ground.

Subthreshold Current Regime

The subthreshold current is the current flowing between source and drain when the transistor goes from the OFF to the ON state. In an inorganic device, this current is observed just below the transition between the so-called weak inversion and strong inversion regimes, where, because of the low density of charge carriers (less than the bulk majority carrier density), the current is essentially due to charge diffusion between the

two electrodes. By considering the $p-n-p$ structure of an inorganic MOSFET under weak-inversion , it is easy to demonstrate that the conditions for charge carriers drift are, in this case, not satisfied. The junction between the drain electrode and the channel is, indeed, close to a reverse biased metal/semiconductor junction, so that the applied source to drain voltage drops primarily on this interface, practically without no effect on the channel. Charge diffusion is therefore predominant in weak inversion, because, in this case, there is no electric field to drift the charges along the semiconductor between the source and drain electrodes. This condition is also evidenced by the fact that the subthreshold current is practically independent from the drain voltage. [28, 30]
Because of its exponential dependence on the applied gate voltage, the subthreshold current is usually described in term of the so-called subthreshold slope (or subthreshold swing), which is given by:

$$S = \frac{\mathrm{d}V_G}{\mathrm{d}(\log I_D)} = \frac{kT}{q} \ln 10 \left(1 + \frac{C_D + C_{it}}{C_i}\right) \tag{3.11}$$

Here, I_D is the drain current and V_G the gate voltage; C_D, C_{it} and C_i are the depletion layer, interface states and gate dielectric capacitance, respectively. k is Boltzmann's constant, T the absolute temperature and q the elemental charge. S is a measure of how rapidly the device switches from the OFF to the ON state and it is typically reported in Vdecade^{-1} or mVdecade^{-1}. A large subthreshold swing generally implies a large influence of traps on the charge carrier diffusion. This statement is clearly visible in Eq. 3.11, considering that the capacitance C_i is linearly proportional to the density of interface state.
Looking to the reported equation is clear that, once again, the inorganic description cannot be used with an organic device, working in accumulation. [29, 133] In this case, the transition between the OFF and the ON states occurs when passing from the depletion regime to the accumulation regime. At the transition point, the depletion layer width falls to zero, meaning that the respective capacitance rises to infinity. Under such circumstances, equation 3.11 becomes meaningless. Moreover, the subthreshold current has often been found to be non-exponential below the threshold, pointing to charge transport mechanisms that are different to charge diffusion. [22] A plausible explanation can be traced, in any case, from the one provided for the inorganic TFTs [29] in which the current is seen to be limited by the influence of localized energy trap states, that need to be filled by the gate-induced charge. We will develop this concept in Chap. (8), by presenting our analytical description of the current below threshold in an organic single crystal FET.

Part II

From Materials to Devices

Chapter 4

Rubrene Single Crystals

Rubrene single crystals represent one of the most useful samples for the understanding of the properties of organic materials. In this chapter we describe in detail these systems, starting from the description of the material characteristics and concluding with the presentation of the single crystal field effect devices. The motivations and the choices at the base of this thesis should therefore be clear: to reach a deeper understanding about the working principles of an organic FET, by using one of most important and well characterized organic materials.

4.1 General Description

Rubrene is an aromatic polycyclic derivative of tetracene, in which the hydrogen atoms of the two interior rings are replaced by four phenyl-groups (Fig. 4.1).

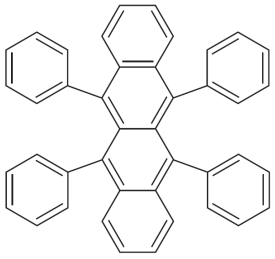

Figure 4.1: Molecular structure of rubrene. This is a non planar molecule in which the aryl substituents reduce the reactivity of the inner tetracene bone.

Because of the aryl substituents, this is a more stable molecule against oxidation, with respect to the other acenes. [134] However, its decomposition upon exposure to light and air is a well document process; [135] clear evidence on the complete oxidation of rubrene thin film has been reported, [136] pointing out the importance of control the photo-oxidative effects during the material processing, also when single crystals are used. [137, 138] Oxidation of rubrene single crystals, in air and at room temperature, occurs in any case only at the surface, thanks to the compact packing of the constituent units. [139]

Rubrene is a non-planar molecule, with tendency to solidify in an amorphous state when deposited on foreign substrates. [140] Only recently, evidence for the formation of crystalline thin films on the surface of high order single crystals has been reported. [141, 142] This important peculiarity limits the utilization of rubrene thin films as active layer in a large area device.
In spite of this limitation, rubrene is considered, nowadays, one of the most interesting molecules in the field of organic electronics. [143] Starting from this compound, high mobility single crystals, with a low density of defects and impurity related traps [20], can be easily obtained and efficient field effect transistors can be fabricated. The latter are considered unique tools for determining the intrinsic properties of organic materials; they permit to explore the upper limit of mobility in an organic device. Other techniques have also shown the importance of these materials for fundamental studies: time-of-flight (TOF) analysis, from which the high mobility of the charge carriers in the bulk has been extracted, [144] and combined optical and electrical methods from which the dynamics of the charge carriers in an anisotropic molecular material has been elucidated. [145] A point to note is that, in any case, a peculiarity limits the development of an electronic based on rubrene single crystals: the difficulty to integrate the active layer into a complex electronic system. [146, 147]

4.2 Morphological and Structural Properties

Among the single crystal growth methods available for organic semiconductors [74], the most exploited technique remains the physical vapor transport (PVT). In spite of the important results obtained by working in solution, [148] or by sublimation of the raw powder, [149] PVT is still the methods that provides higher purity materials. Impurities crystallize at different temperature along the temperature gradient present from the source to the end of the growth tube; this permits their separation, even if several cycles are in general used to achieve a high degree of purity. The temperature profile in the reactor and the gas flow are the most important parameters to control in this widely used single crystal growth technique. [150, 151] After molecular condensation, millimeter size single crystals with tabular habit [152] and with an extremely low density of defects [153] are generally obtained. A higher crystalline quality is reached, when low temperatures and high gas flow rates are used. [154] Argon is the most common gas for the single crystal growth by PVT, even if important results in terms of field effect mobility have been obtained growing rubrene single crystal in a stream of pure H_2. [155, 24]
With the PVT technique and under the stream of a controlled mixture of argon and H_2, rubrene crystallizes in an orthorombic phase with unit cell parameters $a = 26.86$ Å, $b = 7.19$ Å, $c = 14.43$ Å, containing four molecules arranged in a herringbone motif in the (100) plane and forming layers along the a-axis direction with spacing $a/2 = 13.43$ Å. [156] As apparent in Fig. 4.2(a), in the high mobility direction b the molecules present a slipped-cofacial configuration along the long molecular axis, but no displacement along the short-molecular axis (Fig. 4.2(b)) This characteristic is strongly different from pentacene or tetracene single crystals, in which the short-axis displacement between adjacent molecules is so high that

only weak interactions exist between them. The very efficient electronic coupling and therefore the high mobility of rubrene single crystals in the b crystallographic direction are due therefore to the absence of short-axis displacement and a favorable molecular sliding parallel to the long molecular axis. [21] The intermolecular distance corresponds in this case to a maximum of the electronic coupling (and therefore of the band-width) that, on the long axis displacement, is an oscillating function.

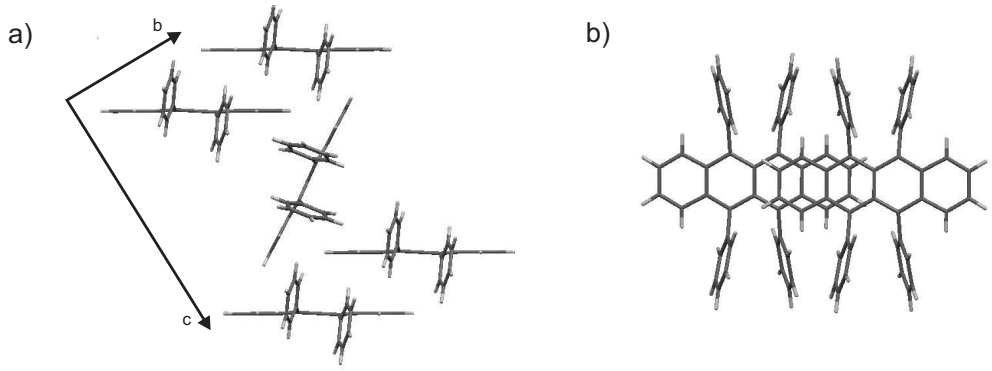

Figure 4.2: Projection of the single crystal packing of rubrene in the bc plane, showing the herringbone motif and b) π-staking in adjacent molecular units due to minimal shot-axis slip.

4.3 Rubrene single crystal FETs

4.3.1 Device Performances

Rubrene single crystal field effect transistors are the highest mobility devices in the field of organic electronics. [143] Aside from the common polymeric dielectric structures with a mobility now in excess of 10 $\mathrm{cm^2V^{-1}s^{-1}}$, high-performance devices with a thin free-space gap between the gate and the crystal have been prepared. [157] With these devices the surface properties of the active layer can be investigated, without taking into account the effects associated with the dielectric layer. The high mobility found in these systems is also gate-voltage independent, in contrast to what is generally observed in organic thin film transistors. [120] In the latter, a reduction of the mobility with an increase of the gate voltage at constant drain voltage has been attributed to the different, more defective, morphology of the semiconductor film next to the dielectric interface as compared with that in the bulk of the film; [122] this is not a feature of the air-gap structure. However, also in rubrene single crystal devices with solid gate insulator, the density of trap states close to the insulator/semiconductor interface is orders of magnitude higher that the one on the semiconductor bulk. [158] The performances of these devices are, in any case, higher than for the thin film case. Moreover, even if thin films remain the most appropriate systems for applications in large area organic electronics, the first step toward the employment of rubrene single crystals in practical devices has been reported. [159]

The printing of octadecyltriethoxysilane (OTS) domains onto the source/drain electrodes offers a direct nucleation and growth of semiconductor crystals over the electrodes, giving an array of high mobility transistors (2.4 $cm^2V^{-1}s^{-1}$) working on flexible substrates of large dimensions. An even higher mobility (4.6 $cm^2V^{-1}s^{-1}$), as well as a high ON/OFF ratio and low subthreshold swing can also be obtained by electrostatically bonding a thin single crystal to a plastic substrate equipped with patterned gold electrodes [160]. The performance of these flexible transistors are higher with respect to all the flexible organic transistors made of thin films.

4.3.2 Dependence on the Dielectric Properties

When using single crystals deposited on a dielectric surface, it has been shown that in order to maximize the mobility of the organic transistors, great attention has to be paid to the choice of the dielectric layer. [121] For instance, a higher mobility can be obtained if an insulating organic crystal is used instead of a disordered polymer, because in that case the effects of the random surface potential present in the polymer is minimized; the motion of carriers is therefore less affected by the process of charge trapping and thermal release. This effect is described by the analytical model of Sirringhaus and coworkers, [161] which develops the important concept introduced earlier by Veres *et al.:* [162] the static dipolar disorder in the polymer is the explanation for the dependence of the mobility on the applied gate voltage and the insulator dielectric constant. The effect of a high constant dielectric is to broaden the distribution of states (DOS), which in turn leads to a lowering of the mobility. A similar behavior has been experimentally found in rubrene single-crystals transistors, [25, 66] where an increase of the dielectric constant directly affects the charge transport, which change from metallic-like to insulating-like. A strong decrease of the mobility with an increase of the dielectric constant has been identified and, between the used dielectric, parylene C has been recognized as the insulator with which the higher mobility can be reached (μ=10 $cm^2V^{-1}s^{-1}$). This trend is in good agreement with the result found by other authors with the same active layer and air or vacuum as the dielectric medium. [60, 163] In this case, an even higher mobility can be obtained (μ=15 $cm^2V^{-1}s^{-1}$).
By modifying the dielectric surface with a self assembled monolayer (SAM) and therefore by reducing the number of interface states, the highest reported mobility for an organic device to date (a four-point mobility of 40 $cm^2V^{-1}s^{-1}$) has been found by Takeya and coworkers. [164] In the present case the mobility is not constant with respect to the V_G. The authors attribute it to the decrease of the channel width as the gate voltage increases (the charge carriers tend to be located closer to the dielectric interface). In other words, the region of the crystal explored at low gate bias would correspond to the bulk, while at high voltage the mobility is that of the interfacial region, which can be expected to be more defective than the bulk. Thus, the slope of the transfer curve at low V_G gives the bulk mobility, whereas that at high V_G the interface one.

4.3.3 Charge Transport Mechanisms

Similar to the inorganic case, the mobility in a rubrene single crystal FET has been demonstrated to be an inverse function of the temperature [60], pointing to a band-like charge transport mechanism. This result has been also confirmed by simultaneously measuring the $I - V$ characteristic and the Hall current on similar rubrene crystals; also in this case a diffusive band-like transport in an organic semiconductor with a low density of scattering centers and electronic trap states has been observed. [26, 165] The Hall effect makes it possible to distinguish between the motion of the carrier in delocalized states and transport by thermally activated hopping and suggests the band-like motion as a possible process in these highly ordered systems. Dissenting opinions on these two works do not permit firm establishment of the real transport mechanism near the insulator-semiconductor surface. However, the higher density of defects in the first monolayers of the semiconductor suggests that a hopping process is a more probable mechanism in this region, while a band-like transport is the dominant one in the bulk of the crystal.
A deeper knowledge on the properties of rubrene single crystals has been reached by Batlogg's group by measuring the Seebeck coefficient of the single crystals in a field effect structure. [166] First, high-performance single-crystal devices, with a low subthreshold swing and very weak hysteresis, have been realized by using a fluorinated dielectric layer. [167] On these transistors, the Seebeck coefficient could then be measured as a function of the applied gate voltage. In this way, simultaneous information about the position of the Fermi level and the entropy transported by the carriers could be derived, and the charge transport mechanism in the semiconductor determined. The interesting result is once again that, the band-like transport is a likely picture to describe the motion of carriers.

4.3.4 Structure-Mobility Relations

As previously said, the high mobility generally observed in rubrene single crystal devices has been theoretically attributed to the high electronic coupling between adjacent molecules in the *b*-direction. A clear experimental linear relation, between the charge carriers mobility and the intermolecular distance, has been also provided by applying different high pressures to a working rubrene single crystal FET. In this way the intermolecular distance can be reduced and a linear increase of the mobility observed, because of the higher transfer integral between adjacent molecules. [168] Using field effect devices, the charge transport has found to be clearly anisotropic and to reflect the corresponding anisotropy of the molecular packing in the crystal. [23] These results point out to the high quality of the active layer and to the validity of the band-like charge transport mechanism in a high performance single crystal FET. In fact, an anisotropic mobility, that is also linearly dependent with the intermolecular distance, only occurs when no relevant trapping is present. Other evidence about the favorable molecular arrangement in rubrene single crystals has been found, by analysing the polymorphs of a rubrene derivative. By adding alkyl-groups on two rubrene lateral aromatic rings, single crystals with different packing compared with the unsubstituted compounds have been obtained. [169] In spite of the same molecular composition, field effect transistors made with the two polymorphs show different characteristics. One of the devices is similar to a rubrene single crystal FET (with mobility of the

order of 10 $cm^2V^{-1}s^{-1}$), whereas in the devices made on the second polymorph no current flows. This peculiarity reflects the different structure of the two materials and points to the low influence of the composition with respect to the molecular arrangement in the single crystal. The in-plane motif in the high mobility single crystal is in fact comparable to that of rubrene, whereas a significantly higher intermolecular distance is found in the second case. The latter does not permit an efficient π-staking between adjacent units, with a clear effect on the molecular coupling and therefore on the device mobility.

Chapter 5

Device Fabrication

In this section, starting from the single crystal growth, we give an overview of the methods we have used to fabricate our rubrene single crystal transistors. Along with the techniques used to prepare the final devices, morphological and structural properties of these materials are also described.

5.1 Semiconducting Active Layer

5.1.1 Single Crystal Growth

Two different techniques have been employed to grow rubrene single crystals: the floating-drop (FD) [170] and the physical vapour transport (PVT) techniques. However, only the PVT method has provided easy-to-hand and high quality single crystals, suitable for electrical characterizations. In this case, single crystal growth takes place in a horizontal furnace, by physical transport of the sublimated raw material under a stream of pure argon (flow rate 50 ml/min). A controlled temperature gradient assures compound sublimation in the furnace hottest region and its crystallization at a well defined position close to the end of the tube. Several recrystallization processes have been used to achieve an acceptable separation between the compound and its impurities. Proper cleaning processes for all the used glasses avoid also contamination with unexpected organic substances.

5.1.2 Morphological and Structural Characterization

The surface morphology of the crystals and the characteristics of the channels (shape and real length) have been analyzed by using a Digital Nanoscope III*a* atomic force microscope (AFM) in tapping mode. Moreover, in order to determine the crystal dimensions and their thickness, an optical microscope Olympus SZX12 and a Dektak 8 stylus surface profiler have been used respectively (except for the sub-micron samples, whose thicknesses were determined with the AFM).
Rubrene single crystals present a tabular morphology with a well-developed (100) face and elongated parallel to the [010] direction. Samples with different thickness have been used for the SCLC analysis (in the range 500 nm-40 μm), whereas FETs have been fabricated

always with active layers not thicker than 2 µm. Fig. 5.1 shows the optical and morphological analysis of a representative crystal, on which two gold electrodes have been deposited via thermal evaporation of the metal.

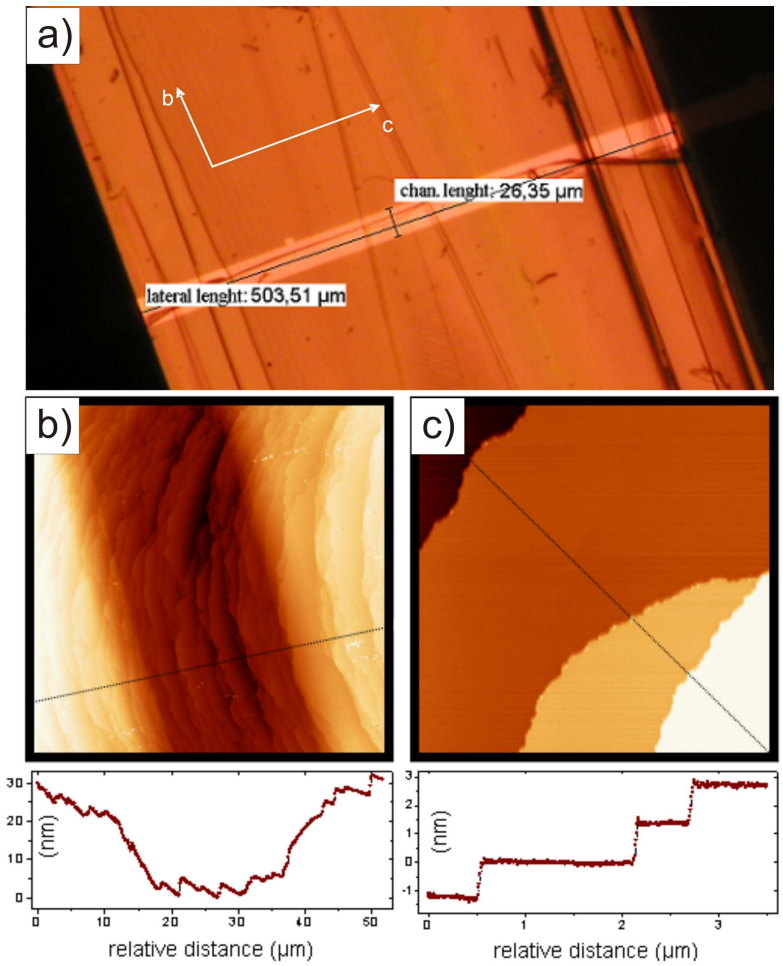

Figure 5.1: Optical microscope a) and AFM [b) and c)] images of a rubrene crystal equipped with two gold planar contacts defined by means of a 25 µm *shadow mask. b) is a general and c) a close view of the channel; in the bottom part of the figure their respective profiles are reported.*

The AFM analysis (Fig. 5.1(b-c)) shows the shape of the channel and the morphology of the crystal surface (the thickness of the steps corresponds to the value $a/2$), while the optical microscope image (Fig. 5.1(a)) shows the homogeneity of the channel and its lateral dimension W. Note the presence of some non-uniformity parallel to the crystalline b-axis. This has been found to characterize the bulk of the sample and not its surface, as already described in the literature. [152] All the crystals also exhibit uniform extinction under cross-polarizers, thanks to their high crystalline quality and the absence of multiple crystalline domains.

Other interesting analysis have been carried out with the scanning tunneling microscopy technique (STM). The single crystal structural characterization has been made possible by the high conductivity of the sample (also in the direction normal to the crystal plane). The latter is a thin flat crystal (h <1 µm), that was placed on an indium doped tin oxide

(ITO) substrate covered by a thin PEDOT:PSS film. By using a low noise instrument (pA resolution), images resolved down to the molecular scale can be obtained, as reported in Fig. 5.2; no Fourier Transform filtering was applied in this case.

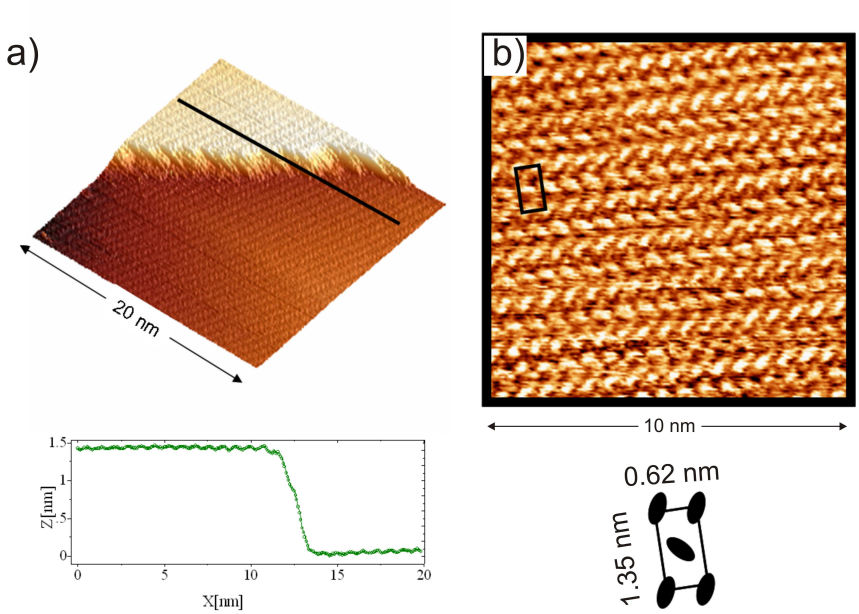

Figure 5.2: STM analysis of a rubrene single crystal. a) is a 20x20 nm^2 *image showing a single molecular step and b) is a* 10x10 nm^2 *image in which the herringbone motif, typical of an organic material, can be seen. In the bottom part of the figure, two drafts, showing the height of the molecular step and the unit cell parameters, are reported.*

A molecular step of $\simeq$ 1.3 nm, between two large and flat terraces is visible in the 20x20 nm^2 image (Fig. 5.2(a)), whereas molecular resolution can be observed in Fig. 5.2(b). Molecules are arranged in a herringbone motif, according to what was previously established and reported in Fig. 4.2. The draft in figure 5.2(b) also shows the lattice parameters extracted from the analysis of the 10x10 nm^2 image. The slight difference between these parameters and those obtained from the XRD data is not yet fully understood. However, because both the STM values are smaller than the XRD ones, we speculate that it is related to the calibration of the instrument in the xy-plane. Another contribution could be given by the piezo-scanner thermal drift.
These results demonstrate the possibilities of conducting STM experiments on high conductivity bulky organic single crystals; a peculiarity that has already been highlighted by other authors. [101] In any case, aside from what was previously stated, we believe that the reported images refer to an inner part of the crystal, close to the interface with the ITO/PEDOT:PSS back electrode. Evidence shows that, in a broad range of approaching current set-points, the STM tip penetrates the first molecular layers and that the scan occurs in the bulk of the sample. Moreover, on the basis of our electrical characterizations of asymmetrical single crystal diodes (to be reported in Chap. (7)), we do not believe that the Schottky model can be used to analyze the current-voltage trends they have obtained with the STS technique.

5.2 Single Crystal Devices

5.2.1 Two Terminal Symmetric Structures

Rubrene single crystal bulk characterizations have been carried out by using two terminal gap-type devices, in which the active layer, attached to an insulating glass substrate, is equipped with two coplanar gold electrodes (approximate thickness of 30 nm). Even if more "soft" contact fabrication techniques, as the lamination or the metal ion assisted deposition [171, 172, 173] have already been proposed, electrodes were fabricated by simple thermal evaporation and by defining the gap with a 25 μm diameter gold wire shadowing the semiconductor surface. However, when this method is used, introduction of structural defects is an inevitable and well-known problem [174] and metal penetration into the volume of the organic active layer is often observed. [175, 176, 177] For this reason, in order to assure the applicability of the SCLC theory, (the metal/semiconductor contact must be ohmic as explained in Chap. (3)) several electrical characterizations were initially carried out to determine the quality of the gold/rubrene contact. Reduction of the thermal load on the crystal surface was found to be crucial for this purpose. Ohmic contacts were obtained only by using a thin tungsten wire ($\emptyset = 0.5$ mm), as the thermal source, and by using small metal plates to mask the infrared radiation emanating from the warmest part of the wire itself. Accordingly, to prevent thermal damage, the sample was placed not closer than 30 cm from the source. After metal evaporation the samples were left under vacuum for some hours to avoid uncontrolled oxidation after the unavoidable Joule heating effect.
All the measurements were performed in the *bc* plane of the crystals, in the dark and under argon atmosphere, with a Keithley 4200 semiconductor parameter analyzer, using a linear stepwise increase of the applied voltage and measuring the quasi-equilibrium current (the transit time of the electron is less than the period of the applied electrical signal). The maximum applied voltage was 210 V corresponding to an electric field of 8.4×10^4 V/cm.

5.2.2 Asymmetric Diodes and MESFET

Single layer asymmetric contact diodes were obtained by electrostatically sticking a thin rubrene single crystal ($h \leq 1$ μm) on a glass substrate coated with ITO, or on a thermally evaporated gold electrode, and depositing an aluminum cathode on the other side of the crystal. For the gold-aluminum system the reverse configuration has also been tested, but no substantial differences have been observed in the $I - V$ characteristics.
Organic single crystal MESFETs were fabricated with an aluminum gate electrode and two coplanar gold electrodes on the opposite surface. The static electrical responses of all devices were recorded in the dark. Impedance measurements were carried out by means of a HP 4292A LF Impedance Analyzer (5 Hz-13 MHz). The time elapsed between this measure and the collection of the impedance data was reduced to a minimum to avoid any change at the cathode-semiconductor interface. The experimental data were then analyzed with the freely available fitting software LEVM [178].

5.2.3 MISFET

Different MISFET configuration were tested during this work, but significant results were obtained only with TC/BG and BC/BG devices (ref. to Fig. 3.3). The former are staggered transitors, in which the source and drain gold electrodes are evaporated on top of the active layer surface, which consists of a thin crystal of ≈ 1 μm thickness, electrostatically bonded on the insulator. [164] The length of the semiconducting channel has been defined by means of a calibrated metal wire laid down across the crystal, and its width corresponds to the lateral dimension of the crystal, typically less than 1 mm. The gate is formed by an ultrasonically cleaned electrode of ITO, covered with a spin-coated insulating polymethylmethacry1ate (PMMA) film $C_i = 3 \pm 1$ nF/cm^2, prepared as in [179]. On the contrary, single crystal FETs, with bottom-contacts, bottom-gate geometry, were fabricated by using a spin coated fluoropolymer (Teflon AF) thin film $C_i = 2.8 \pm 3$ nF/cm^2 on ITO and by evaporating two gold contacts on its surface. In this case, the single crystal was in direct contact with the insulator, and to the source and drain electrodes.
The $I - V$ characteristics were recorded in the dark both in constant gate voltage (output characteristic), and constant drain voltage (transfer characteristic) modes.
Model calculations were performed with programs developed in Mathcad.

Part III

Analysis and Results

Chapter 6

Bulk Charge Transport Properties

By analyzing the $I-V$ characteristics of rubrene single crystal two-terminal devices, we have found evidence for a 3D charge transport mechanism also in a planar configuration, when this is allowed by the high thickness of the active layer. In the range of validity of the Mott-Gurney treatment, a set of electrical bulk parameters for the preferential single crystal growth direction have therefore been obtained. Particular attention is dedicated to the analysis of the trap-free regime in the $I-V$ curves, from which it is possible to estimate the free-electron drift mobility and the density of the traps. We also show that the crystals electrical response can be interpreted in terms of a discrete trap level at 0.48 eV above the valence band edge. The different nature of an organic semiconductor in respect to an inorganic one is here highlighted.

6.1 Charge Injection

Prior to SCLC analysis, we have checked the quality of the two gold contacts on the rubrene surface. Good contacts should behave as infinite reservoirs of charge, so that only a negligible fraction of the applied voltage is absorbed across the interface. When this condition is fulfilled, the total current across the crystal is dominated by the bulk properties of the sample and no asymmetries are observed in the $I-V$ characteristics. [180]
Two representative examples are illustrated in Figs. 6.1 and 6.2, for a good and a bad contact, respectively. Since, in a real device, area and quality of the two contacts always present some differences (because of the non-homogeneity of the crystal surface) the perfectly symmetrical curve in Fig. 6.1 tells us that the current in this case is limited by the bulk of the crystal, i.e. the current is bulk limited rather than contact limited. The linear regime at very low bias (inset in Fig. 6.2) also indicates that potential barrier effects at the metal-semiconductor interface are in this case negligible. On the other hand, the unsymmetrical character of the $(I-V)$ curve in Fig. 6.2 can be interpreted as the sign that the current is limited by the contacts. These characteristics show that a low thermal load evaporation of gold on an organic single crystal surface can provide good contacts, but that the quality of the latter has to be checked at the beginning of each analysis. In all the remainder of the work, such devices, for which unsymmetrical curves were recorded, have been systematically disregarded without further investigations about the causes of

this problem.

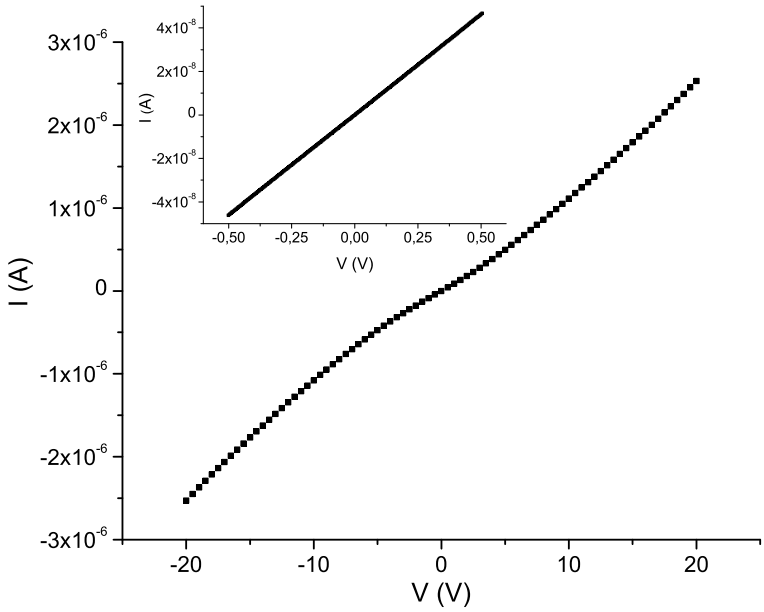

Figure 6.1: Current vs applied voltage for an Ohmic rubrene-gold system. The inset shows the lack of non-Ohmic effect of a low voltage.

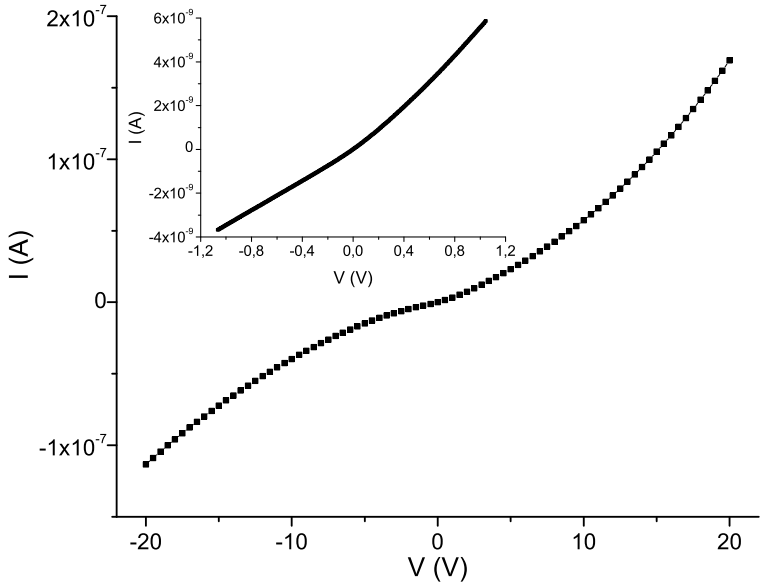

Figure 6.2: Current vs applied voltage for an asymmetrical rubrene-gold contact. The inset shows problems linked to the different behavior of the contacts.

6.2 Space-Charge-Limited Current in a Gap-Type Structure

It has been already pointed out that, in a rubrene single crystal, the higher molecular overlap and therefore the higher mobility is in the *bc* plane. Significant characterizations about the bulk properties have therefore to be conducted along the (100) face, by using a 2D gap-type structure, where both electrodes are deposited on the same side of the crystal. From the point of view of the SCLC analysis, this is a non-conventional architecture that can not be formally described in the framework of the Mott-Gurney treatment. It is important therefore to check if, also in this case, the devices characteristics can be analyzed with the latter theory. Only in this way can the bulk properties of the active layer be correctly determined.
As mentioned in Chap. (3), two limiting cases can be considered in a gap structure. In the first one, the thickness h of the semiconductor is very small $h \to 0$, which corresponds to the 2D geometry first analyzed by Geurst. The second case intervenes when the thickness is higher than the distance between the electrodes L; under such circumstances, the current is h-dependent and can be described by an equation similar to that originally developed by Mott and Gurney for the 3D architecture (Eq. (3.1)). In these limiting cases, the current I can be expressed rewriting the equations of Geurst ((Eq. (3.3)) and Mott-Gurney, obtaining respectively Eqs. (6.1) and (6.2):

$$I\frac{L^2}{W} = \frac{2}{\pi}\varepsilon\mu V^2 \qquad \text{(film)} \tag{6.1}$$

$$I\frac{L^2}{W} = \frac{9}{8}\varepsilon\mu\frac{h}{L}V^2 \qquad \text{(bulk)} \tag{6.2}$$

where L is the distance between the two electrodes, W the width of the channel, and h the thickness of the sample. μ is the mobility, ε the permittivity, and V the applied voltage. On account of previous considerations, it is plausible to assume that a single crystal of thickness $h >> 0$, with both electrodes on the same face, is in an intermediate situation between the 2D and 3D cases, depending on the ratio between h and L; when varying the ratio h/L, the coefficient in the Mott-Gurney's equation actually assumes a different weight with respect to $2/\pi$. Accordingly, it can be expected that the 2D law will dominate as long as $h/L << 1$, while the 3D law will be valid when $h/L >> 1$, or more precisely as long as $(9/8)(h/L) >> (2/\pi)$. A common practice to discriminate between the two limiting cases consists of plotting the current at a given voltage as a function of the electrodes distance, which is expected to vary as L^{-2} in a film structure ($h << L$) and as L^{-3} in a bulk structure ($h >> L$). [88] Unfortunately, such an analysis could not be performed with our single crystal devices. The reason is that the transition point between the Ohmic and SCLC regimes increases as L^2. With the technique used in this work, where, as previously stated, the length of the channel is defined by a mask made of a calibrated gold wire, practical values of L are 25 µm, 50 µm, and above. The transition can therefore be expected to be four times larger with 50 µm than with 25 µm, with the consequence that, in the former case, the SCLC regime starts outside the explored voltage $(0 - 200V)$. In order to investigate about the applicability of the Mott-Gurney law also in the 2D cases, we have therefore restricted our analysis to devices with $L = 25$ µm and we

have analyzed the dependence of the free-electron mobility μ (the mobility extracted from the $I - V$ curves in the trap-free regime) on the crystal thickness using both Eqs. (6.1) and (6.2).
Figure 6.3 illustrates the variation of the calculated mobility for crystals with various thicknesses and identical channel lengths $L = 25$ μm.

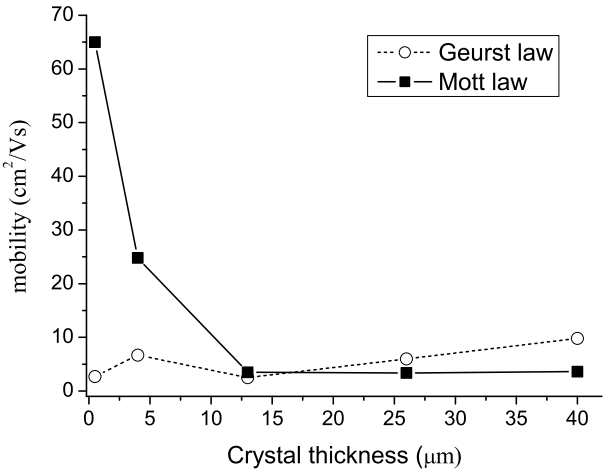

Figure 6.3: Calculated mobility vs crystal thickness as derived from Eqs. (6.1) and (6.2). The channel length is constant and equal to 25 μm. *The mobility value extracted with the Mott-Gurney law for the thick samples is approximately equal to* 3.5 $\mathrm{cm}^2/\mathrm{Vs}$

It can be seen that, for thicknesses comparable to or greater than the channel length (15 μm $< h <$ 40 μm), the Mott-Gurney law gives a thickness independent mobility of around 3.5 $\mathrm{cm}^2/\mathrm{Vs}$. At lower thicknesses, a sharp rise of the calculated mobility occurs. This is because, when the cathode-anode spacing becomes larger than the crystal thickness, Eq. (6.2) loses its physical meaning and, although it is an approximate description of the system, the Geurst law has to be used (a more reliable theory would have to consider the finite thickness of the crystal, as pointed out by Grinberg and coworkers [90]). A converse behavior is followed by the 2D mobility; that is, at low thicknesses, the 2D mobility magnitude is comparable to that of the 3D mobility at high thickness, while it tends to depart from this mean value as the thickness increases. In conclusion, Fig. 6.3 brings evidence for a transition between a $2D$ and a $3D$ regime. The fact that the transition point occurs at $h \approx 13$ μm, that is, when $(9/8)(h/L) \approx (2/\pi)$ brings additional evidence for such a transition. We note that above this point, the 3D mobility is independent of the thickness of the crystal, which can be interpreted by stating that the current density is uniform over the whole section of the crystals.
At this point, the question arises as to how can the charge carriers be uniformly injected in the whole thickness while the contacts are only located on one side? 3D modeling would be required to give a definitive answer to that, but we can put forward a simple image where the mobility in the direction across the crystal of the charges is high enough to provide a uniform repartition of the injected charge. Of course, such a process would not operate for

very thick crystals; however, this limitation is not reached in the present case.

6.3 Bulk Parameters Extraction

Within the thickness domain where the Mott-Gurney model provides a good description of the system, a set of electrical parameters have been extracted from the experimental curves. A significant example is reported in Fig. 6.4 in linear and double-logarithmic scales. It is easy to observe the similarity between this behavior and the ideal one, reported in Fig. 3.1.

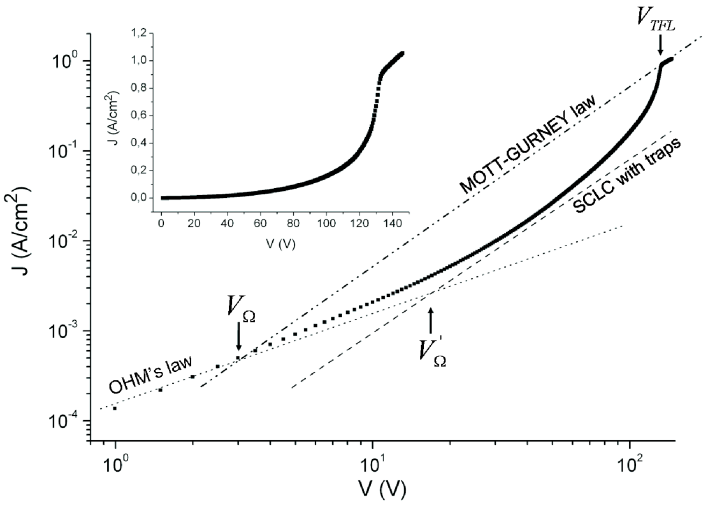

Figure 6.4: Current density vs applied voltage in double-logarithmic and linear (inset in the figure) scale for an 13 µm *thick rubrene single crystal at room temperature. Four different regimes are clearly observable: (i) at low voltage the current rises linearly and (ii) becomes SCL at higher field. Up till the (iii) transition point V_{TFL} the properties are still determined by traps, to the point they become filled and a regime given by the Mott-Gurney law (iv) [see Eq. (6.2)] takes place.*

At low voltages, the curve follows an Ohmic (linear) regime, due to the presence of thermal free carriers; these ones are related to shallow defect states that at room temperature do not act like effective charge traps. Upon increase of the applied voltage, a transition from this regime to a square law one occurs. The latter is linked to the presence of a discrete trap level that reduces the measured (or effective) charge carrier mobility $\mu_{eff} = \theta\mu$ and affects the space-charge limited current. From the Mott-Gurney theory we know that such a trend can be described by Eq. (3.1), where the trap parameter θ has a non zero value. The voltage $V_{\Omega'}$, at which the transition between the Ohmic and traps-dependent SCLC regimes occurs, can be easily extracted from the experimental curve. An estimation of the thermally generated electron density n_0 is therefore possible by using equation (3.2). At higher voltages, the current experiences an almost vertical rise and reaches the trap-free regime at the applied voltage V_{TFL}. As previously said, the knowledge of V_{TFL} makes it possible to estimate the density of traps N_t from the experimental $I-V$ curves. However, it should be pointed out that this is only valid under the assumption that the traps are

uniformly distributed in the volume of the crystal, which is most often an oversimplification, because the density of traps at the interface is always different from that in the bulk. [19] When analyzing the experimentally determined triangle of Lampert and Mark [78], we also see that the presence of shallow trapping delays the finish of the Ohmic regime from the critical voltage V_Ω to $V_{\Omega'} = (1/\theta)V_\Omega$, in agreement with the discrete trap level theory. We also underline that all the curves used to estimate the reliance of the mobility on the crystal thickness (Fig. 6.3) present the same trend: a square-law dependence at low voltage followed by a sharp current increase and a second square-law region at higher current. The $I - V$ curve for a 560 nm thick rubrene crystal is reported as a further example in logarithmic and linear scales (Fig. 6.5). Also in this case, the trap-free region is preceded by a square-law section and by an increase of the current due to trap filling. We also observe a second vertical rise, a characteristic found also in some thick crystals, that could represent either the filling of another discrete trap level, or the breakdown of the system at high injected current density.

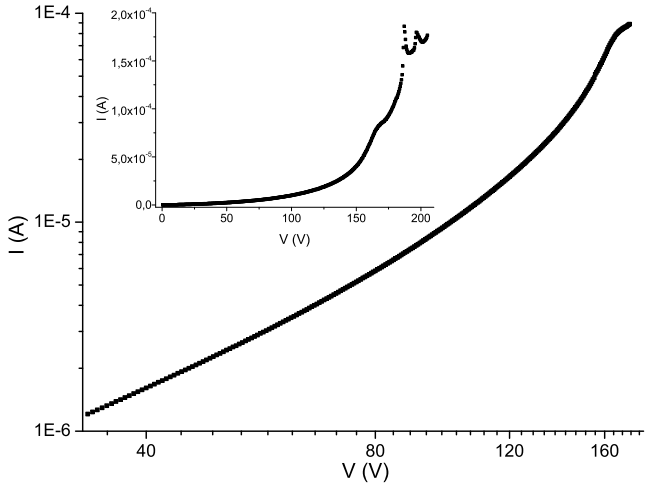

Figure 6.5: $I - V$ characteristic of a 560 nm thick rubrene crystal with gold electrodes on the surface and a channel length of 25 μm in double-logarithmic and linear scales (the latter is in the inset). The inset shows the complete experimental characteristic, whereas, for clarity, in the logarithmic plot only the SCLC behavior is reported.

The described analysis of the experimental characteristics has permitted us to fully determine the bulk properties of a rubrene single crystal. The electrical parameters for two thick samples are reported in Table 6.1, as an example. All the values have been extracted by using the Mott-Gurney's equation [Eq. (3.1)]

The trap constant θ is calculated from the ratio between the effective μ_{eff} and trap-free μ mobility, but the same value can be found by considering that in the $logJ - logV$ plot the trap limited curve is shifted below the trap-free curve by θ. The density of thermal carriers n_0 is estimated knowing θ and the transition potential $V_{\Omega'}$. The in-plane rubrene static dielectric constant was assumed to be $\varepsilon_r = 2.6$, the mean value extrapolated from the crystal full dielectric tensor at $\omega = 0$. [181]

Table 6.1: Set of electrical parameters for two different rubrene crystals, calculated with the Mott-Gurney theory with a discrete trap level.

	sample I[a]	sample II[b]
μ (cm^2/Vs)	3.5	3.4
μ_{eff} (cm^2/Vs)	0.74	0.72
n_0 (cm^{-3})	5.7×10^{11}	8.8×10^{11}
N_t (cm^{-3})	5.2×10^{13}	4.2×10^{13}
θ	0.2	0.2

[a] crystal thickness h = 13 μm
[b] crystal thickness h = 26 μm

We note that the high quality of our crystals is underlined by their extreme low density of traps. This is orders of magnitude lower than in amorphous or polycrystalline thin films [9] and in other rubrene single crystals analyzed with the same technique. [24] On the other hand, the charge carrier mobility is higher that in the disordered case, but it is significantly lower than in rubrene single crystal FETs. However, a point to note is that, in a bulk analysis, the current is normalized on the whole thickness of the active layer, whereas the conduction in a FET is always considered to be a surface process (charge-sheet model [28]). The thickness of the conductive channel is usually not taken into account either in the organic case, [182] even if calculations have already shown that, especially at low V_G, the conductive channel thickness can be of the order of several molecular layers. [122] This contradiction could explain an overestimation of the charge carriers mobility when the latter is obtained from the analysis of a field effect device. Note also that the density of thermal free charges is only one order of magnitude higher that the density of intrinsic free charge presents in Si and GaAs at room temperature. This result demonstrates the semi-insulating character of an organic material.

6.4 SCLC Differential Method: Energy of the Discrete Trap Level

To avoid incorrect interpretation of the SCL trend in the $I-V$ curves, but also because in many samples the complete trap-free regime is followed by an electrical breakdown (Fig. 6.6), we have also analyzed the characteristics by using the SCLC differential method (Ref. Chap.(3)). Besides its spectroscopy character, this technique represents a straightforward tool to prove the consistency of the experimental results with the simple Mott-Gurney model, and to exclude any misinterpretation of the data, such as assigning the square-law dependence to a discrete trap level instead of a monotonously increasing slope, [49] followed by double injection effects. [78, 183, 184]

As previously mentioned, an energy distribution of states can be (in principle) directly extracted from a single experimental $I-V$ curve by using Eqs. (3.4) and (3.5). An obvious problem is that, according to Eq. (3.5), the effective density of states N_v should be previously known in order to find the correct values of the trap energy depth. This

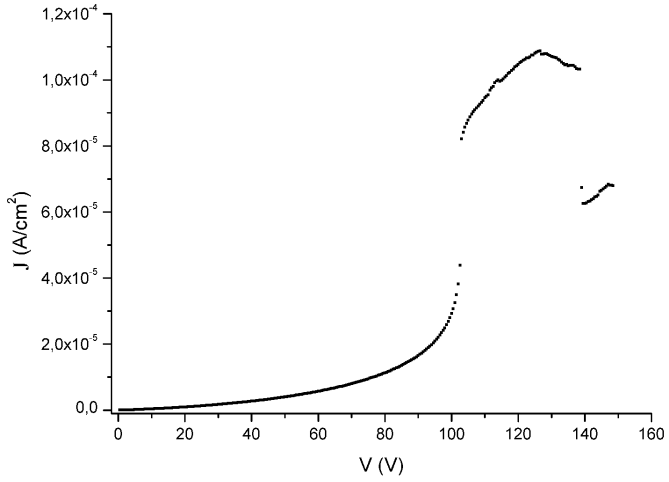

Figure 6.6: Current vs applied voltage in a rubrene single crystal. The trap-free regime is followed by a breakdown of the system. This event could lead up to misunderstanding and bad interpretation of the vertical rise that precedes it.

need, combined with the approximation of uniformity in the trap distribution, makes the calculated trap depth E_t only an estimation of the real value, altered by an error that may be as great as several kT. In any case, the found distribution, if correctly fitted, can be used to properly assign the SCL behavior and hence confirm the reliability of the parameters obtained with the Mott-Gurney treatment.
With this in mind, by taking $N_v = 1 \times 10^{21}$ cm^{-3}, [174] we have used Eqs. (3.4) and (3.5) to estimate the density of those traps whose occupancy changes during the voltage sweep. In order to confirm our previous extraction of the bulk parameters, we have then performed a fitting of the data with the bell-shaped distribution derived by Nešpurek to explain the effect of the temperature on the visibility of discrete trap levels, as follows:

$$n_t(E_F) = N_t \frac{e^{\left(\frac{E_t - E_F}{kT}\right)}}{\left[1 + e^{\left(\frac{E_t - E_F}{kT}\right)}\right]^2} \tag{6.3}$$

where $n_t(E_F)$ is the density of trapped carriers, N_t and E_t are the density and the energy depth of the discrete trap, and E_F the quasi-Fermi level given by Eq. (3.5). N_t and E_t are, in this case, the fitting parameters. Actually, fitting the data with this equation is possible because the experimentally accessible parameter is not the energetic distribution $h(E)$, but the density of trapped carriers $n_t(E)$ (strictly speaking, Eq. (3.4) is only valid at low temperature, under zero-temperature approximation, where $h(E) \simeq n_t(E)$).
Figure 6.7 shows the energetic distributions (scattered data) and the fitting curves (dashed lines) for two samples.

It can be seen that the distributions are satisfactorily fitted to (7.5) at room temperature ($T = 300K$). This confirms that within the voltage explored, the SCL features are essentially related to a discrete trap level located at $E_t = 0.48 \pm 0.02$ eV above the valence

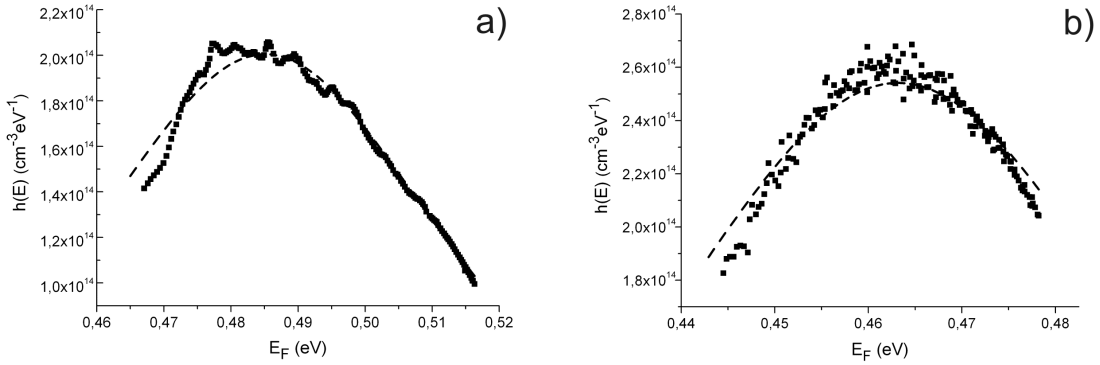

Figure 6.7: Density of states (Eqs. (3.4) and (3.5)) and fitting curve to Eq. (7.5) for two different crystals. The band edge is chosen as the reference level. Using the room temperature value $kT = 25\times10^{-3}$ *eV, the following fitting trap parameters are obtained: a)* $N_t = 4\times10^{14}$ *cm*$^{-3}$ *and* $E_t = 0.485$ *eV and b)* $N_t = 5.1\times10^{14}$ *cm*$^{-3}$ *and* $E_t = 0.462$ *eV. We have removed from the DOS reconstruction the apparent distribution maxima appearing in the low-energy region when it falls down the necessary condition* $\theta \ll 1$.

band and with a density $N_t = 4 \pm 2 \times 10^{14}$ cm^{-3} (the uncertainty is estimated from the spreading of the fitting parameters from one crystal to the other). A comparable discrete trap state level at about the same energy was found in the density of states (DOS) of rubrene recently reported by Krellner *et al.* [185]
It is worth remembering that the thus derived trap distribution is only valid in the region of the forbidden energy gap lying between E_{F0} and E_{Fh}, that is, between the position of the Fermi level at equilibrium and the position of the quasi-Fermi level at the highest voltage applied to the crystal during the experimental run. Here the found discrete level is the predominant one, even if we cannot exclude that a continuum of localized trapping states is also present in this region of the energy gap (and in the energy region closer to the valence band edge). In any case, these states make a negligible contribution to the SCLC characteristic because they act like a background in the presence of the dominant discrete trap. Therefore the free-carrier mobility found through the SCLC analysis is characteristic of charge carriers not affected by a discrete trap level, but it may be guessed that, if higher-energy states could be reached, that is, higher voltages could be applied, even greater mobility values would be found.

6.5 Conclusions

We have analyzed the in-plane hole transport properties of rubrene single crystals by means of the SCLC model and we have established a set of electrical parameters characterizing the carriers motion. The $I-V$ curves show a trap-free SCLC regime that allows us to determine a charge carriers trap-free mobility of 3.5 cm^2/Vs. Working in a gap-type structure and by calculating the mobility within the Geurst 2D and Mott-Gurney 3D models for various crystal thicknesses, we have found a transition between the 2D and 3D regimes at a thickness corresponding to roughly half the distance between the electrodes. From a

differential analysis of the $I - V$ curves, we have also found that the room temperature electrical features are related to a discrete trap level at 0.48 ± 0.02 eV above the valence band.

Our results underline the peculiarity of a rubrene single crystal, that is, its low density of thermal free charges and charge traps, and a high charge carriers bulk mobility. These materials are therefore high quality organic semiconductors, suitable for fundamental studies about the properties of an organic device.

Chapter 7

Organic Diodes and MESFETs

From the study of asymmetric metal-semiconductor-metal structures, further suggestions about the semi-insulating character of an organic material have been found. We did not find any evidence for the formation of a depletion layer in the rubrene single crystal close to the non-ohmic contact. Instead, the dependence of the impedance on the voltage, combined with the analysis of the $I - V$ characteristics, reveals the effect of a built-in potential, arising from the difference between the work function of the two electrodes at both sides of the structure. This peculiarity has been interpreted, by using the previously determined density of intrinsic charges in a rubrene single crystal.
Moreover, efficient single crystal metal-semiconductor field effect transistors have been fabricated and characterized. Thanks to the high resistance of the Au/rubrene/Al structure under reverse bias, these voltage controlled resistors show negligible leakage current and high ON/OFF ratio. The absence of a depletion layer in an organic single crystal diode suggests that the physical principles underlying the operation of the device must be revisited. A first attempt in this direction is given here, suggesting that the current modulation is an interface process in which charge injection is controlled by the applied gate voltage.

7.1 Single Crystal Diodes

7.1.1 Properties of the Rectifying Contact

I-V Characteristics

A typical $I - V$ response of a rubrene single crystal diode is reported in Fig. 7.1 in semi-logarithmic and linear scale. As visible from the characteristic, our two terminal devices are efficient hole-only rectifying diodes, with no detectable current in the reverse direction. A measurable current only flows, when a positive bias is applied to the anode (high work function electrode, ITO or Au); in this case holes are injected into the active layer thanks to a suitable energy level alignment between the metal Fermi level [186] and the rubrene HOMO level, [187, 188] while practically no electrons can go beyond the high injection barrier between the aluminum and the LUMO level of the semiconductor. [189, 6]

However, a satisfying determination of the mechanism governing the charge transport in these devices has not be possible. Several models, developed for the inorganic case (ref.

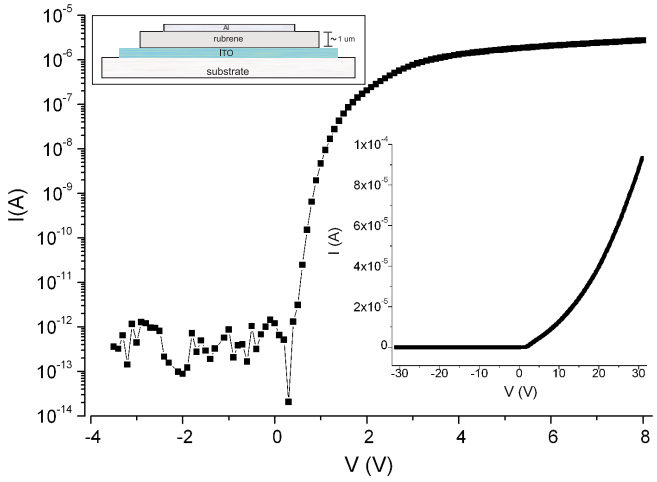

Figure 7.1: $I-V$ characteristic in semi-logarithmic and linear (inset) scales of a rubrene single crystal diode with ITO and aluminum electrodes. No detectable current flows in the device under reverse bias down to -30 V. The diagram gives the structure of the diode.

to Chap. (3), have been used to fitted the experimental curves, but without significant results. The validity of the model depends on the voltage range in which the fitting is performed, making the interpretation of the $I-V$ characteristics a pure speculation. We note that even for our single crystal devices, in which the characteristics are supposed to be not determined by a high density of defects, inorganic theories have been found to be inappropriate.

Rather than providing approximative explanations about the interplay between charge injection and drift, we have therefore focused on the properties of the metal/semiconductor interface. Our discussion, supported by the previous analysis of two terminal symmetric devices, excludes the Schottky model, as the basis understanding of the functioning of an organic diode. The rectifying effect is not dictated by a single metal-semiconductor barrier; instead, it is a consequence of the work function difference between the metal electrodes and of the resulting built-in potential established in the organic semiconductor layer. Fig. 7.2(a) shows a close view of the current onset of Au/rubrene/Al and ITO/rubrene/Al diodes. For an applied voltage $V_a < V_d$ (here, $V_a = V_{anode} - V_{cathode}$), the current remains below the detection limit of our setup (1 pA). Importantly, the onset of the forward current depends on the nature of the anode, 0.55 V for ITO and 0.85 V for gold, in good agreement with the work function difference between the two electrodes. It is worth pointing out that the onset potential for the couple Au/Al agrees fairly well with the built-in potential measured on a sandwich Au/MEH-PPV/Al structure, [190] whereas for the ITO/Al couple it is only slightly different from the reported value of 0.7 ± 0.1 eV [191].

Such a dependence of the turn-on voltage with the nature of the backcontact is not predicted by the theory of the conventional metal-semiconductor (MS) diode. Consequently, the metal-insulator-metal (MIM) image should be preferred. Fig 7.2 gives the energy scheme of both the structures. A critical feature of the Schottky diode (Fig. 7.2(b)) is

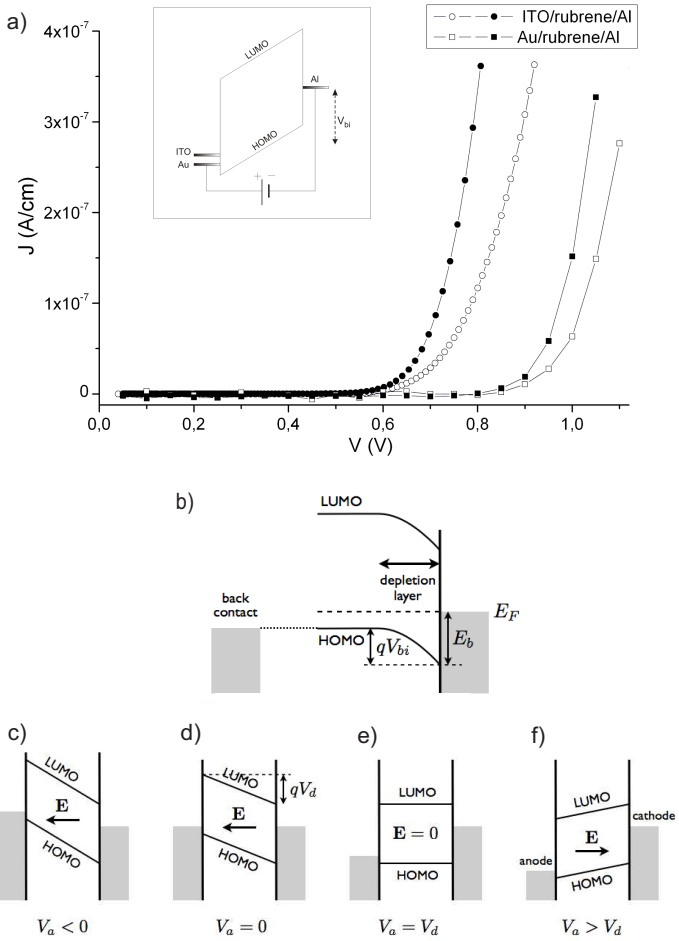

Figure 7.2: a) Close view of the $I-V$ characteristics near the turn-on voltage at which flat band conditions are reached. The response of two different samples for each anode is reported, with the inset showing a draft of the energetic levels alignment in forward bias. b) Energy diagram of the inorganic p-type Schottky diode. c-f) Energy diagrams of an organic diode.

the existence of an equipotential region that extends between the edge of the depletion layer and the back contact (the so-called *neutral region*). It is assumed that no ohmic loss intervenes across this neutral region, which seems reasonable for silicon where the conductivity ranges between 0.1 and 1 S/cm. Under such circumstances, the built-in voltage V_{bi} depends on the nature of the cathode and the Fermi level of the semiconductor, but not on the back ohmic contact; this property becomes questionable in the case of a highly resistive organic semiconductor. By contrast, the hole-only MIM device depicted in Fig. 7.2(c)-(f) is characterized by a diffusion potential V_d (the counterpart of V_{bi} in the Schottky diode) that corresponds to the work function difference between the anode and the cathode. Accordingly, V_d only depends on the nature of the electrodes and not on that of the semiconducting layer. When the anode and cathode are electrically connected and no voltage is applied, the work function difference induces an electric field that prevents hole

injection at the anode. Applying a negative voltage to the higher work function electrode (reverse bias) increases this backward electric field, so that no current is expected to flow though the structure. The electric field is canceled by the application of a voltage V_a that exactly compensates the diffusion potential ($V_a = V_d$); this corresponds to the situation of flat bands (Fig. 7.2(e)). When $V_a > V_d$, the electric field is reversed and a current starts to flow through the diode. This effect is clearly visible in Fig. 7.2(a), where the characteristics are drawn together with a diagram showing the energy level alignment in the case where a net driving force acts on the carriers.

C-V Dependence

Further considerations against the applicability of the inorganic model in the case of a non-intentionally doped, highly resistive organic semiconductors can be put forward by analyzing the dependence of the device capacitance on the applied voltage.
In an inorganic diode, the width W of the depletion layer is given by Eq. (2.1); note its dependence on the dopant density. Because organic semiconductors are non-intentionally doped, it is difficult to estimate this value. The common usage consists of equating N_A with the density of free charge, which can be accessed, for example, by analyzing the $I-V$ characteristics of symmetric diodes with the Space Charge Limited Current (SCLC) theory. As previously explained, from such an analysis, a density of thermal free carriers in the range $10^{11} - 10^{12}$ cm^{-3} has already been found for our rubrene single crystals. This value, combined with a static dielectric constant of $\varepsilon = 2.6 \times \varepsilon_0$, [181] where ε_0 is the permittivity of free space, would correspond to a space charge of around 10 µm, which in most cases largely exceeds the thickness of the semiconductor. This fact is clearly demonstrated, by analyzing the dependence of the device impedance on the applied voltage. When the system is kept under reverse bias, the impedance-voltage data show a purely capacitive behavior, characterized by a constant phase angle of $\theta = -\pi/2$. The measured capacitance (2.3×10^{-11} F) is in this case close to the geometrical capacitance (2×10^{-11} F), as given by $C_{geom} = \varepsilon A/d$, where d is the thickness of the crystal (990 nm) and A the area of the metal contact.
Fig. 7.3 shows the response of the system to an ac perturbation at 1 kHz. Consistent with the previous calculation of the depletion layer width, the impedance curves indicate that the organic semiconductor is fully depleted, with no space charge region close to the metal-semiconductor interface. This characteristic of many organic thin film diodes [15, 192, 193, 194, 195] is observed here in the case of a bulk device with an active layer thickness of $\simeq 1\mu$m, thus illustrating the very low density of accidental dopants in this semiconductor typology.

7.1.2 Impedance Spectroscopy

When a voltage above the turn-on is applied to the anode, a significant decrease of the impedance modulus is observed (Fig. 7.3). Because in this case the resistive behavior prevails, the frequency dependence of the impedance can be readily recorded over a broad frequency range and significant capacitance and resistance values estimated by fitting the impedance response at each forward bias.

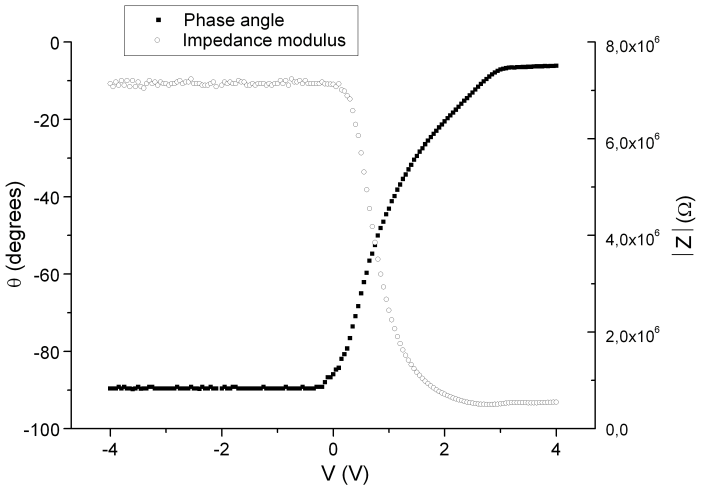

Figure 7.3: Impedance vs. voltage for a rubrene single crystal diode with ITO and aluminium electrodes. The constant impedance and phase angle reveal the insulating behavior of the active layer, when a negative bias is applied to the hole-injecting electrode.

An example of frequency-dependent impedance curve is shown in Fig. 7.4(a), using the Argand representation, and Fig. 7.4(b) with the frequency as an explicit variable. The latter represents the resistance and reactance at an applied voltage 3.5 V, along with the best-fit response of the RC equivalent circuit shown in the inset. Note that this circuit slightly differs from a simple circuit with two parallel RC in series in that C_2, which corresponds to the geometrical capacitance, extends all over the two external contacts. The advantage of this circuit is that the geometrical capacitance is not affected even when C_1 is of similar magnitude to C_2. However, in our case, we always have $C_2 << C_1$ so that the two parallel RC in series would lead to very similar results to the circuit in Figure 7.4.
When drawn in the complex plane (Fig. 7.4(a)), the impedance spectra show two well-resolved semicircles, from which meaningful capacitance and resistance values can be extracted by fitting the experimental curves at each applied voltage. Capacitance and resistance values for each elements of the equivalent circuit are reported in Fig. 7.5. As expected, the high frequency resonance is clearly a geometrical effect, with a practically constant capacitance of 2.4×10^{-11} F, close to the geometrical capacitance. By contrast, the associated resistance varies with the applied voltage and it is comparable to the resistance of the second RC circuit. In the latter, the capacitance is also voltage dependent, with a mean value of 4×10^{-9} F, which suggests that the low frequency resonance arises from a defective, highly resistive thin slab close to the metal-semiconductor interface, of around 5 nm thickness. It is important to remark that, because the low frequency arc is not always a full semicircle, the former has to be consider only as a qualitative analysis that, in any case, gives important information about the phenomena occurring in the diode under forward bias. The injection of charges under forward bias results in charging these traps, and therefore in an increase of the capacitance with the applied voltage. Such an explanation has already been reported in the literature, along with the observation of full

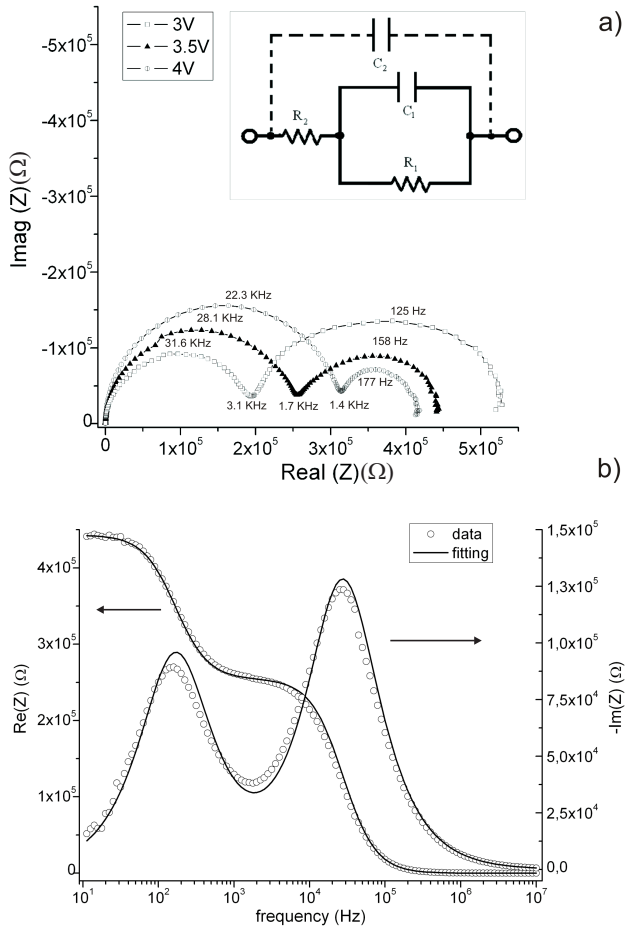

Figure 7.4: a) Complex plane plot of an ITO/rubrene/aluminum diode impedance spectrum and b) the frequency dependence of the impedance real and imaginary part for an applied bias of 3.5 V*. The experimental curves are adequately fitted in the range* $10 - 10^7$ Hz*, using the equivalent circuit reported in the inset.*

depletion under reverse bias. [99, 196, 195] In spite of the high quality of the single crystal under analysis, this contribution can not be excluded because of the inevitable damage done to the active layer by the deposition of the contact. However, the presence of defects at the metal-organic interface does not directly influence the device rectification properties, which are mostly related to the work function difference of the two electrodes.

7.2 MESFET

Using a non-injecting aluminum gate electrode and two gold ohmic contacts on the opposite sides of a rubrene single crystal we have also fabricated efficient and easy-processable organic MESFETs. The output (constant gate voltage V_G) and transfer (constant drain voltage V_D) characteristics are displayed in Fig. 7.6(a) and (b). The inset shows a schematic view of the structure.

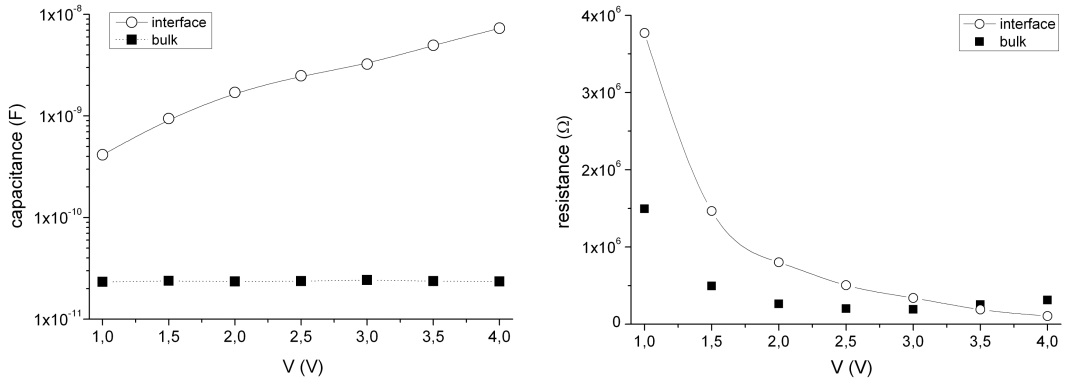

Figure 7.5: a) Capacitance and b) resistance data obtained by the analysis of the impedance spectra at different forward bias. Fitting have been carried out using the equivalent circuit reported in the inset of Fig. 7.4(a).

A specific aspect of an OMESFET is that it is a normally ON device; that is, the device is ON when no voltage is applied to the gate, while the current decreases drastically as the gate bias becomes more positive. (Note that this regime is reverse to that of the metal-semiconductor diode because here the gate voltage is applied to the cathode.) The operating mode and its difference to the conventional (insulated-gate) OFET is further illustrated in Fig. 7.7, which shows the V_G-dependent drain current over a wider range, together with the gate current. Proper operation occurs when the diode is under reverse polarization (no gate current). The maximum drain current coincides with the turn-on point of the forward regime. Beyond this point, we observe a concomitant increase of the gate current and decrease of the drain current, which bring evidence for the fact that the gate is not electrically insulated from the semiconductor.

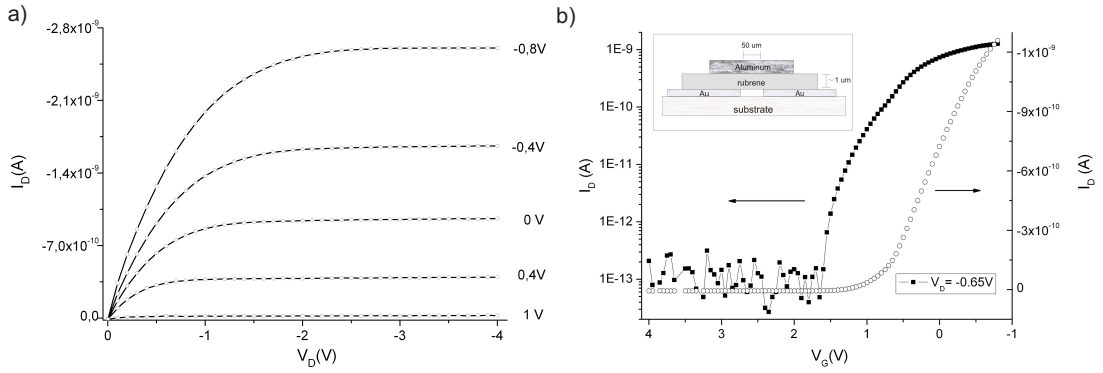

Figure 7.6: Output and transfer characteristics of a rubrene single crystal MESFET with a channel length $\mathrm{L} = 50\ \mu\mathrm{m}$ *and a channel width* $\mathrm{W} = 400\ \mu\mathrm{m}$*. The response of the device is characterized by a strict linearity of the curves at low drain voltage and by an almost perfect channel pinch-off in the saturation region.The ON/OFF ratio and the operating voltage are comparable to that reported for the insulated-gate field effect devices. The inset gives a schematic view of the device.*

Considering the high rectification ratio and the very low reserve current of the respective

diode, it is not surprising that, also in this case, the leakage current (between the source and the gate) and the OFF current are below the detection limit. Accordingly, this single crystal transistors present an ON/OFF ratio comparable to other low-voltage field effect devices. [197, 198, 199]
We propose the conjecture that the current modulation is linked to a gate-dependent charge injection mechanism, in which the ohmic injection process from the source electrode is hampered by the presence of a non-injecting metal gate, forming a parallel-plate capacitor with the latter. The device is therefore a voltage controlled resistor, in which the current is modulated by the potential of a non-injecting gate metal electrode. In the conventional MESFET, there is no electric field in the region that extends between the edge of the depletion layer and the source electrode (the neutral zone), so that charges injected at the source can spread over the neutral zone. In the OMESFET, the depletion layer under reverse bias extends up to the source, so that under this condition the backward field is present also at this electrode. At $V_G = -V_d$, the electric field vanishes and charge carriers injected at the source can readily diffuse all over the semiconductor layer. At this point, the drain current is at its maximum. The electric field that grows under reverse bias is prone to hinder charge injection because it is oriented in a direction that goes against charge injection, up to a point where the drain current completely vanishes. In other words, the current in an OMESFET is controlled by charge injection rather than modulation of the neutral zone width.

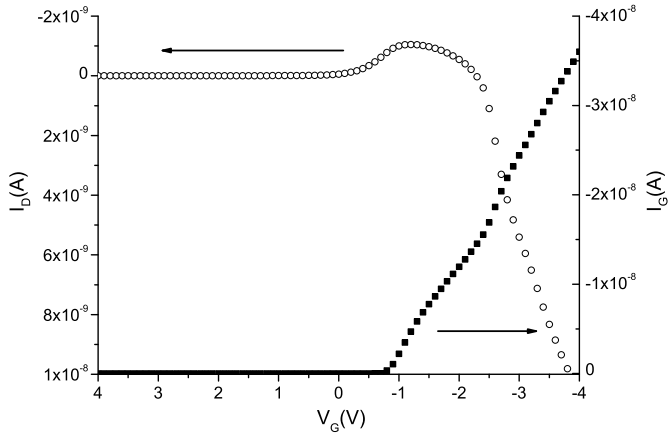

Figure 7.7: Drain I_D and gate I_G currents as a function of gate voltage for a rubrene single crystal OMESFET.

7.3 Conclusions

We have shown that the rectifying behavior of rubrene single crystal diodes is not governed by the presence of a depletion layer at the metal/semiconductor interface, but rather by the difference between the work function of the two metal electrodes and the built-in potential established inside the active layer. This property, already observed in several

thin film diodes, is here demonstrated for thick active layer devices ($d \simeq 1$ μm), thanks to the high quality and low defects density in a rubrene single crystal. As long as the diode is in reverse bias no current flow is registered, while, when the system is polarized in forward bias, injection of holes occurs from the high work function electrode. In this case, the small-signal impedance response of the devices clearly reveals the contributions of a second RC element, in series with the expected high resonance geometrical one.
On this basis, efficient single crystal metal-semiconductor field effect transistors (MESFETs) have been fabricated and characterized. The conventional inorganic theory is not applicable in this case, because of the verified absence of depletion zone close to the metallic non-injecting gate electrode. An alternative interpretation about their functioning has been given here, by considering a gate-controlled charge injection process from the gold ohmic contact into the organic layer.

Chapter 8

Organic Single Crystal Transistors

Besides all the peculiarities described so far, inconsistencies with respect to the inorganic case have been also found in the analysis of insulated-gate rubrene field effect transistors. The drain current at low V_D is, in fact, not linear in a top-contact/bottom-gate transistor, because space charge is formed in the active layer between the conductive channel and the source/drain electrodes. Moreover, the subthreshold current is not exponential. Instead, it appears as an additional current that more or less follows a linear trend. The origin of this current is attributed to the presence of charge traps. A model has been developed to describe the voltage dependence of the current in the transistor subthreshold regime. It is shown that the threshold voltage no longer establishes at the transition between the depletion and accumulation regimes; it rather corresponds to the point at which a discrete trap level is filled. The presence of this charge trap results in a subthreshold current that varies mostly linearly with gate voltage and that, at low drain voltages, increases with the drain voltage.

8.1 Rubrene MISFETs

As previously said, several MISFET configurations have been tested during this work, but significant results have been obtained only with BC/BG and TC/BG. Besides these devices also TC/TG transistors have been fabricated, but their extremely high subthreshold swing (10V/decade) has not permitted a full understanding of the processes occurring in the system. For this reason, these devices will not be considered here.
Output and transfer characteristics of two efficient devices, different in the configuration and for the polymer used as dielectric material, are reported in Figures 8.1 and 8.2.

Fig. 8.1(a) is the output characteristic of a BC/BG transistor with Teflon AF as insulator. It shows a pronounced field effect, with a perfect linearity at low drain voltage and no hysteresis up to $V_D = -40\ V$. Also, the current in the transistor OFF state is below the detection limit of our setup (Fig. 8.1(b)), giving a rectification ratio of 10^5 at $\pm 10\ V$.
The $I - V$ characteristics of a TC/BG rubrene single crystal transistor with PMMA as gate insulator are reported in Fig. 8.2(a) and (b). Also in this case, the OFF current is extremely low and there is a pretty good saturation at high V_D. Even if a direct

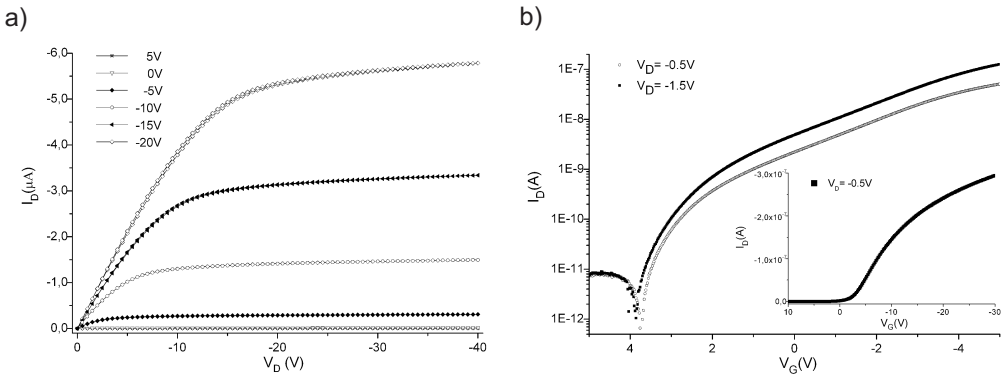

Figure 8.1: Output and transfer characteristics of a BC/BG rubrene single crystal transistor with Teflon AF as gate dielectric.

comparison between the characteristics of the two devices is not possible, we note that the charge carrier mobility in a PMMA-based transistor is substantially lower than that in the fluoro-insulator transistor. The $I_D - V_G$ characteristics of the two devices are, in fact, almost the same, even if the ratio W/L of the BC/BG transistor is half the one of the PMMA-based device (on the contrary, the insulator normalized capacitance is the same). This confirms what reported about the properties of a fluorinated insulator; [167, 200] the high charge carrier mobility in these FETs is attributed to the absence of electrically active trap states at the insulator/semiconductor surface. A point to remark is also that the trend of the current in the subthreshold regime is, in both cases, different from that in conventional MOSFETs: the current is not exponential, but it presents two tendencies, the more pronounced of which is clearly linear.

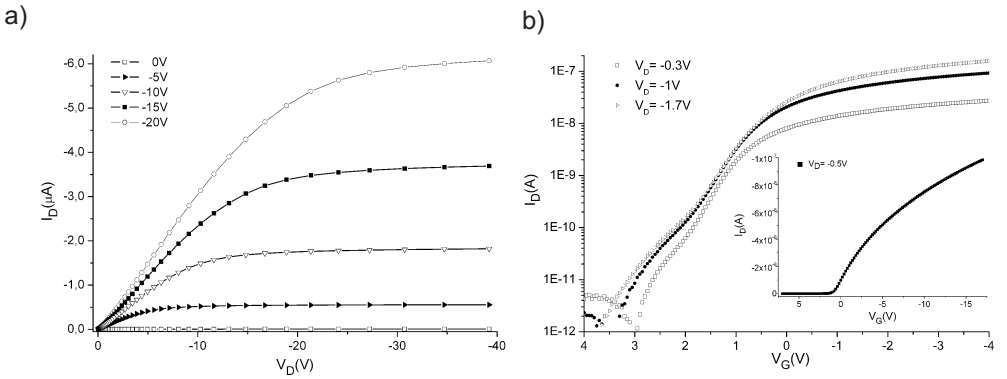

Figure 8.2: Output and tranfer characteristics of a TC/BG rubrene single crystal transistor with PMMA as gate dielectric. Note that the subthreshold regime is not exponential as in a conventional MOSFET.

An important difference between the output characteristics we have reported can be found in the low V_D region: the response of the TC/BG transistor is linear until 1 V, but it becomes superlinear for higher applied voltage (Fig. 8.3(a)). We believe that, in this case, the source to drain current is limited by a non-ohmic resistance in series with the conductive channel. A similar trend has already been observed in top contact organic single crystal

FETs [51, 201] and has been explained by considering space charge effects in the region between the conductive channel and the source/drain electrodes. As we can see in Fig. 8.3(b), in a top-contact FET, the channel is in series with two parallel-plate capacitors, that are due to the overlap between the source/drain and gate electrode. The portion of the semiconducting layer between the electrodes acts like a resistive element, in which space charge formation occurs. The latter causes the source to drain current to be not linear on the applied voltage. It is also interesting to note that the occurrence of current crowding at exactly 1 V can be explained in the framework of the SCLC theory if, different from the case reported in Chap. (3), diffusion of injected carriers is considered. [202] However, space charge effects influence the transistor properties only in the case of high active layer thickness h, when the resistance associated to the semiconductor bulk is comparable or higher than the resistance of the metal/semiconductor contacts. [203, 204, 205]

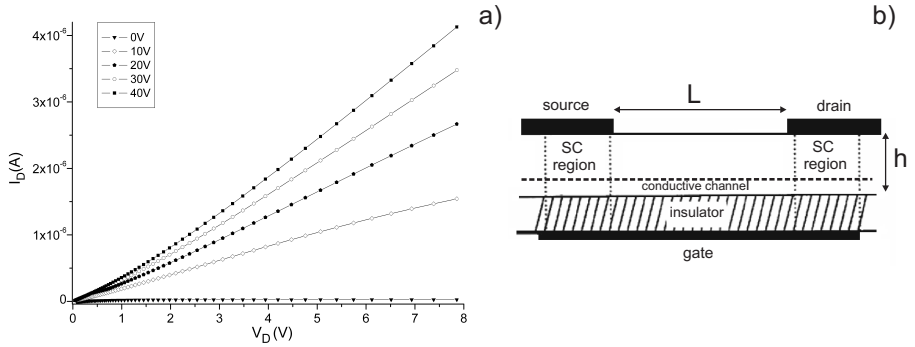

Figure 8.3: a) Particular of the output characteristics of a rubrene single crystal transistor at low V_D and b) a diagram showing a top contact FET. Current crowding at low V_D is attributable to space charge formation in the overlap region between the gate and the source/drain electrodes.

8.2 Analysis of the Subthreshold Voltage Regime

8.2.1 Current Trend below Threshold

As noted above, the characteristics of our single crystal transistors present a peculiarity that cannot be explained in the framework of the inorganic theory: the linear regime above the threshold voltage is anticipated by a non-exponential region. Moreover, when we augment the voltage between source and drain, a shift of the threshold voltage can be observed, along with an increase of the subthreshold current, (Fig. 8.2(b)). Also this effect cannot be explained by the conventional theory, because no dependence of the subthreshold current on the drain voltage is predicted in that case (ref. to Chap. (3)). On the other hand, it is remarkable that the behavior we found is similar to what predicted in terms of bulk traps effect by the numerical simulation reported in Ref. [206]. The trap density affects the carrier distribution in the channel as well as the quasi-Fermi level, causing a dependence of the subthreshold current on the applied V_D. On the basis of the results we have obtained with the SCLC technique, we believe that this explanation of the subthreshold current trend in an organic FET is extremely plausible. However, the

strong effect reported in Ref. [206], where a polymeric semiconductor has been considered, is noticeably more accentuated that in our case. By means of our analytical model, we will show that this peculiarity is probably due to the higher density of traps present in a polymer compared to that in a high quality single crystal made of a small molecular weight molecule.

8.2.2 Threshold Voltage Extraction

In order to compare the subthreshold characteristics at different V_D, the exact knowledge of the threshold voltage is required. As pointed out during the previous discussion, several methods can be used to extract this parameter, but not all of them provide meaningful results (Chap. (3)). For example, by applying the extrapolation method to our characteristics, an incorrect determination of V_T would be carried out. Figure 8.4 shows the transfer curve of a rubrene FET in the saturation regime ($V_D = -40V$) (full line), along with the plot of the transfer characteristic square root vs. V_G (dotted line). By looking to the latter curve, it is evident its upward curvature at low voltage followed by a downward curvature at high gate voltage. We note, therefore, that the linearity between the two tendencies cannot be ascribed to a constant mobility, like express by Eq. 3.10, but it represents, rather, the transition between two opposite curvatures. A direct consequence of this non-linearity is that the final estimation of the mobility and threshold voltage would largely depend on the gate voltage range used for the fitting procedure. [122, 207]

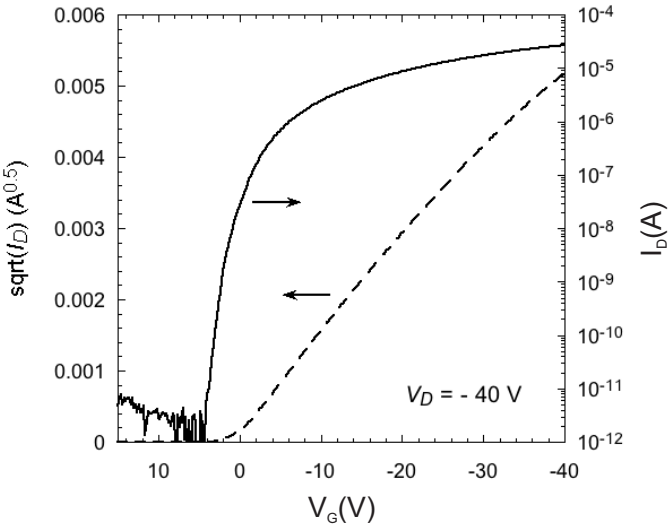

Figure 8.4: Transfer curve of a rubrene OFET in the saturation region, plotted in semi-log coordinates. Also shown is the square root of the drain current. Note that the latter is not linear but presents an upward curvature at low voltage followed by a downward curvature at higher V_G.

For this reason, the Transconductance Change method has been preferred during our analysis. The TC method yields a separate extraction of the threshold voltage, and a subsequent determination of the V_G-dependent mobility by simply using the linear regime equation. Thanks to the low noise presents in our experimental curves, on performing the second derivative, sharp peaks have been obtained, without applying error suppres-

sion algorithms. [208, 209] Only a mild smoothing procedure has been applied to the experimental data. In Figure 8.5 we report an example of V_T extraction from the second derivative. In this case, the second derivative presents a sharp peak at $V_T = 3$ V that is clearly visible over the smooth oscillating background due to the experimental data noise.

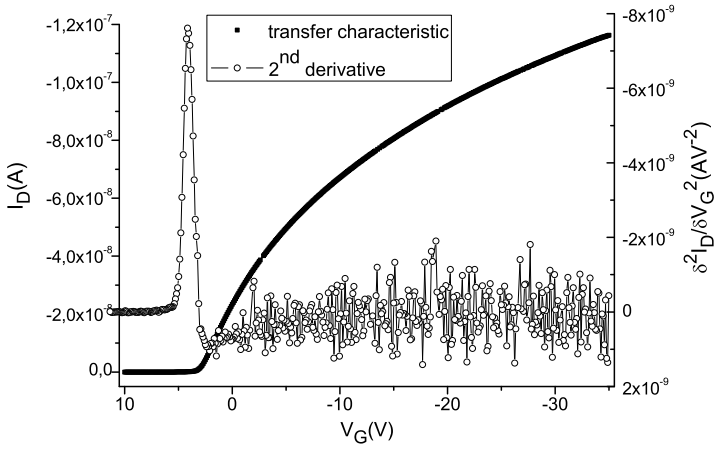

Figure 8.5: Transconductance Change method for the threshold voltage extraction through the analysis of a transfer characteristic at low drain voltage ($V_D = -0.5$ V). V_T is given by the position of the sharp peak in the second derivative of the curve. The transistor geometrical parameters are $L = 180$ μm and $W = 700$ μm. The threshold voltage is in this case $V_T = 3$ V.

Thanks to the TC technique, we have performed an accurate analysis about the threshold voltage characteristics, in particular about its dependence on the applied V_D. The resulting consideration is that V_T is not constant with the applied drain voltage, as shown in Figure 8.6 and in the inset. The slope of the $V_T - V_D$ curve in all the crystals tested falls within the range 0.65 ± 0.15, slightly higher about what could be expected by extrapolation from the transfer characteristics in the linear regime. Indeed, according to Eq. 3.9, the extrapolated value at the V_G-axis should be equal to $(V_T - V_D/2)$. An important point to remark is that, even if this trend is a peculiarity of all the considered transistors, we have found a large scattering of V_T from sample to sample, indicating the dependence of this parameter on the devices preparation procedure.
By further analysis, we have also found a plausible explanation for the non-linearity of the transfer curves. A V_G-dependent mobility is not the only possible contribution; the above threshold current trend can also be reproduced by simply introducing a V_G-independent resistive term R_c in series with the conducting channel. Actually, in a real device, the applied drain voltage V_D, is not equal to the drain to source voltage, but to an effective voltage $V_D(eff) = (V_D - R_c I_D)$ in which the potential drop on the resistance R_c is considered. Including the latter term in the equation for the ideal transistor in the linear regime, yields:

$$I_D = \frac{V_D}{R_c + 1/\left[\frac{W}{L}\mu_0 C_i (V_G - V_{Teff})\right]} \tag{8.1}$$

where V_{Teff} is the effective threshold voltage given by $V_{Teff} = (V_T + V_D/2)$.

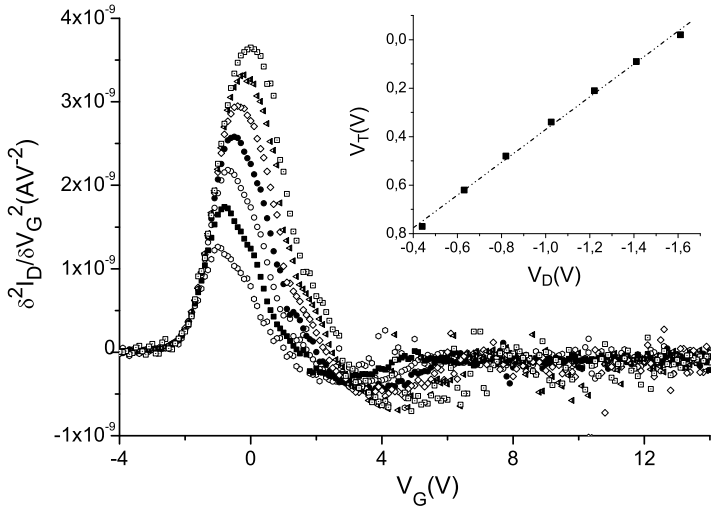

Figure 8.6: Second derivative of the transfer characteristics at different drain voltage for the determination of the threshold voltage and, in the inset, the dependence of the extracted V_T on V_D. Because of the term $V_D/2$ in the equation for the linear regime, the found threshold voltage has no real physical meaning and an extrapolation of the experimental values is necessary. The slope of the fitting straight line in the inset is 0.6.

By using this equation, fitting of noticeable quality have been carried out on the transfer characteristics, with only three free parameters (series resistance, mobility and threshold voltage). A representative example of the method is reported in Figure 8.7, where a transfer characteristic obtained at low V_D is reported along with a fitting curve. In the inset of the figure the trend of the fitted parameter V_T on the applied V_D is also shown. We note that also in this case V_T is found to derive with V_D, with a linear fitting slope of 0.63.
At variance with the description given in Ref. [124], we believe that the origin of this resistance is directly connected to the device geometry, rather than to the contacts. In our previous analysis on two terminal symmetric devices, we have shown, in fact, that there are no visible contact effects on the $I-V$ characteristics and the current is limited only by the bulk of the semiconductor. As a consequence, we can exclude the metal contacts as the source of the series resistance R_c (we are not assuming the contact resistance to be zero; rather, we believe it is not the limiting factor). Instead, as previously stated, we assign it to the region of the crystal located between the injecting electrodes and the conductive channel. In the range of applied V_D, this contribution is independent of the drain and gate voltage. At higher V_D the series resistance is expected not to be constant with the applied bias, because of space charge formation. However, this case is not considered here, because several attempts made to resolve the problems did not yield satisfactory results.

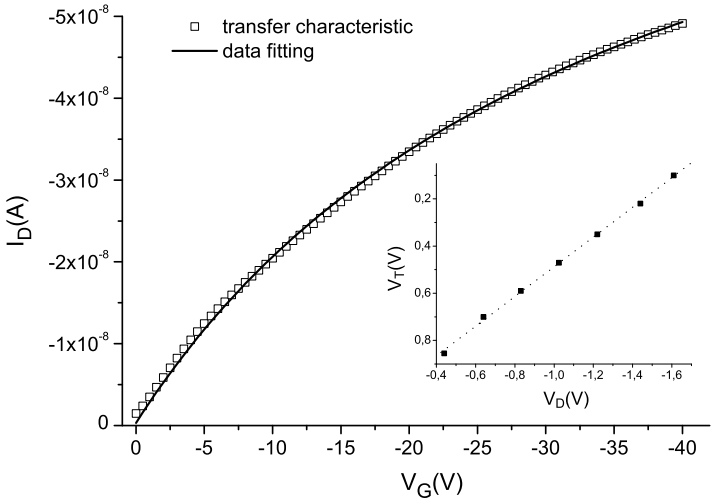

Figure 8.7: Transfer characteristic of a rubrene single crystal transistor taken at $V_D = -0.5$ V, with a fitting to Equation (8.1). The inset shows the variation of V_T with V_D.

8.3 A model for the Subthreshold Regime

8.3.1 Basic Equations

In order to explain the subthreshold current trend observed in the single crystal FETs characteristics, we propose an extension of the multiple trapping and thermal release concept. The latter describes the effect of a single shallow trap level, located close to the transport band edge, on the current-voltage characteristics of an organic field effect transistor. [27, 210]. Starting from the basic equations derived during the elaboration of the MTR model, we concentrate here on the advent of the threshold voltage and subthreshold current. All the subsequent calculations will be carried out for an n-type semiconductor; their extension to p-type is straightforward.
The geometry of the system we are considering is depicted in Figure 8.8. W and L are the channel width and length; the x axis is along the channel and the y axis across it.

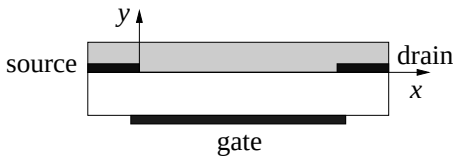

Figure 8.8: Schematic view of an organic thin-film transistor, showing the direction of the x and y axes.

In the gradual channel approximation, the component of the electric field along the channel is neglected, so we will only consider the component F_y across the channel. Under such circumstances, the drain current is given by:

$$I_D = -\frac{W}{L}\mu_0 \int_0^{V_D} Q_f(V_G - V_{FB} - V)\mathrm{d}V. \tag{8.2}$$

Here, V_D and V_G are the drain and gate voltages, respectively, μ_0 the trap free mobility and Q_f the free surface charge. The total charge, induced by the application of a gate voltage V_G, amounts to:

$$Q_{tot} = Q_f + Q_t = -C_i V_i = -C_i(V_G - V_{FB} - V_s), \tag{8.3}$$

where Q_t is the trapped surface charge, C_i the capacitance of the gate dielectric, and V_i and V_s the potential drop through the gate dielectric and the accumulation layer, respectively. V_{FB} is the flat-band potential, which will be neglected in the following.

Upon formation of the accumulation layer, a slight band bending of the conduction band edge emerges at the insulator-semiconductor interface. This is depicted in Figure 8.9, where the level alignment in the MIS structure (described in Chap. (2)), is presented again by considering an n-type semiconductor. Note that, apart at very low gate voltages, most of the voltage drop across the interface appears in the insulator, so that $|V_s| \ll |V_G|$.

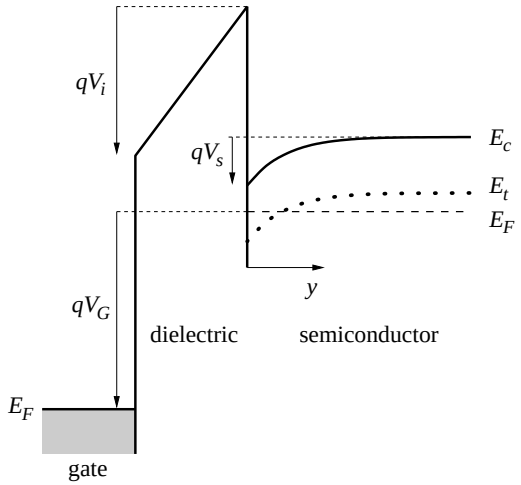

Figure 8.9: Energy diagram of an accumulation layer for an n-type semiconductor with a single trap level at energy E_t. V_s is the voltage drop (or band bending) through the accumulation layer, V_i the voltage drop through the gate dielectric and $V_G = V_s + V_i$ the gate voltage.

Generally speaking, the charge density (per unit area) in the accumulation layer is related to the volume density of charge through:

$$Q = \int_{surface}^{bulk} \rho \mathrm{d}y. \tag{8.4}$$

Here, Q and ρ pertain either to the free (Q_f and ρ_f) or to the trapped (Q_t and ρ_t) charge. Making use of $F = -\mathrm{d}V/\mathrm{d}y$, Equation (8.4) can be rewritten as:

$$Q = \int_0^{V_s} \frac{\rho}{F}\mathrm{d}V. \tag{8.5}$$

In turn, the electric field at the insulator-semiconductor interface is connected to the total charge through Gauss's law:

$$Q_{tot} = -\varepsilon_s F_s, \tag{8.6}$$

where ε_s is the permittivity of the semiconductor. The electric field is also related to the bulk charge through Poisson's equation:

$$\frac{dF}{dy} = -F\frac{dF}{dV} = \frac{\rho_{tot}}{\varepsilon_s}, \tag{8.7}$$

which can be integrated to:

$$F^2 = -\frac{2}{\varepsilon_s}\int_0^V \rho_{tot}\mathrm{d}V. \tag{8.8}$$

8.3.2 Calculation of the Drain Current

The volume densities n_f and n_t of free and trapped charge carriers in an n-type semiconductor with a single trap level of energy E_t and volume density N_t are given by:

$$n_f = \frac{N_c}{1 + e^{(E_c - E_F - qV)/kT}}, \tag{8.9}$$

$$n_t = \frac{N_t}{1 + e^{(E_t - E_F - qV)/kT}}. \tag{8.10}$$

where N_c is the density of states at the conduction band edge. The variation of n_f, n_t and $n_{tot} = n_f + n_t$ as a function of the accumulation band bending is shown in Figure 8.10.

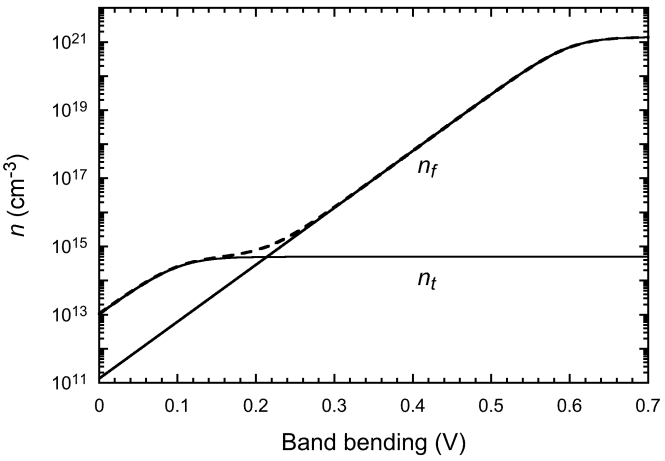

Figure 8.10: Free (n_f) and trapped (n_t) charge distribution as a function of the accumulation band bending for an n*-type semiconductor with a single shallow trap level. The dotted line corresponds to the total charge $n_{tot} = n_f + n_t$.*

The electric field across the conducting channel can be estimated by integrating Equation (8.8):

$$F^2 = \frac{2kT}{\varepsilon_s}\left[N_c \ln \frac{1+e^{-(E_c-E_F-qV)/kT}}{1+e^{-(E_c-E_F)/kT}} + N_t \ln \frac{1+e^{-(E_t-E_F-qV/kT}}{1+e^{-(E_t-E_F)/kT}}\right] \tag{8.11}$$

The free surface charge is obtained from a numerical integration of (8.5). The drain current can now be estimated from Equation (8.2) with $V_{FB} = 0$. In the linear regime, $V_D \ll V_G$, so (8.2) simply becomes:

$$I_{D,lin} = -\frac{W}{L}\mu_0 \int_{V_G-V_D}^{V_G} Q_f(V)\mathrm{d}V. \tag{8.12}$$

Note that here, the dependence of the free surface charge Q_f is on V_G, not on V_s. For this, the gate voltage is derived from (8.3) and (8.6):

$$V_G = \frac{\varepsilon_s}{C_i}F_s + V_s \tag{8.13}$$

From Equations (8.5) and (8.13), the V_G dependent free surface charge is obtained through a numerical interpolation.

The curves in Figure 8.11 have been calculated with the parameter given in Table 8.1. Note that the discrete trap level has been considered at the same energy, as that found by analyzing the $I-V$ characteristics of rubrene single crystal diodes with the SCLC analysis.

Table 8.1: Parameters used for the calculation of the drain current in Figure 8.11

$E_c - E_F$ (eV)	0.60
$E_t - E_F$ (eV)	0.10
N_c (cm^{-3})	1.4×10^{21}
N_t (cm^{-3})	5×10^{14}
ε_s	$3 \times \varepsilon_0$
C_i ($\mathrm{nF/cm}^2$)	3
μ_0 (cm^2 /Vs)	3
W/L	10

It clearly appears in Figure 8.11, that the trap level introduces an additional threshold (the mobility threshold) that corresponds to a trap-filled limit. The mobility threshold roughly occurs when the free carrier density becomes higher that that of the trapped carriers. From Figure 8.10, this coincides with the point where n_f crosses n_t, that is, when $n_f = N_t$.

Other important features in Figure 8.11 can be summarized as follows.

- In the subthreshold regime, the current is linear with gate voltage, not exponential. The current follows a superlinear variation, that could be assimilated to an exponential one, only in a narrow transition range between the substhreshold and above threshold regimes. However, we note that the range of this superlinear variation is quite limited in current (less that one decade).

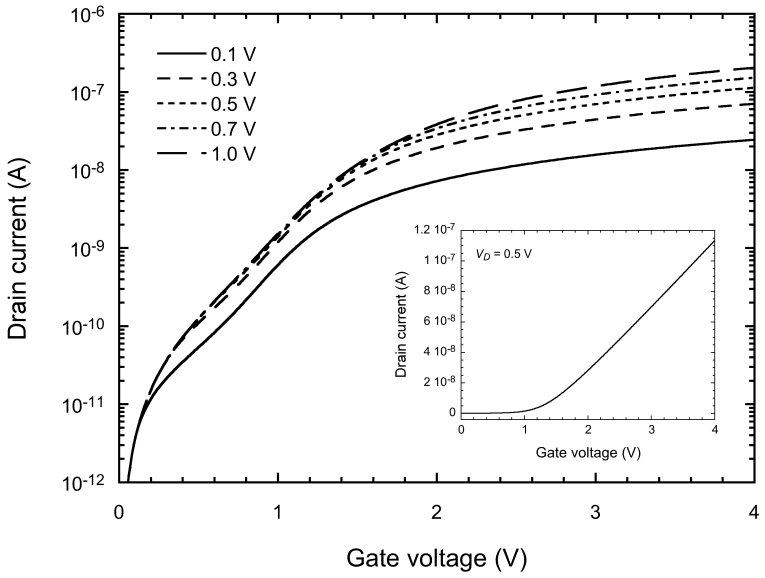

Figure 8.11: Calculated transfer characteristic at various drain voltages for an n*-type semiconductor with a single level trap. The inset shows the curve for* $V_D = 0.5$ V *in linear coordinates.*

- The subthreshold current becomes independent on the drain voltage only at high V_D. For V_D between 0.1 and 0.5 V, the subthreshold current is clearly drain voltage dependent.

Essentially, our model shows that the presence of a discrete shallow trap-level induces a shift of the threshold and that it causes the subthreshold current to be non-exponential. This effect becomes more and more pronounced as the density of trap-states increases. This statement is in a good agreement with the experimental results. However, a point to remark is that the large scattering founded in the experimental analysis is in variance with the model developed above, which predicts V_T to be only dependent on the trap distribution. We think the reason of such a discrepancy has to be sought in the fact that we have neglected the flat-band potential V_{FB}. In practice, V_{FB} is mainly determined by the charges located at the insulator-semiconductor interface, [28] a contribution that has not be included in our model. This could account for both the scattering of the data, and the discrepancy with the analytical model.

8.3.3 Determination of the Threshold Voltage

The TC method, when applied to the transfer characteristics calculated above, yields a dependence of V_T on V_D that manifests itself as a shift of the peak of the second derivative. This peculiarity is shown in Figure 8.12, along with the variation of the peak maximum on the applied drain voltage (in the inset).

Actually, the slope of the V_T vs. V_D curve, being 0.62, is extremely close to what experimentally found. On the contrary, when the extrapolation method is applied to the calculated characteristics, a value of 0.52 has been found, in agreement with the conventional theory (Chap. (3)). We can not provide a clear explanation of this discrepancy.

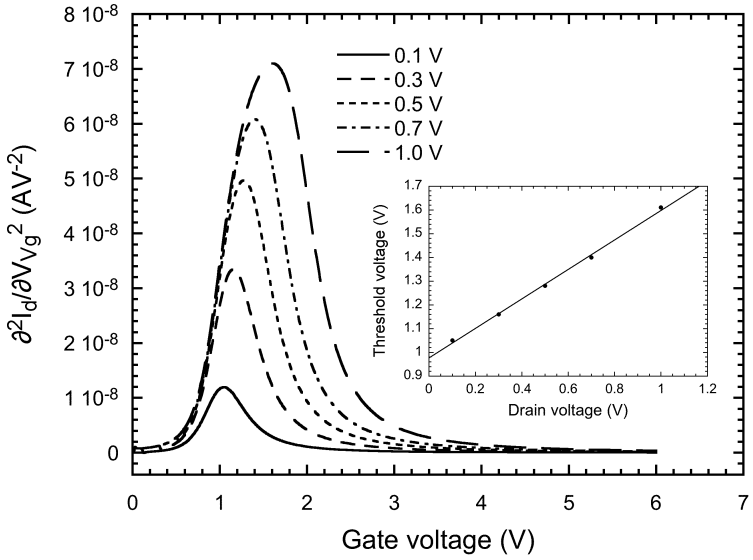

Figure 8.12: Threshold voltage extraction by the transconductance change method for the data reported in the previous figure. The inset shows the variation of V_T with the drain current. The slope of the linear fit is 0.62.

We think that the TC method introduces some deviation form the real value. However, as previously stated, the extrapolation technique is not applicable in most real cases because of non-ideal effects such as contact resistance and non-constant mobility, hence the usefulness of the TC method.

8.4 Conclusions

Rubrene single crystal MISFETs have been fabricated and characterized by using the knowledge gained from the previous analysis. Moreover, by starting from an already developed analytical model, we have theoretically studied the effect of a localized level on the transfer characteristic of organic FETs below the threshold voltage. From a derivation of the electrical field across the conducting channel, based on the free and trapped charge distribution as a function of the accumulation band bending, we could simulate some salient features, that have been found during the analysis of our rubrene single crystal devices. In particular, the subthreshold current does not follow an exponential variation as predicted by the diffusion theory developed for the inorganic MOSFET; instead, it is linear with the gate voltage both below and above threshold, and it only follows a pseudo-exponential behavior in a narrow transition region. This effect is attributed to a discrete energy level in the HOMO-LUMO gap that needs to be filled before the conduction can be considered as related to free carriers. The simulated curves are in good qualitative agreement with the subthreshold trends in the experimental transfer characteristics.

Conclusions

Understanding the characteristics of organic devices is not a simple task, especially because there are no consistent descriptions on the properties of an organic semiconductor. Because of the great importance of organic thin films in several innovative technological applications, attention is particularly given to these systems, with which low cost and efficient devices can be fabricated. However, these materials do not permit an easy determination of the mechanisms governing the device operation. Single crystals are certainly more suitable for this purpose, thanks to their lower density of defects; generally, the latter hide the intrinsic characteristics of the system under analysis.
For this reason, in spite of their poor mechanical properties, we have used high quality rubrene single crystals as ideal materials useful to clarify the fundamentals of organic devices. Through the chapters of this manuscript it has been attempted to demonstrate that organic field effect transistors cannot be treated in the same way as conventional MOSFETs. Because of the semi-insulating nature of an organic semiconductor, their operating principles are considerably different from those of inorganic devices.
First to consider metal-insulator-field effect transistors (MISFETs), we have obtained a detailed picture about the properties of a rubrene single crystal, by analyzing the current-voltage ($I-V$) characteristics of symmetric diodes with the Space Charge Limited Current (SCLC) theory. A low density of defects and a low density of intrinsic thermally generated carriers have been found to characterize this semiconductor. The SCLC method has given also full evidence of the presence of a discrete charge trap level in the active layer and, through the achievement of the trap-free regime, it has provided the "effective" charge carrier mobility in the crystal. After this characterization, in order to verify the reliability of the results obtained, we have fabricated rubrene single crystal rectifying diodes. By analyzing their responses to an applied static or alternate electric field, we did not find any evidence of a depletion layer in the rubrene single crystal close to the non-ohmic contact. This peculiarity reflects well the low density of free charges in this semiconductor, as extracted from the SCLC analysis. However, we have also seen that the absence of depletion layer close to the non-ohmic interface does not prevent the functioning of organic metal-semiconductor-field-effect-transistors (MESFETs) made on the same semiconductor. For this reason, in order to describe their functioning, we have proposed a different picture with respect to the inorganic case. These efficient organic field effect transistors, in which the semiconducting layer is in direct contact with a non-injecting gate metal, are seen to be interface controlled devices, in which the carriers injection from the ohmic source contact is modulated by the applied gate voltage.

Finally, rubrene single crystal MISFETs have been analyzed. Inconsistencies with respect to the inorganic case have been found also in this case. Indeed, the current-voltage trend observed below the threshold voltage can not be explained with the conventional theory. An alternative semi-analytical description, based on the multiple trapping and thermal release (MTR) concept, has been therefore provided. The latter takes into account the effect of a localized trap level on the distribution of free charges in the channel. The presence of this discrete trap level in a rubrene single crystal was highlighted by the analysis of two terminal symmetric devices.

In spite of the results obtained, several important aspects on the properties of the material and their influence on the characteristics of the devices are still to be clarify. Even if we have been able to identify a discrete trap level in the semiconductor energy gap, our analysis has been limited to a narrow energy range. Some evidence on the presence of another trap level closer to the HOMO level has been found, but this characteristic has not been deeply investigated. A wider analysis about the properties of the bulk of these crystals should be carried out, for example, by reducing the spacing between the electrodes in the two terminal symmetric structure. Moreover, by analysis both organic rectifying diodes and organic MESFETs, we have shown that the inorganic theories are not applicable in these cases. However, the conjecture we have proposed to explain the functioning of an organic MESFET needs to be demonstrated. For this purpose, an analytical model, that can supports our assumptions, should be developed. Finally, even if we have provided a consistent picture that explains the results obtained with high quality single crystal MISFETs, the latter should be expanded in order to provide a complete analytical treatment useful for the analysis of thin film devices. This should be made by considering a wider distribution of localized states in the semiconductor gap. However, we conjecture that the presence of distributed trap levels should lead to a less pronounced transition between empty and filled traps; in this case the subthreshold current trend could look like (and be confused with) that in a conventional inorganic device.

References

[1] Z. Bao and J Locklin, editors. *Organic field-effect transistors.* CRC Press, (2007).

[2] A. Tsumura, H. Koezuka, and T. Ando. *Macromolecular electronic device: Field-effect transistor with a polythiophene thin film.* Appl. Phys. Lett., **49**:1210, (1986).

[3] C. W. Tang and S. A. VanSlyke. *Organic electroluminescent diodes.* Appl. Phys. Lett., **51**:913, (1987).

[4] T. Hasegawa and J. Takeya. *Organic field-effect transistors using single crystals.* Sci. Tech. Adv. Mater., **10**:024314, (2009).

[5] J. Fraxedas. *Molecular organic materials : From molecules to crystalline solids.* Cambridge University Press, (2006).

[6] I.H. Campbell and D.L. Smith. *Physics of Organic Electronic Devices.* Academic Press, (2001).

[7] H Hoppe and N.S. Sariciftci. *Organic solar cells: An overview.* J. Mater. Res., **19**:1924, (2004).

[8] G. Horowitz. *Organic thin film transistor: From theory to real devices.* J. Mater. Res, **19**:1946, (2004).

[9] W Brutting, editor. *Physics of Organic Materials.* Wiley-VCH, (2005).

[10] J.S. Campbell. *Metal–organic interface and charge injection in organic electronic devices.* J. Vac. Sci. Technol. A, **21**:521, (2003).

[11] S. Karg, M. Meier, and W. Riess. *Light-emitting diodes based on poly-p-phenylene-vynylene: I. Charge carrier inj and transport.* J. Appl. Phys., **82**:1951, (1997).

[12] S. Karg, M. Meier, and W. Riess. *Light-emitting diodes based on poly-p-phenylene-vynylene: II. Impedance spectroscopy.* J. Appl. Phys., **82**:1961, (1997).

[13] Y.S. Lee, J.H. Park, and J.S Choi. *Electrical characteristics of pentacene-based Schottky diodes.* Optic. Mater., **21**:433, (2002).

[14] G. Garcia-Belmonte, A. Munar, E. M. Barea, J. Bisquert, I. Ugarte, and R. Pacios. *Charge carrier mobility and lifetime of organic bulk heterojunctions analyzed by impedance spectroscopy.* Org. Electr., **9**:847, (2008).

[15] I. D. Parker. *Carrier tunneling and device characteristics in polymer light-emitting diodes.* J. Appl. Phys., **75**:1656, (1994).

[16] P Stallinga, H.L. Gomes, M. Murgia, and K. Müllen. *Interface state mapping in a Schottky barrier of the organic semiconductor terrylene.* Org. Electr., **3**:43, (2002).

[17] E.A. Silinsh and V. Čapek. *Organic Molecular Crystals: Interaction, Localization and Transport Phenomena.* AIP Press, Woodbury, (1994).

[18] M.E. Gershenson, V. Podzorov, and A. F. Morpurgo. *Colloquium: Electronic transport in single-crystal organic transistors.* Rev. Mod. Phys., **78**:975, (2006).

[19] R. W. I. de Boer, M. E. Gershenson, A. F. Morpurgo, and V. Podzorov. *Organic single-crystal field-effect transistors.* Phys. Stat. Sol. (a), **201**:1302, (2004).

[20] R. Zeis, C. Besnard, T. Siegrist, C. Schlockermann, X. L. Chi, and C. Kloc. *Field effect studies on rubrene and impurities of rubrene.* Chem. Mater., **18**:244, (2006).

[21] D. A. da Silva Filho, E.-G. Kim, and J.-L. Brédas. *Transport Properties in the Rubrene Crystal: Electronic Coupling and Vibrational Reorganization Energy.* Adv. Mater., **17**:1072, (2005).

[22] D. Braga and G. Horowitz. *Subthreshold regime in rubrene single-crystal organic transistors.* Appl. Phys. A, **95**:193, (2009).

[23] C. Reese and Z. Bao. *High-Resolution Measurement of the Anisotropy of Charge Transport in Single Crystals.* Adv. Mater., **19**:4535, (2007).

[24] V. Podzorov, S. E. Sysoev, E. Loginova, V. M. Pudalov, and M. E. Gershenson. *Single-crystal organic field effect transistors with the hole mobility* $8\,cm^2/Vs$. Appl. Phys Lett., **83**:3504, (2003).

[25] A.F. Stassen, R.W.I. de Boer, N.N. Iosad, and A.F. Morpungo. *Influence of the gate dielectric on the mobility of rubrene-single-crystal-field-effect-transistors.* Appl. Phys.Lett, **85**:3899, (2004).

[26] V. Podzorov, E. Menard, J. A. Rogers, and M. E. Gershenson. *Hall Effect in the Accumulation Layers on the Surface of Organic Semiconductors.* Phys. Rev. Lett., **93**:226601, (2005).

[27] P. G. Le Comber and W. E. Spear. *Electronic transport in amorphous silicon films.* Phys. Rev. Lett., **25**:509, (1970).

[28] S. M. Sze. *Physics of Semiconductor Devices.* John Wiley, New York, 2nd edition, (1981).

[29] M. Shur. *Physics of semiconductor devices.* Prentice-Hall, Englewood Cliffs, (1990).

[30] J.P. Colinge and C. A. Colinge. *Physics of Semiconductor Devices.* Kluwer Academic Publishers, (2002).

[31] U.K. Mishra and J. Singh. *Semiconductor Device Physics and Design*. Springer, The Netherlands, (2008).

[32] S. Kasap and P. Capper, editors. *Springer handbook of electronic and photonic materials*. Springer, (2006).

[33] Y. Sun and J. A. Rogers. *Inorganic Semiconductors for Flexible Electronics*. Adv. Mater., **19**:1897, (2007).

[34] R.A Levy. *Microelectronic Materials and Processes*. Kluwer Academic Publishers, (1989).

[35] D. Braga, N. Battaglini, A. Yassar, G. Horowitz, M. Campione, A. Sassella, and A. Borghesi. *Bulk electrical properties of rubrene single crystals: Measurements and analysis*. Phys. Rev. B, **77**:115205, (2008).

[36] E.H. Nicollian and J.R. Brews. *MOS Physics and Technology*. Wiley, New York, (1982).

[37] H. E. Katz, Z. Bao, and S. L. Gilat. *Synthetic Chemistry for Ultrapure, Processable, and High-Mobility Organic Transistor Semiconductors*. Acc. Chem. Res., **34**:359, (2001).

[38] O. Ostroverkhova, D. G. Cooke, S. Shcherbyna, R. F. Egerton, F. A. Hegmann, R. R. Tykwinski, and J. E. Anthony. *Bandlike transport in pentacene and functionalized pentacene thin films revealed by subpicosecond transient photoconductivity measurements*. Phys. Rev. B, **71**:035204, (2005).

[39] W. Warta and N. Karl. *Hot holes in naphthalene: High, electric-field-dependent mobilities*. Phys. Rev. B, **32**:1172, (1985).

[40] A.R. Murphy and J.M.J. Frechet. *Organic Semiconducting Oligomers for Use in Thin Film Transistors*. Chem. Rev. , **107**:1066, (2007).

[41] V. Kazukauskas, H. Tzeng, and S. A. Chen. *Trap levels and effect of oxygen in poly[2-methoxy-5- (2'-ethyl-hexyloxy)-1,4-phenylene vinylene] diodes*. Appl. Phys. Lett., **80**:2017, (2002).

[42] L.-L. Chua, J. Zaumseil, J.-F. Chang, E. C.-W. Ou, P. K.-H. Ho, H. Sirringhaus, and R. H. Friend. *General observation of n-type field-effect behaviour in organic semiconductors*. Nature, **434**:194, (2005).

[43] T. Takahashi, T. Takenobu, J. Takeya, and Y. Iwasa. *Ambipolar organic field-effect transistors based on rubrene single crystals*. Appl. Phys. Lett., **88**:033505, (2006).

[44] Th. B. Singh, F. Meghdadi, S. Günes, N. Marjanovic, G. Horowitz, P. Lang, S. Bauer, and N. S. Sariciftci. *High-Performance Ambipolar Pentacene Organic Field-Effect Transistors on Poly(vinyl alcohol) Organic Gate Dielectric*. Adv. Mater., **17**:2315, (2005).

[45] K. Fujimori, F. S., T. Hamano, T. Minari, T. Miyadera, K. Tsukagoshiam, and Y. Aoyagi. *Current transport in short channel top-contact pentacene field-effect transistors investigated with the selective molecular doping technique.* Appl. Phys. Lett., **90**:193507, (2007).

[46] T. Minari, T. Miyadera, K. Tsukagoshi, Y. Aoyagi, and H. Ito. *Charge injection process in organic field-effect transistors.* Appl. Phys. Lett., **91**:053508, (2007).

[47] C. Vanoni, S. Tsujino, and T. A. Jung. *Reduction of the contact resistance by doping in pentacene few monolayers thin film transistors and self-assembled nanocrystals.* Appl. Phys. Lett., **90**:193119, (2007).

[48] Y. Shen, A. R. Hosseini, M. H. Wong, and G. G. Malliaras. *How To Make Ohmic Contacts to Organic Semiconductors.* Chem. Phys. Chem, **5**:16, (2004).

[49] E. A. Silinsh. *Organic Molecular Crystals: Their Electronic States.* Springer-Verlag, Berlin, (1980).

[50] H. Klauk, editor. *Organic Electronics: Materials, Manufacturing and Applications.* WILEY-VCH, Weinheim, (2006).

[51] G. Horowitz, F. Garnier, A. Yassar, R. Hujhoui, and F. Kouki. *Field-Effect Transistor Made with a Sexithiophene Single Crystal.* Adv. Mater, **8**:52, (1996).

[52] V. Podzorov. *Charge Carrier Transport in Single-Crystal Organic Field-Effect-Transistors*, chapter 2.1, pages 27–72. CRC Press, (2007).

[53] J. E. Anthony, J. S. Brooks, D. L. Eaton, and S. R. Parkin. *Functionalized pentacene: Improved Electronic Properties from Control of Solid-State Order.* J. Am. Chem. Soc., **123**:9482, (2001).

[54] M. David Curtis, Jie Cao, and Jeff W. Kampf. *Solid-State Packing of Conjugated Oligomers: From π-Stacks to the Herringbone Structure.* J. Am. Chem. Soc., **126**:4318, (2004).

[55] D. E. Janzen, M. W. Burand, P. C. Ewbank, T. M. Pappenfus, H. Higuchi, D. A. da Silva Filho, V. G. Young, J.-L. Bredas, and K. R. Mann. *Preparation and Characterization of π-Stacking Quinodimethane Oligothiophenes. Predicting Semiconductor Behavior and Bandwidths from Crystal Structures and Molecular Orbital Calculations.* J. Am. Chem. Soc., **126**:15295, (2004).

[56] Y. Shirota and H. Kageyama. *Charge Carrier Transporting Molecular Materials and Their Applications in Devices.* Chem. Rev., **107**:953, (2007).

[57] Y. C. Cheng, R. J. Silbey, D. A. da Silva Filho, J. P. Calbert, J. Cornil, and J. L. Bredas. *Three-dimensional band structure and bandlike mobility in oligoacene single crystals: A theoretical investigation.* J. Chem. Phys., **118**:3764, (2003).

[58] G. Brocks, J. van den Brink, and A. F. Morpurgo. *Electronic Correlations in Oligoacene and -Thiopene Organic Molecular Crystals.* Phys. Rev. Lett., **93**:146405, (2004).

[59] W. Warta, R. Stehle, and N. Karl. *Ultrapure, high mobility organic photoconductors.* Appl. Phys. A, **36**:163, (1985).

[60] V. Podzorov, E. Menard, A. Borissov, V. Kiryukhin, J. A. Rogers, and M. E. Gershenson. *Intrinsic charge transport on the surface of organic semiconductors.* Phys. Rev. Lett., **93**:086602, (2004).

[61] O. D. Jurchescu, J. Baas, and T. T. M. Palstra. *Effect of impurities on the mobility of single crystal pentacene.* Appl. Phys. Lett., **84**:3061, (2004).

[62] O. Ostroverkhova, D. G. Cooke, F. A. Hegmann, J. E. Anthony, V. Podzorov, M. E. Gershenson, O. D. Jurchescu, and T. T. M. Palstra. *Ultrafast carrier dynamics in pentacene, functionalized pentacene, tetracene, and rubrene single crystals.* Appl. Phys. Lett., **88**:162101, (2006).

[63] Z. Q. Li, V. Podzorov, N. Sai, M. C. Martin, M. E. Gershenson, M. Di Ventra, and D. N. Basov. *Light Quasiparticles Dominate Electronic Transport in Molecular Crystal Field-Effect Transistors.* Phys. Rev. Lett., **99**:016403, (2007).

[64] N. Karl. *Charge carrier transport in organic semiconductors.* Synth. Metal, **133-134**:649, (2003).

[65] V. Coropceanu, J. Cornil, D. A. da Silva Filho, Y. Olivier, R. Silbey, and J.-L. Bredas. *Charge Transport in Organic Semiconductors.* Chem. Rev., **107**:926, (2007).

[66] I. N. Hulea, S. Fratini, H. Xie, C. L. Mulder, N. N. Iossad, G. Rastelli, S. Ciuchi, and A. F. Morpurgo. *Tunable Frohlich polarons in organic single-crystal transistors.* Nat. Mater., **5**:982, (2006).

[67] S. Fratini, H. Xie, I.N. Hulea, S. Ciuchi, and A.F. Morpurgo. *Current saturation and Coulomb interactions in organic single-crystal transistors.* New Journ. Phys., **10**:033031, (2008).

[68] A. Troisi. *Prediction of the Absolute Charge Mobility of Molecular Semiconductors: the Case of Rubrene.* Adv. Mater., **19**:2000, (2007).

[69] G. Nan, X. Yang, L. Wang, Z. Shuai, and Y. Zhao. *Nuclear tunneling effects of charge transport in rubrene, tetracene, and pentacene.* Phys. Rev. B, **79**:115203, (2009).

[70] S. E. Fritz, S. M. Martin, C. D. Frisbie, M. D. Ward, and M. F. Toney. *Structural Characterization of a Pentacene Monolayer on an Amorphous SiO_2 Substrate with Grazing Incidence X-ray Diffraction.* J. Am. Chem. Soc., **126**:4084, (2004).

[71] C.D. Dimitrakopoulos and D.J. Mascaro. *Organic thin-film transistors: A review of recent advances.* IBM J. Res. Dev, **45**:1, (2001).

[72] T. Kelley. High-performance pentacene transistors. In *Organic Electronics*, page 33. Wiley-VCH, (2006).

[73] S. F. Nelson, Y.-Y. Lin, D. J. Gundlach, and T. N. Jackson. *Temperature-independent transport in high-mobility pentacene transistors.* Appl. Phys Lett., **72**:1854, (1998).

[74] M. Schwoerer and H.C Wolf. *Organic molecular solids.* Wiley-VCH Verlag GmbH, (2007).

[75] H. Bässler. *Charge Transport in Disordered Organic Photoconductors a Monte Carlo Simulation Study.* Physica Status Solidi (b), **175**:15, (1993).

[76] G. Horowitz. *Organic Field-Effect Transistors.* Adv. Mater., **10**:365, (1998).

[77] G. Horowitz and M.E. Hajlaoui. *Mobility in Polycrystalline Oligothiophene Field-Effect Transistors Dependent on Grain Size.* Adv. Mater., **12**:1046, (2000).

[78] M. A. Lampert and P. Mark. *Current injection in solids.* Academic Press, New York, (1970).

[79] N. F. Mott and R. W. Gurney. *Electronic Processes in Ionic Crystals.* Clarendon Press, Oxford, (1940).

[80] M. Pope and C.E. Swemberg. *Electronic Processes in Organic Crystals and Polymers.* Oxford University Press, (1999).

[81] S. Nespurek, O. Zmeskal, and J. Sworakowski. *Space-charge-limited currents in organic films: Some open problems.* Thin Solid Films, **516**:8949, (2008).

[82] A. Rose. *Space-Charge-Limited Currents in Solids.* Phys. Rev., **97**:1538, (1955).

[83] K.C. Kao. *Electrical transport in solids.* Pergamon Press, Oxford, (1981).

[84] P.N. Murgatroyd. *Theory of space-charge-limited current enhanced by Frenkel effect.* J. Phys. D: Appl. Phys., **3**:151, (1970).

[85] JS Bonham and DH Jarvis. *Theory of space-charge-limited current with one blocking electrode.* Aust. J. Chem., **31**:2103, (1978).

[86] P. Kumar, S.C. Jain, V. Kumar, A. Misra, S. Chand, and M.N. Kamalasanan. *Current-voltage characteristics of an organic diode: Revisited.* Synth. Metal, **157**:905, (2007).

[87] A. Rose. *An Outline of Some Photoconductive Processes.* RCA Review, **12**:362, (1951).

[88] J. A. Geurst. *Theory of space-charge-limited currents in thin semiconductor layers.* Phys. Stat. Sol., **15**:107, (1966).

[89] R. Zuleeg and Peter Knoll. *Space-charge-limited currents in heteroepitaxial films of silicon grown on sapphire.* Appl. Phys. Lett., **11**:183, (1967).

[90] A. A. Grinberg, S. Luryi, M. R. Pinto, and N. L. Schryer. *Space-charge-limited current in a film.* IEEE Tans. Electron Devices, **36**:1162, (1989).

[91] S. Nešpurek and J. Sworakowski. *Use of space-charge-limited current measurements to determine the properties of energetic distributions of bulk traps.* J. Appl. Phys., **51**:2098, (1980).

[92] O. Zmeškal, F. Schauer, and S. Nešpurek. *The bulk trap spectroscopy of solids by temperature-modulated space-charge-limited currents (TMSCLC) in the steady-state.* J. Phys. C, **18**:1873, (1985).

[93] J. Sworakowski and S. Nešpurek. *Determining local state densities in spatially inhomogeneous samples from steady-state space-charge-limited currents.* IEEE Trans. Electr. Ins., **24**:223, (1989).

[94] S. Steudel, K. Myny, V. Arkhipov, C. Deibel, S. De Vusser, J. Genoe, and P. Heremans. *50 MHz rectifier based on an organic diode.* Nat. Mater., **4**:597, (2005).

[95] M. Bohm, A. Ullmann, D. Zipperer, A. Knobloch, W.H. Glauert, and W. Fix. *Printable electronics for polymer RFID applications.* In Solid-State Circ. Conf. ISSCC 2006. Digest of Tech. Papers. IEEE Internat., page 1034, (2006).

[96] K. Walzer, B. Maennig, M. Pfeiffer, and K. Leo. *Highly Efficient Organic Devices Based on Electrically Doped Transport Layers.* Chem. Rev., **107**:1233, (2007).

[97] W.R. Salaneck, K. Seki, and J.J Pireaux, editors. *Conjugated Polymer and Molecular Interfaces Science and Technology for Photonic and Optoelectronic Applications.* Marcel Dekker, NY, (2002).

[98] S. Dailey, A.P. Monkman, and I.D.W. Samuel. *Electrical Characterisation of polymer heterojunction light-emitting diodes.* Synth. Metal, **102**:945, (1999).

[99] I. H. Campbell, D. L. Smith, and J. P. Ferraris. *Electrical impedance measurements of polymer light-emitting diodes.* Appl. Phys Lett., **66**:3030, (1995).

[100] L. Diao, C. D. Frisbie, D. D. Schroepfer, and P. P. Ruden. *Electrical characterization of metal/pentacene contacts.* J. Appl. Phys., **101**:014510, (2007).

[101] E. Menard, V. Marchenko, A. Podzorov, M.E. Gershenson, D. Fichou, and J.A. Rogers. *Nanoscale Surface Morphology and Rectifying Behavior of a Bulk Single-Crystal Organic Semiconductor.* Adv. Mater., **18**:1552, (2006).

[102] T. Kaji, T. Takenobu, A. F. Morpurgo, and Y. Iwasa. *Organic Single-Crystal Schottky Gate Transistors. Adv. Mater.*, **21**:3689, (2009).

[103] S. K. Cheung and N. W. Cheung. *Extraction of Schottky diode parameters from forward current-voltage characteristics.* Appl. Phys Lett., **49**:85, (1986).

[104] W. Brütting, S. Berleb, and A. G. Mückl. *Device physics of organic light-emitting diodes based on molecular materials.* Org. Electr., **2**:1, (2001).

[105] V. I. Arkhipov, H. von Seggern, and E. V. Emelianova. *Charge injection versus space-charge-limited current in organic light-emitting diodes.* Appl. Phys. Lett., **83**:5074, (2003).

[106] P. L. Bullejos, J. A. J. Tejada, M. J. Deen, O. Marinov, and W. R. Datars. *Unified model for the injection and transport of charge in organic diodes.* J. Appl. Phys., **103**:064504, (2008).

[107] J. C. Scott and G. G. Malliaras. *Charge injection and recombination at the metal-organic interface.* Chem. Phys. Lett., **299**:115, (1999).

[108] M. A. Baldo and S. R. Forrest. *Interface-limited injection in amorphous organic semiconductors.* Phys. Rev. B, **64**:085201, (2001).

[109] U. Wolf, S. Barth, and H. Bassler. *Electrode versus space-charge-limited conduction in organic light-emitting diodes.* Appl. Phys. Lett., **75**:2035, (1999).

[110] E. E. Barsoukov and J.R. Macdonald. *Impedance spectroscopy: Theory, Experiment, and Applications.* Wiley, New York, (2005).

[111] D.M. Taylor and H.L. Gomes. *Electrical characterization of the rectifying contact between aluminum and electrodeposited poly(3-methylthiophene).* J. Phys. D: Appl. Phys., **28**:2554, (1995).

[112] I. Torres and D.M. Taylor. *Interface states in polymer metal-insulator-semiconductor devices.* J. Appl. Phys., **98**:073710, (2005).

[113] C.A. Mead. *Schottky Barrier Gate Field-Effect-Transistor.* Proc. IEEE, **54**:307, (1966).

[114] D. J. Gundlach, L. Zhou, J. A. Nichols, T. N. Jackson, P. V. Necliudov, and M. S. Shur. *An experimental study of contact effects in organic thin film transistors.* J. Appl. Phys., **100**:024509, (2006).

[115] L. A. Majewski, R. Schroeder, and M. Grell. *Organic field-effect transistors with electroplated platinum contacts.* Appl. Phys. Lett., **85**:3620, (2004).

[116] I. N. Hulea, S. Russo, A. Molinari, and A. F. Morpurgo. *Reproducible low contact resistance in rubrene single-crystal field-effect transistors with nickel electrodes.* Appl. Phys. Lett., **88**:113512, (2006).

[117] E.J. Meijer, C. Detcheverry, P.J. Baesjou, E. Van veenendaal, D.M. de Leeuw, and T.M. Klapwijk. *Dopant density determination in disordered organic field-effect transistors.* J. Appl. Phys., **93**(8):4831, (2003).

[118] A.R. Brown, C.P. Jarrett, D.M. de Leeuw, and M. Matters. *Field-Effect tranisistors made from solution-processed organic semiconductors.* Synth. Metal., **88**:37, (1997).

[119] A.R. Brown, D.M. de Leeuw, E.E. Havinga, and A. Pomp. *A universal relation between conductivity and field-effect mobility in doped amorphous organic semiconductors.* Synth. Metal, **68**:65, (1994).

[120] G. Horowitz, M. E. Hajlaoui, and R. Hajlaoui. *Temperature and gate voltage dependence of hole mobility in polycrystalline oligothiophene thin film transistors.* J. Appl. Phys., **87**:4456, (2000).

[121] J. Takeya, M. Yamagishi, Y Tominari, and Y. Nakazawa. *Gate dielectric materials for high-mobility organic transistors of molecular semiconductor crystals.* Solid-State Electron., **51**:1338, (2007).

[122] M. Mottaghi and G. Horowitz. *Field-induced mobility degradation in pentacene thin-film transistors.* Org. Electron., **7**:528, (2006).

[123] M.J. Panzer and D. Frisbie. *Contact Effect Organic Field Effect Transistor*, chapter 2.4, page 139. CRC Press, (2007).

[124] D. Natali, L. Fumagalli, and M. Sampietro. *Modeling of organic thin film transistors: Effect of contact resistance.* J. Appl. Phys., **101**:014501, (2007).

[125] J. Zaumseil, K. W. Baldwin, and J. A. Rogers. *Contact resistance in organic transistors that use source and drain electrodes formed by soft contact lamination.* J. Appl. Phys., **93**:6117, (2003).

[126] R. J. Chesterfield, J. C. McKeen, C. R. Newman, C. D. Frisbie, P. C. Ewbank, K. R. Mann, and L. L. Miller. *Variable temperature film and contact resistance measurements on operating n-channel organic thin film transistors.* J. Appl. Phys., **95**:6396, (2004).

[127] I. Yagi, K. Tsukagoshi, and Y. Aoyagi. *Direct observation of contact and channel resistance in pentacene four-terminal thin-film transistor patterned by laser ablation method.* Appl. Phys. Lett., **84**:813, (2004).

[128] M. Koehler and I. Biaggio. *Space-charge and trap-filling effects in organic thin film field-effect transistors.* Phys. Rev. B, **70**:045314, (2004).

[129] G. Horowitz, R. Hajlaoui, H. Bouchriha, R. Bourguiga, and M. Hajlaoui. *The concept of "threshold voltage" in organic field-effect transistors.* Adv. Mater., **10**:923, (1998).

[130] A. Ortiz-Conde, F. J. Garcia Sanchez, J. J. Liou, A. Cerdeira, M. Estrada, and Y. Yue. *A review of recent MOSFET threshold voltage extraction methods.* Microelect. Reliab., **42**:583, (2002).

[131] L. Dobrescu, M. Petrov, D. Dobrescu, and C. Ravariu. *Threshold voltage extraction methods for MOS transistors.* In 23rd International semicondutor conference CAS 2000, page 371, (2000).

[132] H. S. Wong, M. H. White, T. J. Krutsick, and R. V. Booth. *Modeling of transconductance degradation and extraction of threshold voltage in thin oxide MOSFET's.* Solid-State Electron., **30**:953, (1987).

[133] P. Servati and A. Nathan. *Modeling of the Reverse Characteristics of a-Si:H TFTs.* IEEE Trans. Electr. Dev., **49**:812, (2002).

[134] J. E. Anthony. *The Larger Acenes: Versatile Organic Semiconductors.* Angewandte Chemie, **47**:452, (2008).

[135] H. H. Wasserman, J. R. Scheffer, and J. L. Cooper. *Singlet oxygen reactions with 9,10-diphenylanthracene peroxide.* J. Am. Chem. Soc., **94**:4991, (1972).

[136] M. Kytka, A. Gerlach, F. Schreiber, and J. KovaC. *Real-time observation of oxidation and photo-oxidation of rubrene thin films by spectroscopic ellipsometry.* Appl. Phys. Lett., **90**:131911, (2007).

[137] M. Fischer, M. Dressel, B. Gompf, A. K. Tripathi, and J. Pflaum. *Infrared spectroscopy on the charge accumulation layer in rubrene single crystals.* Appl. Phys. Lett., **89**:182103, (2006).

[138] O. Mitrofanov, C. Kloc, T. Siegrist, D. V. Lang, W.-Y. So, and A. P. Ramirez. *Role of synthesis for oxygen defect incorporation in crystalline rubrene.* Appl. Phys. Lett., **91**:212106, (2007).

[139] C. Kloc, K. Tan, M. Toh, K. Zhang, and Y. Xu. *Purity of rubrene single crystals. Appl. Phys. A*, **95**:219, (2009).

[140] D. Käfer, L. Ruppel, G. Witte, and Ch. Wöll. *Role of Molecular Conformations in Rubrene Thin Film Growth.* Phys. Rev. Lett., **95**:166602, (2005).

[141] M. Campione. *Rubrene Heteroepitaxial Nanostructures With Unique Orientation.* J. Phys. Chem. C, **112**:16178, (2008).

[142] X. Zeng, L. Wang, L. Duan, and Y. Qiu. *Homoepitaxy Growth of Well-Ordered Rubrene Thin Films.* Crystal Growth & Design, **8**:1617, (2008).

[143] D. Braga and G. Horowitz. *High-Performance Organic Field-Effect Transistors.* Adv. Mater., **21**:1473, (2009).

[144] M. Saleh. *Transit Time Measurements of Photogenerated Charge Carriers in Orthorhombic Rubrene Crystals.* Physica Scripta, **21**:220, (1980).

[145] A. Saeki, S. Seki, T. Takenobu, Y. Iwasa, and S. Tagawa. *Mobility and Dynamics of Charge Carriers in Rubrene Single Crystals Studied by Flash-Photolysis Microwave Conductivity and Optical Spectroscopy.* Adv. Mater., **20**:920, (2008).

[146] C. Goldmann, S. Haas, C. Krellner, K. P. Pernstich, D. J. Gundlach, and B. Batlogg. *Hole mobility in organic single crystals measured by a "flip-crystal" field-effect technique.* J. Appl. Phys., **96**:2080, (2004).

[147] C. Reese, W.-J. Chung, M. Ling, M. Roberts, and Z. Bao. *High-performance microscale single-crystal transistors by lithography on an elastomer dielectric.* Appl. Phys Lett., **89**:202108, (2006).

[148] T. Matsukawa, Y. Takahashi, T. Tokiyama, K. Sasai, Y. Murai, N. Hirota, Y. Tominari, N. Mino, M. Yoshimura, M. Abe, J. Takeya, Y. Kitaoka, Y. Mori, S. Morita, and T. Sasaki. *Solution Growth of Rubrene Single Crystals Using Various Organic Solvents.* Jpn. J. Appl. Phys., **47**:8950, (2008).

[149] K. Kim, M. K. Kim, H. S. Kang, M. Y. Cho, J. Joo, J. H. Kim, K. H. Kim, C. S. Hong, and D. H. Choi. *New growth method of rubrene single crystal for organic field-effect transistor.* Synth. Metal., **157**:481, (2007).

[150] R. A. Laudise, Ch. Kloc, P. G. Simpkins, and T. Siegrist. *Physical vapor growth of organic semiconductors.* J. Cryst. Growth, **187**:449, (1998).

[151] Ch. Kloc, P. G. Simpkins, T. Siegrist, and R. A. Laudise. *Physical vapor growth of centimeter-sized crystals of [alpha]-hexathiophene.* J. Crys. Growth, **182**:416, (1997).

[152] X. Zeng, D. Zhang, L. Duan, L. Wang, G. Dong, and Y. Qiu. *Morphology and fluorescence spectra of rubrene single crystals grown by physical vapor transport.* Appl. Surf. Science, **253**:6047, (2007).

[153] B. D. Chapman, A. Checco, R. Pindak, T. Slegrist, and C. Kloc. *Dislocations and grain boundaries in semiconducting rubrene single-crystals.* J. Cryst. Growth, **290**:479, (2006).

[154] A. R. Ullah, A. P. Micolich, J. W. Cochrane, and A. R. Hamilton. *The effect of temperature and gas flow on the physical vapour growth of mm-scale rubrene crystals for organic FETs.* In Proc. SPIE, volume 6800, pages 680005–8. SPIE, (2007).

[155] V. Podzorov, V. M. Pudalov, and M. E. Gershenson. *Field-effect transistors on rubrene single crystals with parylene gate insulator.* Appl. Phys. Lett., **82**:1739, (2003).

[156] O. D. Jurchescu, A. Meetsma, and T. T. M. Palstra. *Low-temperature structure of rubrene single crystals grown by vapor transport.* Acta Cryst. B, **62**:330, (2006).

[157] E. Menard, V. Podzorov, S.H. Hur, A. Gaur, E. Gershenson, and J. A. Rogers. *High performance n- and p-type single-crystal organic transistors with free-space gate dielectrics.* Adv. Mater., **16**:2097, (2004).

[158] C. Goldmann, C. Krellner, K. P. Pernstich, S. Haas, D. J. Gundlach, and B. Batlogg. *Determination of the interface trap density of rubrene single-crystal field-effect transistors and comparison to the bulk trap density.* J. Appl. Phys., **99**:034507, (2006).

[159] A. L. Briseno, S. C. B. Mannsfeld, M. M. Ling, S. Liu, R. J. Tseng, C. Reese, M. E. Roberts, Y. Yang, F. Wudl, and Z. Bao. *Patterning organic single-crystal transistor arrays.* Nature, **444**:913, (2006).

[160] A. L. Briseno, R. J. Tseng, M. M. Ling, E. H. L. Falcao, Y. Yang, F. Wudl, and Z. Bao. *High-performance organic single-crystal transistors on flexible substrates.* Adv. Mater., **18**:2320, (2006).

[161] T. Richards, M. Bird, and H. Sirringhaus. *A quantitative analytical model for static dipolar disorder broadening of the density of states at organic heterointerfaces.* J. Chem. Phys., **128**:234905, (2008).

[162] J. Veres, S. Ogier, and G. Lloyd. *Gate insulators in organic field-effect tranisistors.* Chem. Mat., **16**:4543, (2004).

[163] V. C. Sundar, J. Zaumseil, V. Podzorov, E. Menard, R. L. Willett, T. Someya, M. E. Gershenson, and J. A. Rogers. *Elastomeric Transistor Stamps: Reversible Probing of Charge Transport in Organic Crystals.* Science, **303**:1644, (2004).

[164] J. Takeya, M. Yamagishi, Y. Tominari, R. Hirahara, Y. Nakazawam, T. Nishikawa, T. Kawase, T. Shimoda, and S. Ogawa. *Very high-mobility organic single-crystal transistors with in-crystal conduction channels.* Appl. Phys. Lett., **90**:102120, (2007).

[165] J. Takeya, J. Kato, K. Hara, M. Yamagishi, R. Hirahara, K. Yamada, Y. Nakazawa, S. Ikehata, K. Tsukagoshi, Y. Aoyagi, T. Takenobu, and Y. Iwasa. *In-Crystal and Surface Charge Transport of Electric-Field-Induced Carriers in Organic Single-Crystal Semiconductors.* Phys. Rev. Lett., **98**:196804, (2007).

[166] K. P. Pernstich, B. Rossner, and B. Batlogg. *Field-effect-modulated Seebeck coefficient in organic semiconductors.* Nat. Mat., **7**:321, (2008).

[167] W. L. Kalb, T. Mathis, S. Haas, A. F. Stassen, and B. Batlogg. *Organic small molecule field-effect transistors with Cytop gate dielectric: Eliminating gate bias stress effects.* Appl. Phys. Lett., **90**:092104, (2007).

[168] Z. Rang, M. I. Nathan, P. P. Ruden, V. Podzorov, M. E. Gershenson, C. R. Newman, and C. D. Frisbie. *Hydrostatic pressure dependence of charge carrier transport in single-crystal rubrene devices.* Appl. Phys. Lett., **86**:123501, (2005).

[169] S. Haas, A. F. Stassen, G. Schuck, K. P. Pernstich, D. J. Gundlach, B. Batlogg, U. Berens, and H.-J. Kirner. *High charge-carrier mobility and low trap density in a rubrene derivative.* Phys. Rev. B, **76**:115203, (2007).

[170] M. Campione, R. Ruggerone, Tavazzi.S., and Moret M. *Growth and characterisation of centimetre-sized single crystals of molecular organic materials.* J. Mater. Chem., **15**:2437, (2005).

[171] Y-L Loo, T. Someya, K. W. Baldwin, Z. Bao, P. Ho, A. Dodabalapur, H. E. Katz, and J. A. Rogers. *Soft, conformable electrical contacts for organic semiconductors: High-resolution plastic circuits by lamination.* Proc. Nat. Acad. Scie. Unit. Stat. America, **99**:10252, (2002).

[172] Y.-L. Loo, R. L. Willett, K. W. Baldwin, and J. A. Rogers. *Additive, nanoscale patterning of metal films with a stamp and a surface chemistry mediated transfer process: Applications in plastic electronics.* Appl. Phys. Lett., **81**:562, (2002).

[173] S.M. Jeong, D. Y. Lee, W.H. Koo, S.H. Choi, H.K. Baik, S.J. Lee, and K.M. Song. *Improved stability of organic light-emitting diode with aluminum cathodes prepared by ion beam assisted deposition.* Sci. Tech. Adv. Mat., **6**:97, (2005).

[174] R. W. I. de Boer and A. F. Morpurgo. *Influence of surface traps on space-charge limited current.* Phys. Rev. B, **72**:073207, (2005).

[175] P. V. Pesavento, K. P. Puntambekar, C. D. Frisbie, J. C. McKeen, and P. P Ruden. *Film and contact resistance in pentacene thin-film transistors: Dependence on film thickness, electrode geometry, and correlation with hole mobility.* J. Appl. Phys., **99**:094504, (2006).

[176] D. V. Lioubtchenko, I. A. Markov, and T. A. Briantseva. *GaAs surface modifications under Au evaporating flux.* Appl. Surf. Science, **211**:335, (2003).

[177] T. Ohgi, H. Y. Sheng, Z. C. Dong, and H. Nejoh. *Observation of Au deposited self-assembled monolayers of octanethiol by Scanning Tunneling Microscopy.* Surface Science, **442**:277, (1999).

[178] J.R. Macdonald. *CNLS (Complex Nonlinear Least Squares) Immittance, Inversion, and Simulation Fitting Program.* LEVMW version 8.08 (2007).

[179] C. B. Walsh and E. I. Franses. *Ultrathin PMMA films spin-coated from toluene solutions.* Thin Solid Films, **429**:71, (2003).

[180] A. Moliton. *Optoelectronics of Molecules and Polymers.* Springer, New York, (2005).

[181] S. Tavazzi, A. Borghesi, A. Papagni, P. Spearman, L. Silvestri, A. Yassar, A. Camposeo, M. Polo, and D. Pisignano. *Optical response and emission waveguiding in rubrene crystals.* Phys. Rev. B, **75**:245416, (2007).

[182] P. Stallinga and H.L. Gomes. *Modeling electrical characteristics of thin-film field effect tranisistors. I. Trap-free materials.* Synth. Metal., **156**:1305, (2006).

[183] H. T. Henderson, K. L. Ashley, and M. K. L. Shen. *Third side of the Lampert triangle: Evidence of traps-filled-limit single-carrier injection.* Phys. Rev. B, **6**:4079, (1972).

[184] R. H. Bube. *Trap density determination by space-charge-limited currents.* J. Appl. Phys., **33**:1733, (1962).

[185] C. Krellner, S. Haas, C. Goldmann, K. P. Pernstich, D. J. Gundlach, and B. Batlogg. *Density of bulk trap states in organic semiconductor crystals: Discrete levels induced by oxygen in rubrene.* Phys. Rev. B, **75**:245115, (2007).

[186] H.B. Michaelson. *Handbook of Chemistry and Physics.* CRC Press, (1996).

[187] R. Schmechel and H. von Seggern. *Electronic traps in organic transport layers.* Physica Status Solidi (a), **201**:1215, (2004).

[188] N. Sato, K. Seki, and H. Inokuchi. *Polarization energies of organic solids determined by ultraviolet photoelectron spectroscopy.* J. Chem. Soc., Faraday transactions 2, **77**:1621, (1981).

[189] N.C. Greenham and R. Friend. *Semiconductor Device Physics of Conjugated Polymers*, volume 49. Academic, San Diego, (1995).

[190] I. H. Campbell, T. W. Hagler, D. L. Smith, and J. P. Ferraris. *Direct Measurement of Conjugated Polymer Electronic Excitation Energies Using Metal/Polymer/Metal Structures.* Phys. Rev. Lett., **76**:1900, (1996).

[191] X. Wei, S.A. Jeglinski, and Z.V. Vardeny. *Photoresponse and electroresponse studies of polymer light-emitting diodes.* Synth. Metal., **85**:1215, (1997).

[192] A. J. Campbell, D. D. C. Bradley, and D. G. Lidzey. *Space-charge limited conduction with traps in poly(phenylene vinylene) light emitting diodes.* J. Appl. Phys., **82**:6326, (1997).

[193] G. G. Malliaras, J. R. Salem, P. J. Brock, and J. C. Scott. *Photovoltaic measurement of the built-in potential in organic light emitting diodes and photodiodes.* J. Appl. Phys., **84**:1583, (1998).

[194] A. Kaur, M. J. Cazeca, K. G. Chittibabu, J. Kumar, and S. K. Tripathy. *Mechanism of electroluminescence in dye doped thiophene based conjugated polymer.* J. Appl. Phys., **89**:3250, (2001).

[195] V. Shrotriya and Y. Yang. *Capacitance–Voltage characterization of polymer light-emitting diodes.* J. Appl. Phys., **97**:054504, (2005).

[196] P. S. Davids, A. Saxena, and D. L. Smith. *Nondegenerate continuum model for polymer light-emitting diodes.* J. Appl. Phys., **78**:4244, (1995).

[197] M.H. Yoon, H. Yan, A. Facchetti, and T. J. Marks. *Low-Voltage Organic Field-Effect Transistors and Inverters Enabled by Ultrathin Cross-Linked Polymers as Gate Dielectrics.* J. Am. Chem. Soc., **127**:10388, (2005).

[198] K. H. Lee, K. Lee, M. S. Oh, J.-M. Choi, S. Im, S. Jang, and E. Kim. *Flexible high mobility pentacene transistor with high-k/low-k double polymer dielectric layer operating at -5 V.* Org. Electr., **10**:194, (2009).

[199] L. A. Majewski, R. Schroeder, and M. Grell. *Low-Voltage, High-Performance Organic Field-Effect Transistors with an Ultra-Thin TiO_2 Layer as Gate Insulator.* Adv. Funct. Mater., **15**:1017, (2005).

[200] M. Uno, Y. Tominari, and J. Takeya. *Fabrication of high-mobility organic single-crystal field-effect transistors with amorphous fluoropolymer gate insulators.* Org. Electr., **9**:753, (2008).

[201] Y.G. Seol, J.G. Lee, N.-E. Lee, S.S. Lee, and J. Ahn. *Electrical characteristics of poly(3-hexylthiophene) organic thin film transistor with electroplated metal gate electrodes on polyimide.* Thin Solid Films, **515**:5065, (2007).

[202] G. Horowitz, D. Fichou, X. Peng, and P. Delannoy. *Evidence for a linear low-voltage space-charge-limited current in organic thin films. Film thickness and temperature dependence in alpha-conjugated sexithienyl.* J. Phys. France, **51**:1489, (1990).

[203] M. J. Powell and J. W. Orton. *Characteristics of amorphous silicon staggered-electrode thin film transistors.* Appl. Phys Lett., **45**:171, (1984).

[204] R. R. Troutman and A. Kotwal. *A device model for the amorphous-silicon staggered-electrode thin-film transistor.* IEEE Trans. Electron Device, **36**:2915, (1989).

[205] S. M. Gadelrab and S. G. Chamberlain. *The Effects of Metal-n^+ Interface and Space Charge Limited Conduction on the Performance of Amorphous Silicon Thin-Film Transistors.* IEEE Trans. Electron Device, **41**:462, (1994).

[206] S. Scheinert, G. Paasch, and T. Dool. *The influence of bulk traps on the subthreshold characteristics of an organic field effect transistor.* Synth. Metal., **139**:233, (2003).

[207] K. Ryu, I. Kymissis, V. Bulovic, and C.G. Sodini. *Direct extraction of mobility in pentacene OFETs using C-V and I-V measurements.* IEEE Electr. Dev. Lett., **26**:716, (2005).

[208] W. Y. Choi, D. S. Woo, B. Y. Choi, J. D. Lee, and B. G. Park. *Stable extraction of threshold voltage using transconductance change method for CMOS modeling. Simulation and characterization.* Jpn. J. Appl. Phys., **43**:1759, (2004).

[209] W. Y. Choi, H. Kim, B. Lee, J. D. Lee, and B. G. Park. *Stable threshold voltage extraction using Tikhonov's regularization theory.* IEEE Trans. Electron Device, **51**:1833, (2004).

[210] G. Horowitz and P. Delannoy. *An analytical model for organic-based thin-film transistors.* J. Appl. Phys., **70**:469–475, (1991).

Appendix A

Ph.D. activity

Publications

- D. Braga, G. Horowitz, M. Campione, A. Borghesi "Organic metal-semiconductor field effect transistor (OMESFET) made on rubrene single crystal", published on line, Adv. Mat. 21, (2009)
- G. Bussetti, S. Cirilli, A. Violante, V. Chiostri, C. Goletti, P. Chiaradia, A. Sassella, M. Campione, L. Raimondo, D. Braga, A. Borghesi "Reflectance anisotropy spectroscopy: A probe to explore organic epitaxial growth" J. Vac. Sci. Technol. A 27, 1029 (2009)
- D.Braga, G. Horowitz "High-performance organic field-effect transistors" Adv. Mater. 21, 1473 (2009)
- D.Braga, G. Horowitz, "Subthreshold regime in rubrene single-crystal organic transistors" Applied Physics A 95, 193 (2009)
- D.Braga et al. "Bulk electrical properties of rubrene single crystals: Measurement and analysis" Phys Rev B 77, 115205 (2008)

Oral/poster presentations

ORAL

- D.Braga, M. Campione, A. Borghesi, G. Horowitz "Injection barrier effects in rubrene single crystal devices" ICOE 2009, Liverpool (UK)
- D.Braga, G. Horowitz, A. Borghesi "Comparative study of space-charge and field-effect current in rubrene single crystals", E-MRS 2008 Spring Meeting, Strasbourg (FRANCE)
- D. Braga et al. "Bulk electrical properties of rubrene single crystals" ECOER 2007 Varenna (ITALY)

POSTER

- D.Braga, G.Horowitz, A.Borghesi "Comparative study of space-charge and field-effect current in rubrene single crystals", International conference on Advanced Materials, 2008 Palanga (LITHUANIA)
- D. Braga et al. "Bulk electrical properties of rubrene single crystals" nanoSYD summerschool 2007, Alsion (DENMARK)
- D. Braga et al. "Charge transport properties of quaterthiophene single crystal and thin films" V Convegno nationale materiali molecolari avanzati per fotonica ed elettronica, 2006 Arbatax (ITALY)

Patents

- M. Campione, D. Braga, M. Moret, A. Sassella, "Method for the realization of electrical contacts on organic semiconductors", EP09425182, May 12, 2009

Courses attended

- June 2008: "Training course on the electronic devices simulation software ATLAS", Grenoble (FRANCE)
- September 2007: "International School on Organic Photovoltaics" Ventotene (ITALY)
- February 2007: "Winterschool on organic electronics" Planneralm (AUSTRIA)

Other scientific activities

- Referee for "Solid State Communications" from 2009